ISSN 2074-272X

науково-практичний журнал 2018/1

Електротехніка і Електромеханіка

Electrical Engineering & Electromechanics

Електротехніка. Визначні події. Славетні імена
Електричні машини та апарати
Електротехнічні комплекси та системи. Силова електроніка
Теоретична електротехніка та електрофізика
Техніка сильних електричних та магнітних полів. Кабельна техніка
Безпека електрообладнання
Ювілеї
Інформація

З 2016р. журнал індексується у міжнародній наукометричній базі Web of Science Core Collection: Emerging Sources Citation Index

«ELECTRICAL ENGINEERING & ELECTROMECHANICS»

SCIENTIFIC & PRACTICAL JOURNAL

Journal was founded in 2002

Founders:

National Technical University «Kharkiv Polytechnic Institute» (Kharkiv, Ukraine)

State Institution «Institute of Technical Problems of Magnetism of the NAS of Ukraine» (Kharkiv, Ukraine)

ISSUE 1/2018

TABLE OF CONTENTS

Editorial office address: Dept. of Electrical Apparatus, NTU «KhPI», Kyrpychova Str., 2, Kharkiv, 61002, Ukraine
phones: +380 57 7076281, +380 67 3594696, **e-mail:** a.m.grechko@gmail.com (**Grechko O.M.)**

ISSN (print) 2074-272X
ISSN (online) 2309-3404

Printed 16 February 2018. Format 60 x 90 ⅛. Paper – offset. Laser printing. Edition 200 copies.

Printed by Printing house «Madrid Ltd» (11, Maksymilianivska Str., Kharkiv, 61024, Ukraine)

UDC 621.3: 537.8: 910.4 **doi: 10.20998/2074-272X.2018.1.01**

M.I. Baranov

AN ANTHOLOGY OF THE DISTINGUISHED ACHIEVEMENTS IN SCIENCE AND TECHNIQUE. PART 42: ELECTRONICS: RETROSPECTIVE VIEW, SUCCESSES AND PROSPECTS OF ITS DEVELOPMENT

Purpose. Preparation of brief scientific and technical review about sources, retrospective view, basic stages, achievements, problems, trends and prospects of development of world electronics for period of 20th-21st centuries. Methodology. Known scientific methods of collection, analysis and analytical treatment of the opened scientific and technical information of world level in area of a vacuum electronics, semiconductor electronics, vacuum microelectronics and nanoelectronics, and also optical electronics. Results. A brief analytical scientific and technical review is resulted about the primary and present states, achievements, trends and prospects of development of electronics in the developed countries of the world. From positions of approach of the systems advantages and lacks of semiconductor microelectronics are described as compared to a vacuum electronics. Considerable progress is marked in development of semiconductor element base (microtransistors, microprocessors, microcontrollers and other) for creation of different electronic devices and computing engineering. Information, touching the determining deposit of electronic companies of the «Silicon Valley» in the USA in providing of technological breach in area of modern microelectronics, production of computers and their microprocessors, software and creation of devices of mobile communication development, is resulted. The basic problems of space microelectronics are affected. The possible ways of further development are indicated in the world of electronics, including vacuum microelectronics and nanoelectronics, and also optical electronics. The special attention is turned for urgent development of high-efficiency protective facilities specialists against cyber attacks hackers on the computer systems. In a review an accent is done on the sharp necessity of acceptance the proper services of drastic measures for a fight with cyber terrorism. Originality. Systematization of the scientific and technical materials touching world history of development and creation of modern element base of a vacuum electronics and semiconductor microelectronics known from the sources opened in outer informative space is executed. Possible new perspective directions of development in the modern world of microelectronics are formulated. Practical value. Popularization and deepening for students, engineer and technical specialists and research workers of front-rank scientific and technical knowledge in the topical area of development, creation and application in the modern technique of the different setting of high-computer-integrated electronic devices, extending their scientific range of interests and further development of scientific and technical progress in society. References 34, figures 22.

Key words: **vacuum electronics, radio lamp, solid state microelectronics, transistor, integrated circuit, microprocessor, vacuum integrated circuit, vacuum microelectronics and nanoelectronics, trends and prospects of electronics development.**

Приведен научно-технический обзор о ретроспективе, успехах, тенденциях и перспективах развития мировой электроники. Рассмотрены основные этапы развития электроники, связанные с изобретением радиолампы, транзистора, интегральной схемы и высокоинтегрированного микропроцессора. Отмечен вклад электронных компаний «Кремниевой долины» США в технологический прорыв в микроэлектронике. Описано состояние работ в области вакуумной микроэлектроники и наноэлектроники. Библ. 34, рис. 22.

Ключевые слова: **вакуумная электроника, радиолампа, твердотельная микроэлектроника, транзистор, интегральная схема, микропроцессор, вакуумная интегральная схема, вакуумная микроэлектроника и наноэлектроника, тенденции и перспективы развития электроники.**

Introduction. For mankind in the 20th century, the time came when the further development of scientific and technological progress in society became unthinkable without electronics. As is known, by «*electronics*» we mean that area of science and technology that covers the study and practical use of electronic and ionic phenomena occurring in vacuum, gases, liquids, solids and plasmas, and also on their boundaries [1]. That is why electronics is engaged in the study of the interaction of electrons and ions with electromagnetic fields and methods of creating electronic devices for the conversion of electromagnetic energy mainly for the transmission, reception, processing and storage of information [2]. Electronics has become the basis of modern automation, radio engineering, electrical engineering, energy, cybernetics, information technology and other important scientific and technical fields of knowledge. Without electronics, research at a high scientific level in the field of the microworld (for example, plant and animal cells, atoms and molecules of matter), and the macrocosm (for example, objects of the nature of the planet Earth, the secrets of near and far space) have become impossible. Without extensive use of electronics, they do not do without the development and creation of most complex military and civilian facilities (for example, aircraft, rocket and space technology, power stations, audio, television, and video equipment, etc.). Electronics and its successes in all industrialized countries of the world are given increased attention. According to the level of development in the country of electronics and, accordingly, the electronic industry, experts make a reasoned assessment of its scientific and technical potential and economic opportunities in the medium and long term [2]. The emergence of electronics was preceded by the invention at the end of the 19th century (May 7, 1895) by our former compatriot, Professor of Physics Department of the St. Petersburg Electrical Engineering Institute A.S. Popov (1859-1906) wireless radio communication [2, 3]. We would like to point out that the remarkable achievements of the talented Italian

engineer and businessman G. Marconi (1874-1937) awarded in 1909 by the Nobel Prize in Physics [4] contributed to the significant development in the world of radio communications. Radio and radio transmitters immediately found application in military affairs and, first of all, in the Navy [2, 3]. It was then that for practical implementation of actual applied radio engineering tasks, a corresponding elemental base was required, and the study and creation of which was done in detail by electronics.

The goal of the paper is the preparation of a brief scientific and technical review on the sources, main stages, achievements, current trends and prospects of development in the electronics world on the basis of published in open press materials.

1. The stage of the birth of electronics and the invention of a radio lamp. The creation and development of the elemental electronics base in the world actually began with the invention of an electronic lamp (EL) in the early 20th century. So, in 1904, John Fleming received a British patent for «*A device for the conversion of alternating current into direct current*» [2, 5]. It was this two-electrode vacuum device - the diode and served as the opening on the Earth of the age of electronics. Therefore, this electronics is usually called «*vacuum electronics*» [5]. EL or simply a radio lamp is known to be an electrovacuum device that operates by controlling the intensity of the flow of free electrons moving inside a vacuumed sealed glass cylinder between the metal electrodes. These electrons in EL arise because of the phenomenon of their thermionic emission from the surface of a metal cathode heated by direct (alternating) heating current to high temperature (about (800-3000) °C) [2, 5]. It should be noted that the author of the discovery of the phenomenon of thermionic emission from a hot electrode is the famous American electrical engineer and inventor Thomas Edison (1847-1931), who in 1883, in experimental studies, as far as possible, to increase the lifetime of a light bulb containing a carbon filament in a pumped glass flask, recorded the passage of an electric current in a vacuum from the filament of a lamp to a flat metal electrode located near a given filament [5]. Then the importance of the significance of this seemingly local electrophysical phenomenon, but as it turned out in the future of a fundamental scientific discovery, he did not fully understand. But as an experienced inventor, just in case, he still patented it in the US. Over time, it was this discovery that became the basis for the operation of all types of EL and, in fact, the basis for all vacuum electronics up to the creation of semiconductor devices. J. Fleming used this «Edison effect» when creating his electrovacuum diode, which played a prominent role in the history of radio engineering. The main drawback of the Fleming diode was its inability to amplify electrical signals. In 1906, an American engineer Lee de Forest introduced a third electrode to the EL in the form of a control metal grid and invented in this way an electrovacuum triode shown below in Fig. 1 [5, 6].

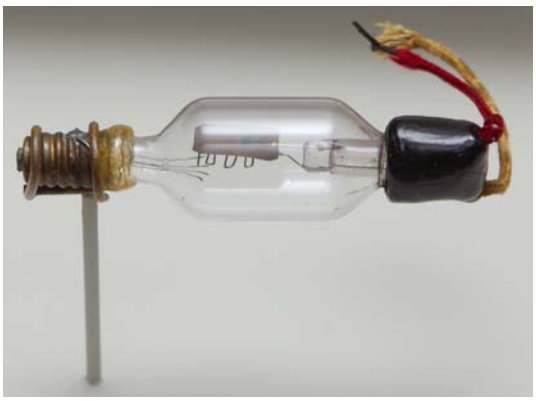

Fig. 1. General view of the triode created by Lee de Forest [5, 6]

The «Forest triode» became the first amplifying lamp and the basis for further improvement of EL with a heated cathode [7]. This EL due to the supply of its control electrode of an alternating electric potential could work as an amplifier of electromagnetic oscillations [7]. In 1913, based on the «Forest triode «, the first autogenerator was created [5, 7]. A major contribution to these pioneering developments for the needs of radio engineering with the use of a tube triode for the generation of electromagnetic oscillations was made by A. Meissner [8]. EL and the lamp amplifiers created on their basis became actively used on radio stations. Under the leadership of the well-known Russian radio engineer M.A. Bonch-Bruevich (1888-1940) at the Nizhny Novgorod Radio Laboratory in 1919 the first Russian radio lamp was created, called «Babushka» («Grandmother») (Fig. 2) [9].

Fig. 2. General view of the first Russian powerful radio lamp «Babushka» («Grandmother») (Nizhny Novgorod Radio Laboratory, 1919) [9]

Later on, after tube diodes and triodes, such types of EL were created: [7] tetrodes (1913), pentodes (1929, Fig. 3), hexodes (1932), heptodes, octodes and nonods. These types of EL differ in design from each other, primarily by the number of metal grids (from two to seven) [5, 7]. ELs using a filament inside the cathode are called indirectly incandescent lamps, and ELs made with a filament in the form of the cathode itself have been called direct-burning lamps. EL cathodes, as a rule, are activated by metals having a small work function of electrons. In EL direct heating for this purpose, radioactive thorium is used, and in indirect filament lamps - barium [7]. On the inner

surface of the EL glass, one can see a brilliant coating-getter intended for the adsorption of residual gases in its internal vacuumed volume and the indication of the vacuum in it (when the air enters the EL, the getter becomes white [7]). The peak of «flowering» in the world of vacuum electronics came in 1930-1950.

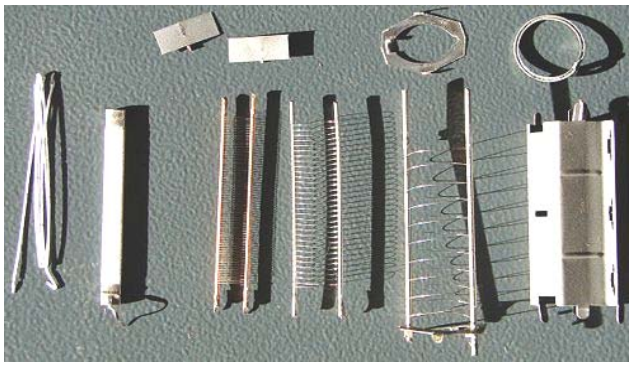

Fig. 3. External view of individual elements of the modern electrovacuum pentode (from left to right: filament, heated cathode, three metal grids, anode, at the top of the mentioned EL elements - details of their attachment) [7]

We point out that in 1913 G. Marconi patented the construction of the anode of a radio lamp in the form of a hollow metal cylinder of various configurations surrounding an internal coaxially placed cathode [7]. In this regard, EL already in the 1930s almost acquired the external view that it now has (Fig. 4). In high-power radio tubes with a high current density of the cathode, purely metallic cathodes perform their refractory tungsten. The anodes in such ELs are most often made in the shape of a box (see Fig. 3, 4) surrounding the cathode and the grid, from nickel or molybdenum (sometimes from tantalum) [7]. The grid in EL is a lattice (see Fig. 2) or a spiral made from a thin refractory metal wire wound around the cathode. A slight change in the difference between the electrical potentials between the control grid and the cathode leads to large changes in the anode current in the external circuit of the EL.

Fig. 4. General view of a modern vacuum radio lamp [7]

Let us pint out the advantages and disadvantages of tube electronic amplifiers using radio tubes in their circuits. The main advantages of amplifiers on EL should be attributed [6, 7]:

- simplicity of circuits (in tube amplifiers, in comparison with semiconductor amplifiers an order of magnitude smaller than composite elements and parts, EL provide more amplification than transistors);
- high reliability in operation (the output parameters of EL depend little on external factors such as temperature, pressure, optical and ionizing radiation, EL are insensitive to electric overloads in their circuits);
- good compatibility with the load (lamp stages have a large input resistance, which helps reduce the number of active elements in the amplifier and reduce losses on them);
- ease of maintenance (with the failure of the EL it is much easier to replace than the transistor);
- absence at their output of certain types of distortion inherent in transistor cascades.

The main disadvantages of electronic amplifiers on radio tubes include the following [6, 7]:

- relatively low efficiency (in used ELs, in addition to powering the anode, it is required to heat the cathode due to the filament, which leads to additional costs of electricity);
- greater inertia in preparation for operation (all EL require preheating);
- certain limitations on safety in their operation (electronic circuits using EL require the use of voltage in their circuits, which is hundreds and thousands of Volts);
- limited lifetime (over time, the cathode EL loses its emissive properties in the emission of free electrons, a relatively high probability of burning the cathode filament EL);
- fragility of their EL with a glass cylinder.

Despite these disadvantages, ELs continue to be actively used and at present when creating electronic circuits of the following techniques [7]:

- powerful broadcasting transmitters having an output power from hundreds of Watts to several Megawatts (electronic circuits of such radio devices use powerful and super-power radiolamps with air or water cooling and a filament current in EL cathode circuits of 100 A and more);
- objects of military equipment that are resistant to the damaging effect of a powerful electromagnetic pulse of natural (from lightning discharges) and artificial (from nuclear explosions) origin;
- rocket and space technology exposed to long-term exposure to radiation fluxes when flying in open space conditions (the radiation degradation of semiconductors limits their use in spacecraft electronics);
- high-quality audio equipment.

Note that the introduction of any gas in the EL degrades its technical characteristics. Nevertheless, radio engineering practice required gas discharge devices in which the control of their electrical ion current is carried out by the voltage applied to their metal electrodes. Such ion devices have been called «thyratrons» one of whose representatives is shown in Fig. 5.

The thyratron is a sealed glass cylinder filled with a gas (usually an inert gas, hydrogen or mercury vapor) and containing at least three electrodes - a cathode, an anode and a grid - inside it [10]. The grid in the thyratron is used to ignite a gas discharge in the space between the cathode and the anode. For this purpose, a high impulse voltage is applied to it from the power supply. The ionized gas (plasma) arising from this electric spark discharge in the closed thyratron volume conducts an electron-ion current between the cathode and the anode. In this way a three-electrode gas-discharge thyratron switches on and off the pulse current in its anode circuit. In high-current circuits

of high-voltage pulse technology using powerful capacitive energy storage (CES) to supply high pulsed currents (HPC) of the nano and microsecond range to electrical loads, three-electrode electronic devices that were termed «trigatrons» were widely used [11]. Usually their working chamber is filled with a gas dielectric (Fig. 6). More rarely it is filled with a liquid dielectric. Trigatrons are one of the varieties of a controlled spark switch [12].

Fig. 5. General view of a large hydrogen thyratron used in pulse electrical circuits of modern radars (manufactured by General Electric, USA) [10]

Fig. 6. General view of the powerful trigatron type CV100 [11]

Trigatrons use a cold cathode. A microsecond voltage pulse with an amplitude of up to ±100 kV is applied to their control (initiating) electrode (an analog of the grid in thyratrons) from the generator of igniting electrical signals, causing the appearance of one of its main spark-discharge electrodes in the local zone and, accordingly, the initial ionization of the plasma channel of the gaseous dielectric surrounding it. As a result of a sharp decrease in the electrical strength of its main insulating gap between the cathode and the anode of the trigatron, an electric breakdown of the working dielectric medium takes place and, accordingly, a discharge of the previously charged CES to the load. The amplitudes of commutated trigatrons of HPC range from tens to thousands of kiloamperes [11, 12]. This type of electronic devices is also used as high-current high-voltage switches in the discharge circuits of generators of high and ultrahigh impulse voltages, performed according to the classical Arkadyev-Marx scheme, in high-voltage devices of high-current accelerators of charged particles and electrodynamic guns [11, 12].

A successful combination of controlled spark switches - trigatrons and thyratrons have become such gas-filled lamps with a cold cathode as «krytrons» [13]. The krytrons (Fig. 7) are characterized by a fast switching on of the electric circuit in order to transmit a powerful signal with high current and high voltage through it. The first samples of krytrons were created in the USA by the firm EG&G Corporation for transmitters of military aircraft radars [13].

Fig. 7. General view of the krytron-key type KN2 «Krytron» (manufactured by EG&G Corporation, USA) [13]

Unlike most gas discharge devices, in krytrons an electric arc discharge is used to initiate a high-current spark discharge between the cathode and the anode of these gas-filled lamps. In this connection, the krytrons have four electrodes: two main or main (cathode and anode), a grid and a keep-alive electrode [13]. In the krytron, the keep-alive electrode to which a small positive-polarity voltage is applied is located next to the cathode, which has a negative electric potential. A high commutated voltage in the krytron is applied to the anode. After the appearance of an electric arc discharge between the keep-alive electrode and the cathode and the initial ionization in this local gas zone, a positive voltage pulse is applied to the control grid in its glass mesh balloon, resulting in a high-current electric spark discharge between the anode and the cathode of the krytron [13]. Electrical breakdown of the insulating gap between the anode and the cathode of the krytron and ensures fast switching of its high-current circuit with load. To facilitate the ionization of the gas of the krytron, an isotope of radioactive nickel-63 emitting β-rays

(electrons) is placed in its glass cylinder [13]. The krytrons created in the second half of the 1940s were used in industrial pyrotechnics and nuclear technology (for example, in high-current control circuits for the operation of electric nuclear detonators [13]) because of their stably high impulse responses compared to semiconductor devices. In connection with the possibility of using krytrons in electric circuits for the detonation of nuclear munitions [13, 14], very strict export restrictions have long been imposed on their export from the United States. At present, the American Company «Perkin-Elmer Components» produces gas-filled and vacuum krytron-keys [13]. The vacuum version of the krytron («sprytron») can operate under conditions of high radiation, when the semiconductor technology is working incorrectly and fails. In conclusion of this section devoted to ELs, let us dwell on such a gas-discharge device as a «xenon arc lamp» [15]. This lamp (Fig. 8) is a powerful source of artificial light, close in its spectral composition to daylight.

Fig 8. General view of a 15 kW xenon arc lamp used in a modern IMAX projector [15]

In this lamp, the electric arc brightly shines in a glass bottle filled with xenon. Its cylinder is made of heat-resistant quartz glass. The cathode and anode in such a lamp are tungsten electrodes doped with radioactive thorium to reduce the work function of electrons from them. The balloon is initially evacuated, and then xenon is fed into it. Pulsed xenon flashbulbs contain a third control electrode surrounding its glass cylinder [15].

2. The stage of development of microelectronics and the invention of a transistor. Electronic devices built on EL had such two significant drawbacks as: large weight dimensions and high levels of consumed electric power (energy) [2, 8]. These shortcomings were critical for the creation of computers, portable electronic devices, electronics for aviation and rocket and space technology. Therefore, semiconductor devices were objectively created and developed. The underlying electronics was called «*solid state electronics*» [2, 8]. Element base of this electronics at the initial stage of its occurrence began to be based on transistors and semiconductor diodes. As is known, a transistor is a semiconductor triode (Fig. 9) which is capable of controlling a significant current from its small input signal in its output circuit. This property of the transistor allowed it to be used to amplify, generate, switch and convert signals. Following the EL, the transistor became the basis for the circuitry of most electronic devices [16]. When and by whom was this device created, which made a «revolution» in electronics?

Fig. 9. General view of bipolar transistors of various designs using three electrodes on a single semiconductor crystal – the base, the control electrode – the emitter and the controlled electrode – the collector) [16, 17]

From the history of the invention of the transistor, it is known that since 1936 in the USA in the experimental development department of Bell Telephone Laboratories of a large Company American Telephone and Telegraph under the leadership of Joseph Becker, work was done to create solid-state amplifiers of electrical signals [17]. Until 1941 (before the start of World War II) it was not possible to produce a semiconductor amplifying device in Bell Labs. In 1945, after the war, under the leadership of theoretical physicist William Shockley in this laboratory, the research related to the creation of a field-effect transistor was resumed. After two years of failure, experimental physicist Walter Brattain working on December 16, 1947 with a germanium crystal unexpectedly received a steady amplification of the signal [17]. His subsequent research with theoretical physicist John Bardeen showed that they, in fact, invented a semiconductor triode, later called a «bipolar transistor.» Fig. 10 shows the external view of the investigated model of this transistor [17].

For the reader it is required to give a little explanation about the field (unipolar) and bipolar transistors. The «field effect transistor» uses a semiconductor (for example, a germanium or silicon crystal) of only one type of conductivity, having a thin channel, which is affected by the electric field of the gate electrode isolated from the channel [16]. A field-effect transistor, unlike a bipolar triode, is controlled not by current, but by the voltage applied to its gate. In the «bipolar transistor» semiconductors with both types of conductivity are used. It works by the interaction of two *p-n* junctions closely spaced on a single semiconductor crystal and is controlled by a change in the current through the base-emitter junction [16]. The output of its emitter is usually common for the control and output currents [3]. Do this so that in circuits with the use of a transistor it would be possible to gain amplification not only by voltage, but also by current. In addition, it should be pointed out that the scientific discovery of the *p-n* junction in crystalline silicon was made in 1940 by the employees of the American laboratory «Bell Labs»

Russell Ol and John Scuff [17]. These solid-state physicists have established that doping the surface of a silicon crystal with boron atoms leads to its positive *p*-conductivity, and phosphorus atoms to its negative *n*-conductivity. Thus, *p*-type silicon and *n*-type silicon were invented, which played a huge role in the development of solid-state electronics [17]. In this regard, it should be noted that in 1941, regardless of US physicists, the Ukrainian physicist V.E. Lashkaryov developed the theory of «blocking layer» and injection of charge carriers at the interface between copper and cuprous oxide [17]. The two types of conductivity found experimentally by means of a thermosonde in a copper-oxide element indicated the presence of a transition layer between them, which prevents the passage of current [17].

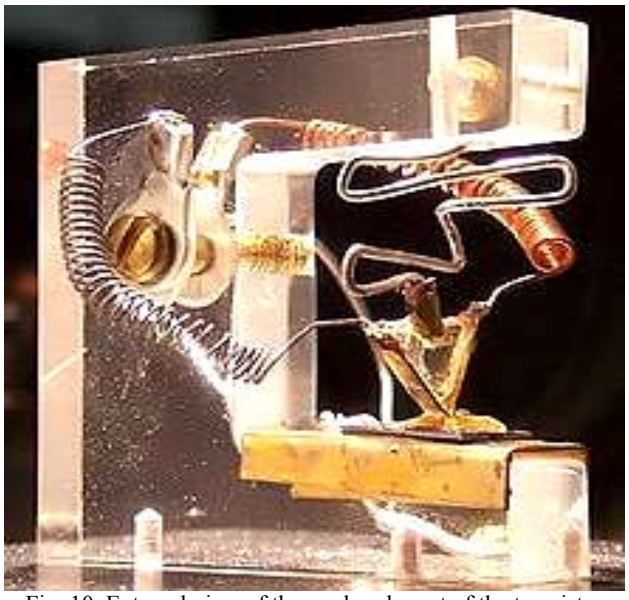

Fig. 10. External view of the modern layout of the transistor By J. Bardeen and W. Brattain (its original is not preserved) [17]

On December 23, 1947, a presentation of the existing original layout (see Fig. 10) of a new semiconductor product – a bipolar transistor to the leadership of the Bell Labs laboratory [17] was held. It is this date that is considered the birthday of the transistor. Having learned about this success of his colleagues, W. Shockley re-connects to semiconductor research and in a short time creates the theory of a bipolar transistor [17]. Fig. 11 shows the American scientists who discovered the transistor effect [17]. Note that at the end of June 1948 in the US Company where the first bipolar transistor was working the first radio transistor was manufactured [17]. However, the world sensation due to the invention in the US and the radio technical use of the transistor at that time did not take place. This was due to the fact that the first point-to-point transistors, in comparison with EL, had low output characteristics. Only in 1956 the scientific discovery of American researchers W. Brattain, J. Bardeen and W. Shockley was appreciated by the Swedish Academy of Sciences for its worth: its authors for the «*semiconductor research and discovery of the transistor effect*» were awarded the Nobel Prize in physics [4].

Fig. 11. Future Nobel Prize Laureates in Physics at the Bell Labs Laboratory (from left to right: John Bardeen, William Shockley and Walter Brattain, USA, 1948) [17]

We point out that the first point-like transistors, despite their small size and economy, were distinguished by a high noise level in useful electrical signals, low power, instability of the characteristics in time, and a strong dependence of the output parameters on temperature [17]. A point transistor, the zones of two *p-n* junctions closely spaced from each other in which a single-crystal germanium was performed on a single crystal, was sensitive to mechanical shocks and vibrations due to its nonmonolithicity. In 1951, the first flat bipolar transistor was constructed, constructively representing a monolithic germanium crystal [17]. At the same time, the first transistors on a silicon crystal appeared (Fig. 12). The output characteristics of such bipolar transistors began to compete successfully with EL parameters [17].

Fig. 12. General view of monocrystalline silicon grown in vacuum by technologists in materials science [18]

Bipolar transistors *p-n-p* (direct conductivity) and *n-p-n* (inverse conductivity) are known [19]. These transistors, in addition to the basic semiconductor material used most often in the form of a single crystal (a thin flat element from the large single crystal shown in Fig. 12), contain in their construction alloying additives (usually

boron or phosphorus) to the base semiconductor, metal leads of the *base*, *emitter* and *collector* as well as the body (metal or ceramic) with insulating parts (see Fig. 9) [17]. The main types of semiconductors in them were silicon, germanium and gallium arsenide. We will point out that in bipolar transistors the charge carriers move from the emitter through a thin base to the collector. The base is separated from the emitter and collector by *p-n* junctions. Current flows through this type of transistor only when charge carriers are injected from its emitter into the base through the corresponding *p-n* junction. In the base they are not the main charge carriers and easily penetrate through its other *p-n* junction between the base and the collector. In the base of the transistor the charge carriers move due to the diffusion mechanism. In this regard, it should be fairly thin. The current control between the emitter and the collector of the bipolar transistor is performed by changing the voltage between the base and the emitter, on which the conditions for injecting charge carriers into the base depend [17, 19].

As for the history of the creation of field-effect transistors, we note that for the first time the electrophysical idea of control (regulation) in a semiconductor triode with an isolated gate electrode by a flux of main charge carriers (electrons) was expressed by J. Lilienfeld (US Patent No. 1745175 of 28.01.1930) [20]. However, the difficulties encountered in realizing this idea in practice made it possible to create the first operating field-effect transistor only in 1960. In 1966, Carver Mead, by shunting the electrodes of such a semiconductor device with Schottky diode, substantially improved the design of the field-effect transistor [20]. Field-effect transistors are classified into devices with a gate in the form of a *p-n* junction and with an isolated gate. The last transistors have received in electronics the name of MDS-transistors («metal-dielectric-semiconductor») [20]. Sometimes, MDS-transistors are also called MOS transistors («metal-oxide-semiconductor»). In addition, field-effect transistors with an isolated gate are divided into instruments with a built-in channel and devices with an induced channel [20]. We will point out that the channel in these transistors is the region through which the flow of their main charge carriers-electrons passes. The electrodes of field-effect transistors have the following names [20]: *source* – an electrode, from which the main charge carriers enter the channel; *drain* – an electrode through which the main charge carriers leave the channel; *gate*-– an electrode that serves to regulate the cross section of the channel. The conductivity of the channel under consideration can be either of the *n*-type or of the *p*-type. In this regard, the type of channel conductivity distinguishes between field-effect transistors with an *n*-channel and a *p*-channel. In a field-effect MOS transistor containing one semiconductor crystal (substrate), the current flows from the source electrode deposited on the highly doped region of the *n*-conductivity semiconductor crystal substrate to the drain electrode deposited on the heavily doped region of the semiconductor substrate with *p*-conductivity, through a channel located under the gate electrode. The distance between heavily doped source and drain regions is of the order of one micron. The surface of the semiconductor crystal between the source and the drain is covered with a thin layer (about 0.1 μm thick) of the dielectric. For a silicon crystal, SiO_2 is used as this dielectric, grown on the surface of a silicon crystal by its high-temperature oxidation [20]. A metal gate electrode is applied to the dielectric layer between the source and the drain. The channel exists in the doped parts of the semiconductor crystal substrate in the gap between the gate and the undoped semiconductor substrate, in which there are no charge carriers. Therefore, it (the substrate) can not conduct a current. Under the shutter, there is a depletion region, in which there are also no charge carriers, due to the formation of a Schottky contact between the doped region of the semiconductor crystal and the metal gate of the Schottky contact [20]. It turns out that in this type of field-effect transistor, the width of the channel is limited by the space between the substrate and the depletion region. The voltage applied to the gate increases or decreases the width of the depletion region of the device in question and thereby adjusts (changes) the channel width of such a transistor. In this way the current passing through its channel changes in this device.

In a field-effect transistor with a control *p-n* junction, a plate-crystal made of a semiconductor (for example, with *n*-conductivity) is used, at the opposite ends of which there is an electrode-source and an electrode-drain included in the controlled circuit of the device. Between these electrodes, a control gate electrode is placed on a region of a semiconductor with a different conductivity (for example, with *p*-conductivity). The power supply included in the input circuit of the device creates on its only *p-n* junction a reverse voltage. In the input circuit of such a transistor, the source of amplified signals is also included. When the input voltage changes on the gate, the reverse voltage on the *p-n* junction also changes. In our case, this will lead to a change in the thickness and, correspondingly, the cross-sectional area of the depletion layer region in the *n*-channel field-effect transistor through which the main carriers (electrons) flow [20]. By varying the cross-sectional dimensions of this channel, a current change is achieved in the output circuit of this type of semiconductor triode.

The main advantages of semiconductor triodes over vacuum ELs are [16, 17]:

- small size and weight, contributing to the wide development of miniature electronic devices;
- low cost, caused by automation of production and technological processes;
- low voltage level, which facilitates the use of transistors in small electronic devices, powered by batteries;
- absence of additional time to warm up their electrodes after switching on the device;
- low power dissipation (energy) indicators, which contribute to improving the energy efficiency of transistors and devices in general;
- high reliability in operation and great mechanical strength to shock loads and vibrations of individual semiconductor triodes and an electronic device as a whole containing a huge number of similar semiconductor devices;

- long service life, counted by dozens of years of continuous operation as part of the device;
- possibility of combination in work with additional electronic circuits and devices.

The main disadvantages of transistors in comparison with vacuum ELs are [17, 21]:

- operating voltage for transistors using crystalline silicon does not exceed 1 kV (when switching circuits with voltages greater than 1 kV, IGBT-transistors are now used);
- use of transistors in high-power broadcasting and microwave transmitters is technically and economically impractical (using high-power generator tubes, magnetrons, klystrons and moving-wave tubes for this purpose provides a better combination of high frequencies, high power and acceptable cost);
- transistors in comparison with EL are more vulnerable to the impact of such a damaging nuclear weapon as a powerful electromagnetic pulse;
- increased sensitivity to the damaging effects of radiation and cosmic radiation.

Note that the input impedance for field-effect MDS- transistors using an isolated gate electrode can be values that vary in the range (10^{10}-10^{14}) Ω. In field-effect transistors with a control *p-n* junction, these parameters are (10^{7}-10^{9}) Ω [20]. High input impedances for field-effect transistors make it possible to use them when creating high-precision electronic devices operating at low voltage with low energy consumption (for example, electronic clocks). A hybrid type IGBT transistor, combining the properties of bipolar and field-effect transistors, can be used in high-voltage technology [8, 20].

Over time, transistors have replaced vacuum EL throughout the world in most electronic devices. These semiconductor devices radically changed all electronics of our world. They became the element base on which «*microelectronics*» arose and integrated circuits and high-speed computers were created [22]. At the beginning of the 21st century, transistors became the most massive product produced by mankind. Note that in 2013 for every inhabitant of the planet Earth electronic industry of the world was released about 15 billion transistors, most of which were part of integrated circuits [16, 17].

3. Intermediate stage of development of microelectronics and the invention of an integrated microcircuit. We point out that in April 1954 the employee of the American Company Texas Instruments Gordon Teal manufactured the first silicon bipolar transistor. Until 1957, this US Company was the only supplier of silicon transistors in the world market of microelectronics [17]. The invention by Karl Frosch in the United States of the process of «wet» (using water vapor) thermal oxidation of silicon in order to obtain a thin SiO_2 layer on a semiconductor substrate made possible the release in 1958 of the «Bell Labs» of the first silicon MES transistors. In March 1959, Jean Ernie created the first silicon planar transistor, in which the meza-technology was replaced by a more promising planar technology for manufacturing transistors. The further development of the physics and technology of semiconductors led to the fact that silicon practically displaced germanium from microelectronics, and the planar process became the main technology of manufacturing transistors in the electronics world and made it possible to create monolithic integrated circuits (ICs) [17, 23]. The IC (Fig. 13) is an electronic scheme of arbitrary complexity made on a semiconductor substrate (crystal plate or film) and placed in a non-separable plastic (ceramic) housing [21, 23].

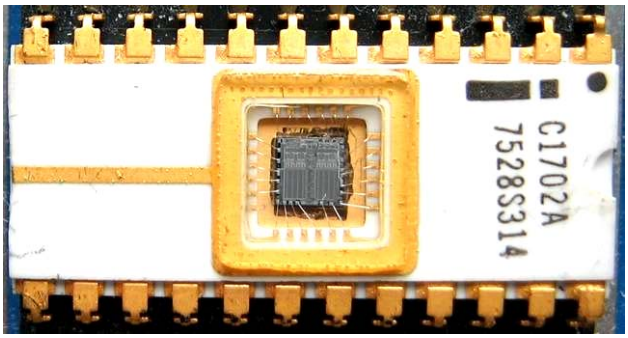

Fig. 13. External view of the IC used in space microelectronics with an increased level of radiation [21]

The vast majority of the IC in the world is manufactured in cases (see Fig. 13, 14) and is intended for their surface mounting on the boards of electronic devices. We will point out that an insignificant part of the IC, which is part of the microassemblies, is manufactured without these enclosures. Often, IC is also called a «chip» (from the English «chip» – «thin plate» [1]). British radio engineer Geoffrey Dummer on May 7, 1952 first put forward the idea of combining a set of standard electronic components in one monolithic semiconductor crystal [23]. This progressive idea for a number of years because of the insufficient level of development in the world of technologies for the production of semiconductor devices remained unrealized in practice. Only in the first half of 1959 there was a real breakthrough in the world semiconductor technology, carried out in practice by three practitioners from three private American Corporations who successfully solved three fundamental problems for the production of IC [23].

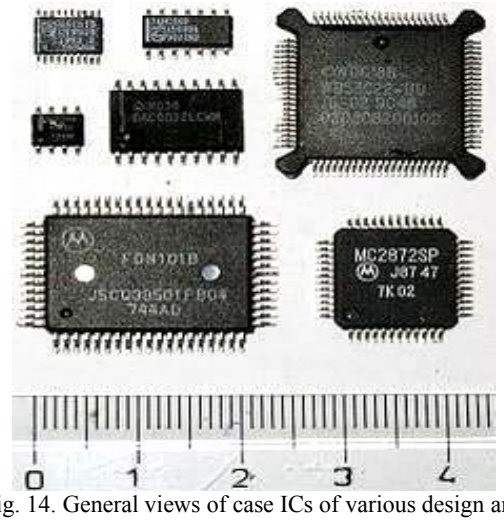

Fig. 14. General views of case ICs of various design and integration degree intended for surface mounting on electronic device boards [23]

So, American physicist and inventor Jack Kilby of Texas Instruments patented the principle of combining electronic components in IC with transistors made with layered *p-n-p* or *n-p-n* junctions (US patent was issued in 1964) [23, 24]. It should be noted that in 2000 J. Kilby (born in 1923) «*for his contribution to the discovery of the integrated circuit*» was awarded the Nobel Prize in physics [24]. Further, at this time, the American engineer Kurt Legovec of the Sprague Electric Company invented a method for electrical isolation of components formed on a single semiconductor crystal (he proposed to use *p-n* junctions as insulation) [23]. It was then that an American specialist Robert Noyce from «Fairchild Semiconductor» invented a method of electrically connecting the components of an IC (due to their metallization with aluminum) [23]. In addition, R. Noyce in those years proposed an improved version of the isolation of components of IC based on the latest planar technology by Jean Hoerni. On September 27, 1960, the group of Jay Last of Fairchild Semiconductor created the first workable IC on the ideas of R. Noyce and J. Hoerni.

Note that, depending on the degree of integration of electronic components in one semiconductor crystal (usually silicon, germanium, gallium arsenide or hafnium oxide), the following IC names are currently used [23]:

- small integrated microcircuit (MIMS), containing up to 100 electronic components;
- medium integrated circuit containing up to 1000 electronic components;
- large integrated circuit containing up to 10,000 electronic components;
- ultra-large integrated circuit containing more than 10,000 electronic components (further increase of electronic components in one chip with bringing their number to 10^9 or more does not change the name of this IC).

Let us emphasize the fact that, in fact, with the invention of IC in electronics, its new section, «microelectronics», objectively studying and manufacturing electronic components objectively appeared, whose linear geometric dimensions of the characteristic elements became a few microns or less. The technological process of manufacturing the IC as a semiconductor element base in microelectronics has been continuously improved and improved to this day [25]. This complicated and complex process includes the sequence of a number of technologies [25-27]: the production of high-purity semiconductor materials, the manufacture of miniature semiconductor elements (transistors, diodes, etc.), the quality control of their manufacture, the assembly of these electronic components and quality control of their assembly. According to the requirements of «electronic hygiene» in the working area of semiconductor wafer processing and in the operations of assembling IC crystals there should not be more than five dust particles with a size of 0.5 μm in 1 liter of air [18]. In the production of IC, the technology of doping a semiconductor crystal is used to obtain *p-n* junctions and photolithography, realized with the help of appropriate lithographic equipment. The resolution (in μm or nm) of this equipment determines the name of the specific technological process used in the manufacture of IC. Reducing the size of semiconductor structures in ICs leads to improved technical characteristics of semiconductor devices (for example, to reduce their power consumption, increase the operating frequency in their electronic circuits, increase their speed, reduce their cost, etc.) [28]. Therefore, the miniaturization of the semiconductor element base of microelectronics has become the main worldwide trend in the production of various electronic devices. Below are the main stages of development in the world of the technological process in the manufacture of IC [23]:

- stage with resolution (3-1.5) μm (1970s);
- stage with a resolution of (0.8-0.5) μm (1980s);
- stage with resolution (350-130) nm (1990's);
- stage with a resolution of (65-10) nm (2000's).

Let us note that in May 2011 Altera Company produced the world's largest IC consisting of 3.9 billion field-effect transistors [23], with the 28 nm resolution technology production process. In 2012, the smallest transistors in the IC contained a few atoms of matter. In one processor of a modern computer, they can contain more than a billion pieces. In the IC, electronic components of conventional electronics such as resistors, capacitors, inductors, diodes, transistors, insulators and conductors are used [28]. Only these components are used in the form of miniature devices made on a single semiconductor chip (Fig. 15) in the integrated version. In microelectronics, ICs are divided into digital, analog-digital and analog. Moreover, digital ICs consist of miniature transistors, and analog ICs contain miniature resistors, capacitors and inductors. Modern digital technology and the ICs used in it are mainly built on field-effect MDS-transistors performed on a single silicon crystal (chip). These transistors have become essentially a «brick» for building circuits of logic, memory and computer processors. The dimensions of modern MDS-transistors are from 90 to 8 nm [28, 29]. At present, up to several billion MDS-transistors can be located on a single semiconductor chip with an area of up to 1 cm^2 [28]. According to Moore law («*the number of transistors in the IC is doubled for every 18 months*»), a further increase in the degree of integration of transistors on a single chip is expected in the coming years [28].

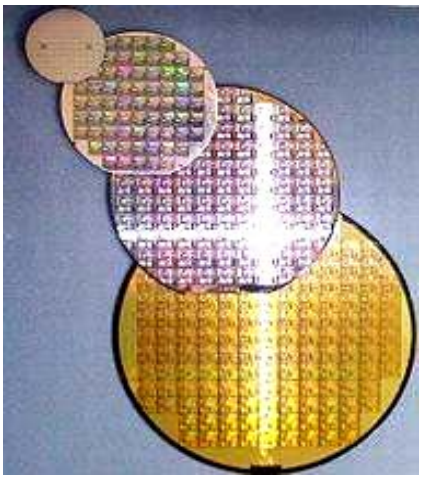

Fig. 15. Thin round silicon plates with prefabricated microcircuits before cutting them with a diamond microdisk into individual crystals of a given semiconductor [28]

4. The current stage of development of microelectronics and the invention of a highly integrated microprocessor. ICs have become the backbone of processors (from Latin «processus» – «advancement» [1]) which are the central part (the «heart») of all computers performing the information conversion programs specified by the program and managing the entire computing process in an electronic computer [28]. As is known, the «microprocessor» forms the core of the computer (Fig. 16), in which additional functions (for example, connections with its peripherals) are performed using specially designed chipsets [23]. The US Company Intel in 1971 was the first to manufacture IC (Intel 4004) which served as a microprocessor [23]. Another American Company IBM based on the advanced microprocessors 8088 and 8086 released their famous personal computers PC/XT series [23]. In the first computers, the number of chipset sets was up to hundreds of pieces. In modern computers, their number does not exceed three. Recently there has been a tendency of gradual transfer of the functions of the chipset (memory controller, etc.) to the microprocessor [23, 28].

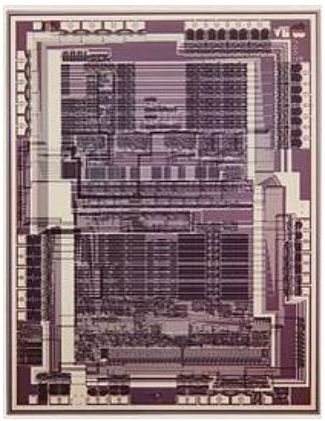

Fig. 16. External view of the internal filling of the modern microprocessor Apple of the US Company of the same name [18]

In this regard, the microprocessor with built-in operational and program memory devices, memory controllers, input-output devices and other additional functions is also called a «microcontroller» [28]. The main feature of the microcontroller is the possibility of programming the logic of its operation. The placement of a whole microprocessor on a single chip of an extremely large degree of integration (Fig. 17) containing hundreds of millions of electronic components led to a significant decrease in its cost [30]. The creation at the end of the 20th century of highly integrated microprocessors on a single crystal determined their wide application in personal computers.

At present microelectronics uses microprocessor systems, which are functionally complete products consisting of one or several microprocessors (microcontrollers, Fig. 18) [30]. In modern electronic devices, massively multi-core processors are also used which are CPUs that contain two or more processing cores on a single processor semiconductor (silicon) crystal [30]. In such a processor, several of its cores are integrated into one ultra-large integrated circuit. The concept of a «multi-core electronic device» can also be used to describe the operation of multi-core systems (for example, Intel MIC [30]).

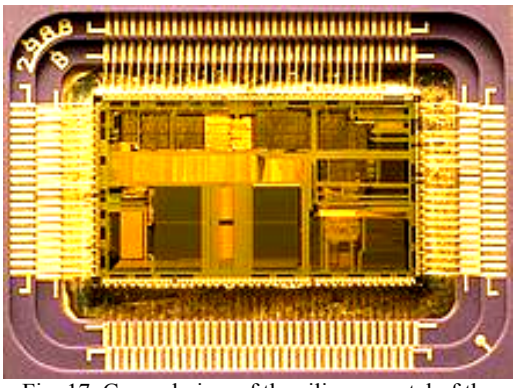

Fig. 17. General view of the silicon crystal of the microprocessor 80486DX2 in the case for a personal computer [30]

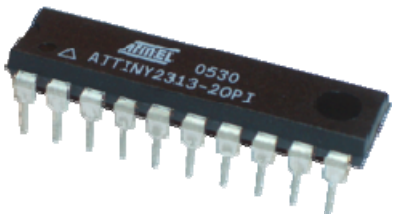

Fig. 18. External view of the modern microcontroller Attiny2313-20PI of the American Company Atmel [30]

The microcontroller (from the English «controller» [1]) is essentially an IC (see Fig. 18), designed to control the operation of various electronic devices. It is, by and large, a single-chip microcomputer. The first US patent for a microcomputer or microcontroller was issued in 1971 to employees of the American Company Texas Instruments, engineers M. Kochren and G. Boone [30]. They were the first to suggest not only a microprocessor on a single semiconductor chip but also a memory with digital I/O devices. In 1976, the American Company Intel released the microcontroller i8048. In 1980, this electronic Company created a microcontroller i8051, on the silicon chip of which placed 128 thousand field-effect transistors were placed. A successful set of peripherals, the ability to flexibly select external and internal program memory and an affordable price have ensured this microcontroller success in the electronics market. To date, there are more than 200 modifications of microcontrollers compatible with i8051, produced by two dozen companies in the world [30].

The continuous increase in the complexity of microprocessors has led the world of electronics to the fact that now one or more microprocessors are used as computational elements in all electronic devices, starting from a mobile phone and ending with mainframes and supercomputers [30]. The achievements of mankind in the exploration of outer space since the late 1960s are due to the use of computer equipment on board space vehicles. Thus, in the US NASA space program associated with the first landing of a man on the Moon (July 20, 1969 [31]), all on-board calculations for guidance, navigation and control on the Apollo 11 spacecraft were provided to small specialized microprocessors on a crystal of silicon

of its on-board computer [30]. These electronic devices were designed and manufactured by the new «young» American Company Fairchild Semiconductor settled in the promising technological area of the United States. At the same time, another US company, Texas Instruments, developed and manufactured germanium ICs for Minuteman-2 intercontinental ballistic missiles [32].

4.1. The «Silicon Valley» of the United States and a technological breakthrough in microelectronics. The northern part of the state of California (near San Francisco) which currently holds about half of the US scientific and technical potential in the field of electronics and computer technology was named «Silicon Valley» [32]. It is the numerous electronic firms of the USA (Fig. 19) formed on the territory of the Silicon Valley, and made a decisive contribution to the beginning of the rapid development of world microelectronics in the 20th century. It was with them that the process of widespread use of ICs in military equipment and civilian technology began [32].

Fig. 19. General view of the buildings of some Companies that are part of the largest technology center in the US [32]

The emergence and active development of this high-tech center of the United States involves the concentration in this area (with the unofficial capital of San Jose) of leading American Universities, cities at a distance of less than an hour from each other, major sources of financing for new companies, and a Mediterranean-type climate . It is commonly believed [32] that the founders of the Silicon Valley were American scientists like William Shockley (Fig. 20) and Frederick Terman (Fig. 21).

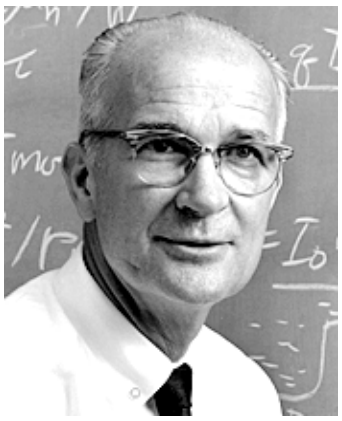
Fig. 20. One of the founding fathers of the Silicon Valley in the US State of California, Professor of Physics William Shockley [32]

It was in this region of the USA that, since the 1960s, the active use of silicon began with the world's most advanced production of semiconductor devices (transistors and ICs). Here in 1956, one of the co-authors of the discovery of the transistor effect, physicist W. Shockley, moved and founded his Company Shockley Semiconductor Laboratory in Mountain View which is developing a new technology for the use of silicon in the production of transistors [32]. Germanium by this time has proved to be an expensive semiconductor material in the production and not resistant to elevated temperatures.


Fig. 21. One of the founding fathers of the Silicon Valley in the US State of California, Stanford University Electrical Engineering Professor Frederick Terman [32]

The authoritarian style of the leadership of W. Shockley and his enthusiasm for his own development of a 4-layer semiconductor diode led to the fact that his eight most talented physicists and specialists (the «Traitorous Eight») left his Company and soon on the funds of his sponsor Sherman Fairchild created a new electronic Company, «Fairchild Semiconductor» [32]. For W. Shockley and his business, this event had a deplorable effect: soon the unprofitable Company «Shockley Semiconductor Laboratory» ceased to exist, and its leader was forced to leave for teaching as a Professor at the nearby Stanford University of the United States. It is important to note that W. Shockley, as the discoverer of the transistor effect, and the author of the most important work on the theory of semiconductors at the end of his life, considered his contribution to genetics as his main scientific achievement, paradoxically [32].

Fairchild Semiconductor Company, led by Robert Noyce, adhered to a new progressive socio-technical ideology: «*Inventions in technology can change the world*». Each of her employees thought about their personal contribution to the progress of microelectronics. This company has a new corporate culture in the development and production of semiconductor devices, which includes a democratic leadership style and strict labor discipline. Fairchild Semiconductor was a successful US commercial project in the field of microelectronics. It became the world leader in the field of creation of transistors and ICs based on silicon crystals. It was this company that laid the foundation for a number of new electronic companies in the Silicon Valley. So,

two of the indicated «Eight» (Gordon Moore and Robert Noyce), having left the electronic Company Fairchild Semiconductor have created a new Company Intel which is engaged in the first stage with magnetic storage devices. Then at Intel followed R. Noyce's invention of the silicon IC and the creation on its basis of the first chip microprocessor (1971) which in the future will became the fundamental basis of all electronic devices of our time [32]. By 1980, the avalanche division of electronic companies in the Silicon Valley led to the creation of a California high-tech park (cluster) comprising 65 companies engaged in the development and production of computers and their components, especially microprocessors, as well as software, mobile devices and biotechnologies. As of 2006, Silicon Valley has become the third technology center in the United States (after New York and Washington) in the area of high technology. About 386,000 highly qualified specialists worked at this center at the indicated time, with an average annual income of about USD 80,000 [32]. Joint efforts of the Companies of the Silicon Valley in the 20th-21st centuries have made a real technological breakthrough in the field of microelectronics.

4.2. Nearest prospects, main trends and problems in the development of world microelectronics. Now in the world of electronics began to develop research on the development and creation of new vacuum micro devices on the basis of IC with field emission [33]. These new semiconductor devices have ultrahigh speed, high radiation resistance, low sensitivity to ambient temperature and high efficiency. This electronics was called «*vacuum microelectronics*», based on vacuum integrated circuits.

4.2.1. Vacuum microelectronics. It is believed that the functionality of vacuum IC will be significantly different from the capabilities of existing ICs. Vacuum microelectronics becomes one of the most important directions in the development of microwave electronics used in radar complexes, telecommunication devices and information processing systems [33]. This is due to the fact that traditional semiconductor technology is no longer able to provide highly reliable transmission, reception, storage and processing in real time of very large volumes of information in conditions of extreme environmental influences. For this reason, in the last decades in all the leading countries of the world intensive work has been carried out related to the study of the fundamental problems of vacuum microelectronics.

4.2.2. Vacuum nanoelectronics. In recent years, experts are increasingly focusing on electronics, which uses autoemission properties of carbon nanotubes (CNT). This new section in electronics was called «*vacuum nanoelectronics*» [33]. The main efforts in this field of electronics are now directed at the development and creation of flat screens of displays and TVs based on CNT. In 2005, Motorola Company announced the creation of a prototype display based on CNT. In 2006, Samsung Corporation demonstrated its prototype display on the basis of CNT, whose panel had a thickness of 30 mm [33]. It should be noted that in its development this corporation successfully cooperates with the American Company Carbon Nanotechnologies Inc., which supplies it with the specified nanotubes. Apparently, it is not «far off» the creation of flat panel TVs based on new technology in electronics. According to [33], the problem of the appearance in the everyday life of people of a display spatially and energetically interfaced with the IC is best solved by creating a flat cathodoluminescent screen with an auto-electronic nanostructured cathode. Therefore, we can say that vacuum microelectronics and vacuum nanoelectronics allow creating fundamentally new microwave vacuum lamps, as well as essentially new and highly efficient flat cathodoluminescent displays [33].

4.2.3. New trends in the creation of IC. In recent decades, the technology of fabricating high-mobility electron transistors (HMETs), which are widely used in microwave communication and radio observation devices, has been rapidly developing. On the basis of the HMET, both hybrid and monolithic microwave integrated circuits are created. At the heart of the HMET operation is the control of their conductive channel by means of a two-dimensional electron gas, the region of which is created under the contact of the gate electrode of the field-effect transistor due to the use of a heterojunction and a very thin dielectric spacer layer [20]. For the practical implementation of ultra-large integrated circuits, ultra-miniature field microtransistors are being created. They are manufactured using nanotechnology with a geometric resolution of equipment less than 100 nm. In such semiconductor devices, the thickness of the gate dielectric of the transistor reaches several atomic layers. Thanks to this, in modern microprocessors of the American Corporation Intel the number of electronic components ranges from tens of millions to two billion pieces [20].

4.2.4. Space microelectronics. To microelectronics intended for use in space and military purposes, there are increased requirements for [21]: reliability of IC (both semiconductor and shell), resistance to instantaneous gamma and neutron radiation, resistance to a powerful electromagnetic pulse of a nuclear explosion, stability to vibrations and mechanical overloads, resistance to high humidity and medium temperature (–40 °C to +125 °C). The biggest problem of space microelectronics is the protection of on-board electronic devices from the damaging effect of heavy space charged particles on them, which have a high energy, sufficient to «break through» their IC through with the formation of a powerful «train» of electric charges [21]. Fig. 22 shows a modern ultra-large integrated circuit for use on artificial satellites and spacecraft.

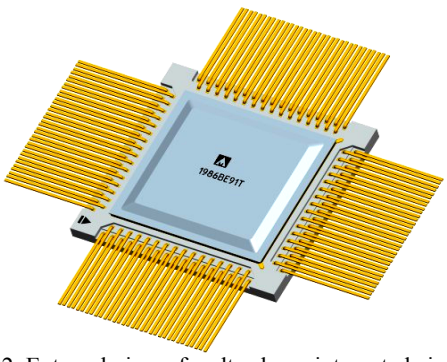

Fig. 22. External view of a ultra-large integrated circuit in cermet body intended for use in space [21]

In addition, it should be noted that around our planet there are two powerful belts of charged particles (the so-called Van Allen radiation belts) [21]: one at an altitude of about 4000 km, consisting of protons, and the other at an altitude of about 17,000 km with an electron flux. The level of cosmic radiation at altitudes (300-500) km above the Earth, where satellites and spacecraft usually fly, such that the annual dose of radiation there reaches 100 rad = = 1 J/kg = 1 Gray [34]. At altitudes of more than 1000 km, the annual dose of radiation can be 10,000 rads or more [21]. For conventional commercial IMS, the «lethal» dose of radiation is about 5000 rad. Therefore, in a few months of flight in such space conditions, conventional ICs will gain their «deadly» dose of radiation and fail. In this connection, for special spacecraft missions in high orbits (≥ 1000 km) and in outer space, special radiation-resistant ICs are needed for their electronic devices [21].

4.2.5. Optoelectronics. At the beginning of the 21st century, the evolution of solid-state electronics in the direction of miniaturization of electronic components gradually stopped and is now practically stopped [2]. This stop was predetermined by the attainment in this kind of electronics of the minimum possible sizes of semiconductor transistors, conductors and other components on a semiconductor crystal capable of removing (dissipating) the heat released to them when electric charges (current) flow through them and not be destroyed. These geometric dimensions in microchips reached units of nanometers, which led to the name of technology for their production - nanotechnology [18]. In this connection, it is possible that in the near future the next stage in the evolution of the world electronics will be «*optoelectronics*» in which a quantum quasiparticle without a rest mass appears as a photon, a much more mobile and less inertial in its physical nature, a representative of the microworld than a free electron («a hole») in a semiconductor crystal of solid-state electronics.

4.2.6. Cybersecurity. A world-class problem in microelectronics is the provision of cybersecurity of computer systems for both private and public Companies and individual computers. In recent years, cyberattacks of hackers around the world have acquired a massive and systemic character. Simple and reliable protective measures and solutions from such attacks in the field of cybersecurity currently do not exist.

Conclusions.

1. The completed scientific and technical review of development for the period of the 20th and 21st centuries of world electronics testifies to the enormous technological breakthrough of mankind in this very complex field of knowledge aimed at serving society. Electronics is on the «threshold» of new discoveries.

2. Electronics has penetrated almost all spheres of human activity. The technosphere of earthlings simply was not conceivable without electronic devices (for example, computers, microprocessors, etc.). The objective process of the development of our civilization has led to the complete dependence of man on electronics and on its scientific and technical achievements. Electronics brought people many benefits and amenities. But along with this, in the monopoly of electronics for mankind lies a hidden threat. Intentional or accidental inadvertent simultaneous failure of the main and back-up electronic devices of control systems at critical technical facilities (for example, nuclear power plants, nuclear facilities and military centers for strategic missile control) can lead to disastrous consequences for large regions of the developed countries of the world.

3. The problem of cybersecurity of electronic devices and computer systems for military and civil purposes is acquiring particular urgency and significance. The development and widespread adoption of effective measures and means to combat cyber-attacks (cyber-terrorism) in electronic practice should always be given the increased attention of the relevant services and specialists.

REFERENCES

1. *Bol'shoj illjustrirovannyj slovar' inostrannyh slov* [Large illustrated dictionary of foreign words]. Moscow, Russkie slovari Publ., 2004. 957 p. (Rus).

2. Available at: https://en.wikipedia.org/wiki/Electronics (accessed 11 June 2012).

3. Baranov M.I. *Izbrannye voprosy elektrofiziki: Monografija v 2-h tomah. Tom 1: Elektrofizika i vydajushhiesja fiziki mira* [Selected topics electrophysics: Monographs in 2 vols. Vol.1: Electrophysics and outstanding physics of the world]. Kharkov, NTU «KhPI» Publ., 2008. 252 p. (Rus).

4. Khramov Yu.A. *Istoriia fiziki* [History of Physics]. Kiev, Feniks Publ., 2006. 1176 p. (Rus).

5. Available at: https://en.wikipedia.org/wiki/Vacuum_tube (accessed 22 May 2013).

6. Available at: http://dic.academic.ru/dic.nsf/ruwiki/1114547 (accessed 10 April 2013). (Rus).

7. Available at: https://wiki.rock63.ru/Радиолампа (accessed 25 September 2014). (Rus).

8. Available at: http://dic.academic.ru/dic.nsf/enc_tech/1440/Электроника (accessed 16 June 2015). (Rus).

9. Available at: http://www.petrofflab.ru/p/blog-page_12.html (accessed 25 January 2014). (Rus).

10. Available at: https://en.wikipedia.org/wiki/Thyratron (accessed 06 August 2014).

11. Available at: https://en.wikipedia.org/wiki/Trigatron (accessed 10 May 2015).

12. Dashuk P.N., Zayents S.L., Komel'kov V.S., Kuchinskiy G.S., Nikolaevskaya N.N., Shkuropat P.I., Shneerson G.A. *Tehnika bol'shih impul'snyh tokov i magnitnyh polej* [Technique large pulsed currents and magnetic fields]. Moscow, Atomizdat Publ., 1970. 472 p. (Rus).

13. Available at: https://en.wikipedia.org/wiki/Krytron (accessed 20 April 2014).

14. Baranov M.I. An anthology of the distinguished achievements in science and technique. Part 40: The scientific opening of the method of explosive implosion for the obtaining above critical mass of nuclear charge and Ukrainian «track» in the «Manhattan» American atomic project. *Electrical engineering & electromechanics*, 2017, no.5, pp. 3-13. **doi: 10.20998/2074-272X.2017.5.01.**

15. Available at: https://en.wikipedia.org/wiki/Xenon_arc_lamp (accessed 21 February 2014).

16. Available at: https://en.wikipedia.org/wiki/Transistor (accessed 12 March 2013).

17. Available at: https://en.wikipedia.org/wiki/History_of_the_transistor (accessed 28 June 2013).

18. Available at: https://en.wikipedia.org/wiki/Semiconductor_device_fabrication (accessed 16 October 2013).
19. Ovsyannikov N.I. *Kremnievye bipoljarnye tranzistory. Spravochnoe posobie* [Silicon bipolar transistors]. Minsk, Higher School Publ., 1989. 302 p. (Rus).
20. Available at: https://en.wikipedia.org/wiki/Field-effect_transistor (accessed 19 July 2013).
21. Available at: https://cont.ws/@nikkuro/514968 (accessed 08 December 2012).
22. Ephimov I.E., Kozyr' I.J., Gorbunov Yu.I. *Mikroelektronika* [Microelectronics]. Moscow, Higher School Publ., 1987. 416 p. (Rus).
23. Available at: https://en.wikipedia.org/wiki/Integrated_circuit (accessed 22 May 2014).
24. Baranov M.I. *Antologija vydajushhihsja dostizhenij v nauke i tehnike: Monografija v 3-h tomah. Tom 3* [An anthology of the distinguished achievements in science and technique: Monograph in 3 volumes. Volume 3]. Kharkiv, PhPB Panov A.N. Publ., 2016. 415 p. (Rus).
25. Chernyaev V.N. *Tehnologija proizvodstva integral'nyh mikroshem i mikroprocessorov* [The technology of production of integrated microcircuits and microprocessors]. Moscow, Radio and Communication Publ., 1987. 464 p. (Rus).
26. Gotra Z.Yu. *Spravochnik po tehnologii mikroelektronnyh ustrojstv* [Handbook of microelectronic devices technology]. Lviv, Kamenyar Publ., 1986. 287 p. (Rus).
27. Ber A.Yu., Minsker F.E. *Sborka poluprovodnikovyh priborov i integral'nyh mikroshem* [The assembly of semiconductor devices and integrated microcircuits]. Moscow, Higher School Publ., 1986. 279 p. (Rus).
28. Available at: https://en.wikipedia.org/wiki/Microelectronics (accessed 11 May 2014).
29. Rabay J., Chandrakasan A., Nikolic B. *Cifrovye integral'nye shemy. Metodologija proektirovanija* [Digital integrated circuits. Methodology of designing]. Moscow, Willyams Publ., 2007. 912 p. (Rus).
30. Available at: https://en.wikipedia.org/wiki/Microprocessor (accessed 18 October 2013).
31. Baranov M.I. *Antologiia vydaiushchikhsia dostizhenii v nauke i tekhnike: Monografiia v 2-kh tomakh. Tom 2.* [An anthology of outstanding achievements in science and technology: Monographs in 2 vols. Vol.2]. Kharkov, NTMT Publ., 2013. 333 p. (Rus).
32. Available at: https://en.wikipedia.org/wiki/Silicon_Valley (accessed 20 May 2014).
33. Available at: http://www.pandia.ru/text/78/325/3338.php (accessed 10 October 2012). (Rus).
34. Kuhling H. *Spravochnik po fizike. Per. s nem*. [Dictonary on Physics. Translated from German]. Moscow, Mir Publ., 1982. 520 p. (Rus).

Received 31.05.2017

M.I. Baranov, Doctor of Technical Science, Chief Researcher,
Scientific-&-Research Planning-&-Design Institute «Molniya»
National Technical University «Kharkiv Polytechnic Institute»,
47, Shevchenko Str., Kharkiv, 61013, Ukraine,
phone +380 57 7076841,
e-mail: baranovmi@kpi.kharkov.ua

How to cite this article:
Baranov M.I. An anthology of the distinguished achievements in science and technique. Part 42: Electronics: retrospective view, successes and prospects of its development. *Electrical engineering & electromechanics*, 2018, no.1, pp. 3-16. **doi: 10.20998/2074-272X.2018.1.01.**

UDC 621.319 **doi: 10.20998/2074-272X.2018.1.02**

G.V. Bezprozvannych, A.V. Roginskiy

DIELECTRIC SPECTROSCOPY OF CASING THERMOSETTING COMPOSITE ELECTRICAL INSULATION SYSTEM OF INDUCTION TRACTION ELECTRIC MACHINES

Introduction. Thermosetting composite electric insulation of traction electric motors undergoes significant heating, moisture, overvoltage, vibration. Purpose. The substantiation of the possibility of using dielectric spectroscopy for monitoring the state of the hull thermosetting composite electric insulating system of induction traction motors (ITM) at the technological stage of manufacturing.. Methodology. In the induction traction motors in which the phases of the stator winding are connected to a «star» and do not have a zero point output, in the case of a two-electrode connection of one of the phases and the housing, the combined characteristics of the capacitance and the dielectric loss tangent of the three-phase hull insulation system are measured. Practical value. It is established that at the second resonant frequency near 10 kHz, the tangent of the dielectric loss is the most sensitive to the state of the composite ITM insulation. Dielectric spectroscopy at alternating voltage of the combined dielectric characteristics makes it possible to evaluate the state of the hull thermosetting electrical insulating system at the final stage of manufacturing of induction traction motors. References 9, tables 1, figures 4.

Key words: **thermosetting composite insulation, induction traction motor, dielectric spectroscopy, replacement circuit, electrical capacitance, dielectric loss tangent, resonance frequency.**

Представлено схему замещения обмоток статора при соединении «звездой» асинхронного тягового двигателя. На основании результатов моделирования частотных зависимостей емкости и тангенса угла диэлектрических потерь установлено наличие двух резонансных частот в диапазоне 1 и 10 кГц. Показано, что измерения тангенса угла диэлектрических потерь изоляционной системы на частоте 10 кГц чувствительны к уровню диэлектрических потерь в корпусной термореактивной электрической изоляции. Результаты математического моделирования согласуются с измерениями совокупных диэлектрических характеристик корпусной композитной электроизоляционной системы трех фаз. Библ. 9, табл. 1, рис. 4.

Ключевые слова: **термореактивная композитная изоляция, асинхронный тяговый двигатель, диэлектрическая спектроскопия, схема замещения, электрическая емкость, тангенс угла диэлектрических потерь, резонансная частота.**

Introduction. Difficult operating conditions for DC and AC traction high-voltage machines present increased requirements for electrical insulation. Thus, thermosetting composite electric insulation of traction electric motors (TEM) undergoes significant heating, moisture, overvoltage, vibration. The insulation must have sufficient electrical and mechanical strength, be heated and moisture resistant. Modern electrical insulating materials and technologies for their manufacture have made it possible to improve the systems of high-voltage thermosetting composite electric insulation of motors, improve their operational and energy characteristics [1]. The use of insulation of the heat resistance class H (180 °C) improves the reliability of the TEM, allows for the same size to realize a greater power. Such isolation systems are capable of operating at least 50,000 hours at temperature of 180 °C and withstanding overvoltages above 10 kV.

For electric insulation with a high content of mica and epoxy resin, the TEM winding is used both as a vacuum-injection impregnation technology and pre-impregnated tapes. The vacuum-injection impregnation procedure guarantees high mechanical strength, especially the frontal part of the winding and high electrical strength. During the process of impregnating the insulation system, the viscosity of the resin is measured; temperature of impregnation and curing; holding time under pressure; reduced and excess pressure.

Problem definition. At all stages of manufacturing TEM: before impregnating the armature and coils, after heat treatment (baking) of the armature and coils, in the finished motor – the insulation resistance and electrical strength are checked [2, 3]. Insulation of rods (coils) of machines with power of more than 5 MW and voltage greater than 6 kV for the control of manufacturing technology is subjected to an additional test [4]: measurement of the dielectric loss tangent tgδ of insulation, depending on the applied test voltage at normal air temperature. Measurement of the tangent of the dielectric loss angle of insulation is performed by the Schering bridge at frequency of 50 Hz. Such tests allow us to indirectly judge the presence of air inclusions caused by the stratification of thermosetting insulation as a result of its incomplete polymerization. Measurements at only one frequency of 50 Hz do not allow to fully reveal the residual moisture and stratification of the thermosetting composite insulation system of TEM. High operational reliability of traction electric motors is determined by the quality of insulation of windings, which must have a high moisture resistance.

In the last decade, **dielectric spectroscopy** has gained considerable theoretical and experimental development. In dielectric spectroscopy, an analysis is made of the function of the complex permeability ε^* of insulation by the frequency and voltage range [5-7]:

$$\varepsilon^* = \varepsilon' - i\varepsilon'' = \varepsilon - i\sigma / \omega\varepsilon_0 ,$$

where ε' is the real part of the complex dielectric permeability (relative permeability ε) which determines the electrical capacity of the insulation; ε'' is the imaginary part that determines the energy loss in

insulation: $\varepsilon'' = \sigma / \omega\varepsilon_o$; σ is the specific volume conductivity of the insulation material, S/m; ω is the circular frequency of the applied current, rad/s; $\varepsilon_0 = 8.85 \cdot 10^{-12}$ F/m is the electrical constant.

The tangent of the dielectric loss angle determines the losses for electrical conductivity and polarization

$$tg\delta = \frac{\varepsilon''}{\varepsilon'}.$$

The frequency dependence of the capacitance and tangent of the dielectric loss angle allows one to judge the state of the thermosetting insulation system of TEM.

The goal of the paper is substantiation of the possibility of using dielectric spectroscopy for monitoring the state of the hull thermosetting composite electric insulating system of induction traction motors at the technological stage of manufacturing.

The method of aggregate measurements of the dielectric parameters of a thermosetting insulating system. In induction traction motors (ITM) in which the phases of the stator winding are connected to a «star» and do not have a zero point output (a blind connection of the phases of the winding), to measure the capacitance and tangent of the phase loss dielectric loss, it is advisable to use two-electrode connection of two phases to the measuring circuit. This is a method of aggregate measurements without shorting the rest of the phases that are not involved in the measurements. For this, it is necessary to perform *three measurements* (indices *a*, *b*, *c* in (1)) based on the results of which, based on the solution of the system of linear algebraic equations for capacitances and the tangent of the dielectric loss angle (1), the dielectric parameters of the windings insulation of each phase (indices 1, 2, 3 in (1)) connected in a «star» [8]

$$\left.\begin{array}{l} \frac{1}{C_1}+\frac{1}{C_2}=\frac{1}{C_a} \\ \frac{1}{C_1}+\frac{1}{C_3}=\frac{1}{C_b} \\ \frac{1}{C_2}+\frac{1}{C_3}=\frac{1}{C_c} \end{array}\right| \begin{array}{l} tg\delta_1\frac{C_2}{C_1+C_2}+tg\delta_2\frac{C_1}{C_1+C_2}=tg\delta_a \\ tg\delta_1\frac{C_3}{C_1+C_3}+tg\delta_3\frac{C_1}{C_1+C_3}=tg\delta_b \\ tg\delta_2\frac{C_3}{C_2+C_3}+tg\delta_3\frac{C_2}{C_2+C_3}=tg\delta_c \end{array}\Bigg\}. \quad (1)$$

Aggregate dielectric characteristics of the hull thermosetting insulation system of ITM. In the case of a two-electrode connection of one of the phases and the housing, the combined characteristics of the capacitance C and the dielectric loss tangent tgδ of the three-phase hull insulation system are measured. Fig. 1 shows the circuit for replacing the stator windings of ITM [9]. The windings are connected according to the «star» circuit. Zero point *O* is not available for measurements. The diagram denotes: *R*1, *L*1, *R*2, *L*2 are the ohmic resistance and inductance of the windings of each phase; *C*3, *R*3 are the capacitance of each phase relative to the body (the capacity of the housing insulation system) and the equivalent resistance of each phase. Resistor *R*3, connected in parallel, reflects the insulation leakage resistance (when measured at a constant voltage) or the equivalent dielectric loss resistance (when measured at alternating voltage). The simplified two-element circuit of substitution of the housing insulation does not reflect the relaxation processes in the insulation associated with the accumulation of space charges.

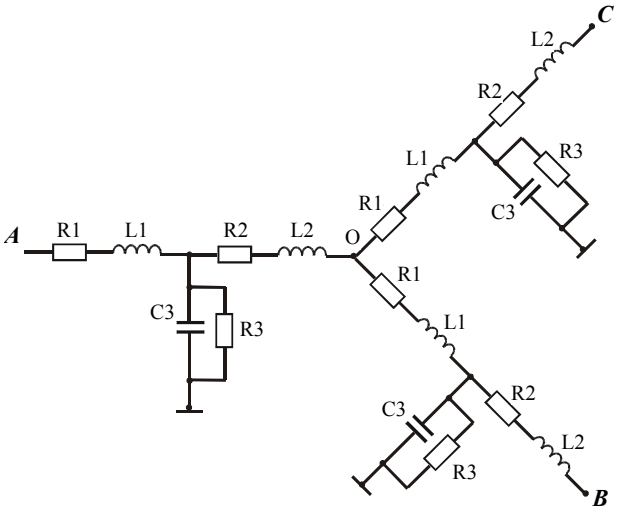

Fig. 1. Circuit of replacement of stator windings of ITM

The complex resistance of phase A is defined as

$$\underline{Z_A} = R_1 + j\omega L_1 + \left[\frac{R_3(-j\frac{1}{\omega C_3})}{R_3 - j\frac{1}{\omega C_3}}\right] \| \left[R_2 + j\omega L_2 + \frac{R_1}{2} + \frac{j\omega L_1}{2} + \frac{\frac{R_3}{2}(-j\frac{1}{\omega 2C_3})}{\frac{R_3}{2} - j\frac{1}{\omega 2C_3}}\right], \quad (2)$$

where by || the parallel connection of fragments of the substitution circuit is indicated.

Assuming the same ohmic resistance and inductance of the half windings of each of the phases $R1 = R2 = R_L$, $L1 = L2 = L$, one can define the complex resistance $\underline{Z_L}$ and conductivity $\underline{Y_C}$ of the half winding

$$\underline{Z}_L = \frac{1}{2}\left(\frac{R_L}{2} + \frac{jw\,L}{2}\right), \underline{Z}_c = r - \frac{j}{w \cdot C}, \ \underline{Y}_c = \frac{1}{\underline{Z}_c}.$$

Complex impedance Z_{LC} (complex conductivity Y_{LC}) of the second half of the winding and two halves of other two windings

$$\underline{Z}_{LC} = \underline{Z}_L + \frac{\underline{Z}_L + \underline{Z}_C}{2}, \ \underline{Y}_{LC} = \frac{1}{\underline{Z}_{LC}}, \underline{Z} = \underline{Z}_L + \underline{Z}_{CLC} \cdot$$

$$\underline{Y}_{CLC} = \underline{Y}_C + \underline{Y}_{LC}, \ \underline{Z}_{CLC} = \frac{1}{\underline{Y}_{CLC}}, \underline{Z} = \underline{Z}_L + \underline{Z}_{CLC} \cdot$$

Then the required total dielectric characteristics of the insulation system of the windings relative to the body are determined on the basis of (3)

$$R_e = \text{real}(\underline{Z}), Ce = -\frac{w}{\text{imag}(\underline{Z})}, \text{tg}\delta_e = R_e \cdot C_e \cdot w. \quad (3)$$

Model frequency dependences of the combined dielectric characteristics of the hull insulation system. Fig. 2, 3 show the frequency dependences of the capacitance and tangent of the dielectric loss angle of the hull insulation system of the ITM windings, constructed on the basis of (2), (3). In the frequency range from 1 to

10 kHz, the windings have two resonant frequencies. The first one is in the 4.2 kHz region; the second one is near the frequency of 10 kHz. Measurements near 10 kHz are very sensitive to the level of dielectric losses in the insulation (Fig. 3). At measuring tgδ of actually *insulation* from 0.074 = 7.4 % to 0.012 = 1.2 % (i.e. almost 6 times – see Fig. 4, frequency 10 kHz), the result of measuring the parameter tgδ_{10kHz} of the entire winding changes tens – hundreds of times (Fig. 3).

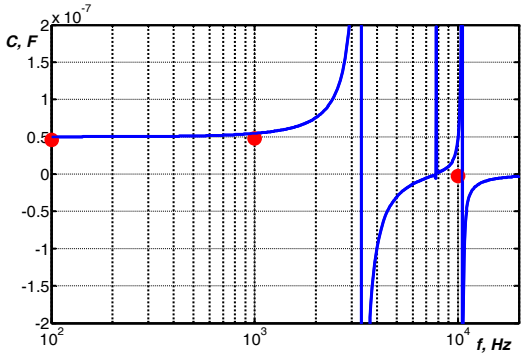

Fig. 2. Dependence on the frequency of the effective capacitance of the windings relative to the housing (capacity of the housing insulation system): points – experimental data; solid line – calculation according to the substitution circuit in Fig. 1

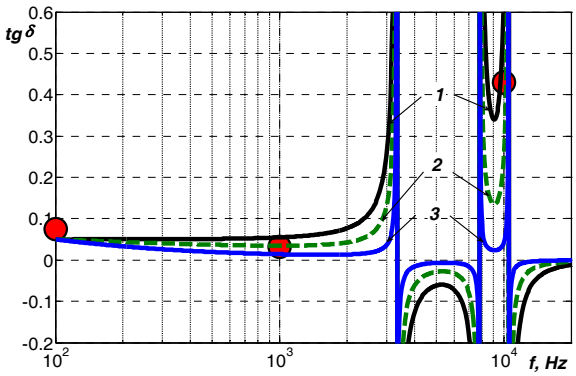

Fig. 3. Dependence on the frequency of the tangent of the dielectric loss angle of the hull insulation system: points – experimental data; solid lines – calculation by the substitution circuit in Fig. 1

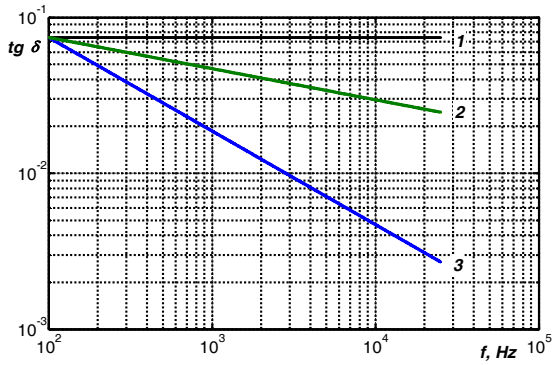

Fig. 4. Dependences on the frequency of the tangent of the dielectric loss angle of the hull thermosetting insulation adopted in calculating the frequency dependences of C and tgδ of the winding insulation system

In Fig. 3 curves 1-3 are constructed under the assumption: curve 1 – with a constant value of tgδ of thermosetting composite insulation; 2 and 3 – with the power law of change of the tangent of the dielectric loss angle of insulation: 2 – at tgδ = tg$\delta_0(f_0/f)^{0.2}$; 3 – at tgδ = tg$\delta_0(f_0/f)^{0.4}$, where the indices «0» correspond to the value at the frequency of 100 Hz.

Table 1 shows the results of measurements of the total dielectric characteristics of the hull insulation system of the ITM windings. The measurements are performed at three frequencies: 100 Hz, 1 kHz and 10 kHz. The first two frequencies turned out to be lower, and the third one was higher than its own resonant frequency (Table 1). Hence, the resonance frequency of the windings (the first resonance frequency) is in the range 1-10 kHz. When measuring at frequencies above resonance, the *aggregate* parameters of both the main and *parasitic* circuits are measured. Thus, when monitoring the capacitance and tangent of the dielectric loss angle tgδ of the hull insulation system at frequency of 10 kHz (above resonant), the readings of the immittance meter become negative: C = –2.8639 nF < 0. This means that the complex resistance of the «three phase-housing» insulation gap at this frequency is no longer capacitive, but inductive.

Table 1

Aggregate dielectric parameters of the induction motor hull system

Induction motor :	Frequencies of measurement, kHz					
	0.1		1		10	
	C, nF	tgδ, %	C, nF	tgδ, %	C, nF	tgδ, %
- voltage 1.875 kV; - power 1200 kW. Insulation class H	45.639	7.435	47.473	3.151	–2.8639	43.016

Conclusions. The results of modeling the frequency dependences of the aggregate dielectric characteristics on the basis of the stator winding replacement circuit for the «star» connection of an asynchronous traction motor indicate the presence of two resonant frequencies in the 1 and 10 kHz range. At frequency of 10 kHz, the tangent of the dielectric loss angle of the entire insulation system of the windings changes by a factor of tens – hundreds which makes it possible to monitor the state of the composite insulation at this frequency. The presence of residual moisture in the body insulation leads to an increase in tgδ of the body thermosetting composite system with decreasing frequency.

Dielectric spectroscopy of aggregate dielectric characteristics at alternating voltage allows to evaluate the state of the body thermosetting electrical insulating system at the final stage of manufacturing of induction traction motors.

REFERENCES

1. Yatsko S.I., Karpenko V.V., Vasilenko D.Yu. Investigations of the stability of isolation systems of traction electric machines to the effect of climatic factors. *Transactions of Kremenchuk Mykhaylo Ostrogradskiy State University*, 2010, iss.4/2010(63), part 1, pp. 134-140. (Rus).

2. IEC 60349-1 Ed. 2.0 b: 2010. Electric traction – Rotating electrical machines for rail and road vehicles – Part 1: Machines other than electronic converter-fed alternating current motors. 2010. 129 p.

3. IEC 60034-18-1:2010. Rotating electrical machines – Part 18-1: Functional evaluation of insulation systems – General guidelines. 2010. 33 p.
4. IEC 60060-1:2010 High-voltage test techniques – Part 1: General definitions and test requirements. 2010. 149 p.
5. Gavrila D.E. Dielectric Spectroscopy, a Modern Method for Microstructural Characterization of Materials. *Journal of Materials Science and Engineering*, 2014, A4, no.1, pp. 18-26.
6. Koch F. Transforming dielectric response measurements from time to frequency domain. *Nordic Insulation Symposium on Materials, Components and Diagnostics (NordIS)*. Session 4, June 15-17, 2009. Gothenburg, Sweden.
7. Bezprozvannych G.V., Kessaev A.G , Shcherba M.A. Frequency dependence of dielectric loss tangent on the degree of humidification of polyethylene cable insulation. *Technical Electrodynamics*, 2016, no.3, pp. 18-24. (Rus).
8. Bezprozvannych G.V, Naboka B.G. Influence of parasitic capacitance on the results of measurements of parameters of multicore cables in assessing their technical condition. *Electricity*, 2011, no.5, pp. 27-36. (Rus).
9. Bezprozvannych G.V., Naboka B.G. *Matematicheskie modeli i metody rascheta elektroizoliatsionnykh konstruktsii* [Mathematical models and methods of calculation of electrical designs]. Kharkiv, NTU «KhPI» Publ., 2012. 108 p. (Rus).

Received 16.12.2017

G.V. Bezprozvannych[1]*, Doctor of Technical Science, Professor,*
A.V. Roginskiy[2]*, Postgraduate Student,*
[1] National Technical University «Kharkiv Polytechnic Institute»,
2, Kyrpychova Str., Kharkiv, 61002, Ukraine,
phone +380 57 7076010,
e-mail: bezprozvannych@kpi.kharkov.ua
[2] SE Plant Electrotyazhmash,
299, Moskovsky Ave., Kharkiv, 61089, Ukraine,
phone +380 50 5158552 49,
e-mail: roginskiy.av@gmail.com

How to cite this article:
Bezprozvannych G.V., Roginskiy A.V. Dielectric spectroscopy of casing thermosetting composite electrical insulation system of induction traction electric machines. *Electrical engineering & electromechanics*, 2018, no.1, pp. 17-20. **doi: 10.20998/2074-272X.2018.1.02.**

UDC 621.313:536.2.24:539.2 **doi: 10.20998/2074-272X.2018.1.03**

V.F. Bolyukh, A.I. Kocherga, I.S. Schukin

INVESTIGATION OF A LINEAR PULSE-INDUCTION ELECTROMECHANICAL CONVERTER WITH DIFFERENT INDUCTOR POWER SUPPLY CIRCUITS

Purpose. ***The goal of the paper is to investigate the influence of the power circuits of the linear pulse-induction electromechanical converters (LPIEC), which form the current pulse of excitation of the inductor from the capacitive energy storage (CES), to its electromechanical parameters.*** ***Methodology.*** ***A circuit mathematical model of LPIEC was developed, on the basis of which recurrence relations were obtained for calculating the interrelated electromagnetic, mechanical, and thermal parameters of the LPIEC. This model makes it possible to calculate the LPIEC parameters for various power circuits, the inductor of which is excited by the CES.*** ***Results.*** ***It is established that electromechanical LPEC parameters with power circuit forming an aperiodic current excitation pulse of an inductor are better than in LPIEC with excitation of an inductor by an unipolar current pulse, but worse than in LPIEC with excitation of an inductor by a vibrationally damped current pulse. In this converter, during operation, the inductor is heated most, and the armature is heated least. It is established that in LPIEC with power circuit that forms an aperiodic current pulse of excitation of an inductor with the connection of an additional CES, all electromechanical parameters are higher in comparison with the LPIEC with a power circuit that forms a vibrationally damped current excitation pulse of the inductor. However, in this LPIEC the excess of the temperatures of the active elements increases, especially strongly in the inductor, and the efficiency of the converter decreases.*** ***Originality.*** ***For the first time, the LPIEC has been investigated using the power circuit that forms an aperiodic current pulse of excitation of an inductor with the connection of an additional CES. It is established that in this LPIEC all electromechanical parameters are higher than for LPIEC with power circuits forming an unipolar or oscillating-damped current excitation pulse of the inductor.*** ***Practical value.*** ***In the LPIEC with power circuit that forms an aperiodic current pulse of excitation of the inductor with the connection of an additional CES, the electromechanical LPIEC parameters increase. This increases the temperature rise of the inductor, and the temperature rise of the armature decreases. The effectiveness of this LPIEC is also reduced.*** References 12, figures 7.

Key words: **linear pulse-induction electromechanical converters, circuit mathematical model, recurrence relations, inductor feed circuits, capacitive energy storage, chain mathematical model, current excitation pulse of inductor.**

На основе разработанной цепной математической модели получены рекуррентные соотношения для расчета взаимосвязанных электромагнитных, механических и тепловых параметров линейного импульсно-индукционного электромеханического преобразователя (ЛИИЭП). ***Показано, что электромеханические показатели ЛИИЭП со схемой питания индуктора, формирующей апериодический токовый импульс возбуждения, лучше, чем у ЛИИЭП с возбуждением индуктора однополярным токовым импульсом, но хуже, чем у ЛИИЭП с возбуждением индуктора колебательно-затухающим токовым импульсом. В данном преобразователе в процессе работы наиболее сильно нагревается индуктор и наименее нагревается якорь. Показано, что в ЛИИЭП со схемой питания индуктора, формирующей апериодический токовый импульс возбуждения с подключением добавочного емкостного накопителя энергии, все электромеханические показатели выше по сравнению с ЛИИЭП со схемой питания индуктора, формирующей колебательно-затухающий токовый импульс возбуждения. Однако в этом ЛИИЭП возрастают превышения температур активных элементов, особенно сильно – индуктора и снижается КПД.*** Библ. 12, рис. 7.

Ключевые слова: **линейный импульсно-индукционный электромеханический преобразователь, цепная математическая модель, рекуррентные соотношения, схемы питания индуктора, емкостной накопитель энергии, токовый импульс возбуждения индуктора.**

Introduction. Linear electric motors of the traditional type (synchronous, induction and direct current) do not allow to provide significant accelerations and impact loads with limited specific indicators. This led to the appearance of special linear pulse electromechanical converters which provide a high speed of the actuator element (AE) on a short active site, and/or create powerful force pulses with a small displacement of it [1-4]. Such converters are used in many branches of science and technology as electromechanical accelerators and shock-power devices [5-7]. They are characterized by [8]:

- pulsating, reciprocating, cyclic or one-time operation mode;
- intermittent nature of the energy conversion due to the presence of a back stroke, and often a long pause during the working cycle;
- long duration of energy storage from a capacitive energy storage (CES) in relation to the duration of the working period;
- intensive electromagnetic loads, significantly exceeding those of traditional linear electric motors.

The most widely used linear pulse-induction electromechanical converters (LPIEC) are coaxial configurations, in which the accelerated arm interacts non-contact with a stationary inductor [1, 2, 9]. When the inductor is excited from the CES, eddy currents are induced in the electrically conducting armature. As a result of this, electrodynamic forces (EDF) act on the armature, causing its axial displacement (Fig. 1,*a*).

However, when operating in a dynamic mode with a rapid change in electromagnetic, mechanical and thermal parameters, the efficiency of the LPIEC is not high enough, which requires new approaches to improve its electromechanical performance. One way to increase these indicators is to generate the necessary current pulses of the inductor due to the power circuits that are located between the CES and the inductor. However, to date, no specific studies have been conducted to determine the

influence of various inductor power circuits on the electromechanical performance of the LPIEC.

The goal of the paper is investigation of the influence of various inductor power circuits forming its current pulses on the electromechanical parameters of the LPIEC.

Mathematical model. We consider the mathematical circuit model of LPIEC which uses the lumped parameters of the inductor and armature (Fig. 1,*b*).

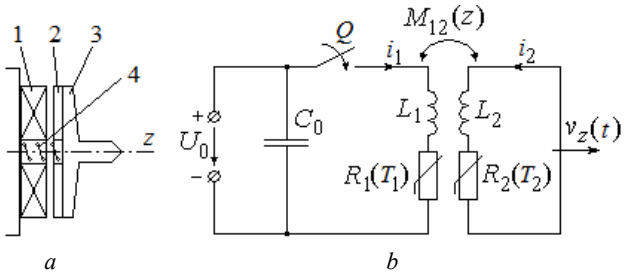

Fig. 1. Design (*a*) and electric (*b*) LPIEC circuits with a free CES discharge on the inductor:
1 – inductor; 2 – armature; 3 – AE; 4 – return spring

In the presented in Fig. 1,*b* electrical circuit after the closure of the key *Q*, a free discharge of the CES occurs to the inductor. Electrical processes in LPIEC can be described by a system of equations [9]:

$$R_1(T_1)i_1 + L_1\frac{di_1}{dt} + \frac{1}{C_0}\int_0^t i_1 dt + M_{12}(z)\frac{di_2}{dt} + $$

$$+ v_z(t)i_2\frac{dM_{12}}{dz} = 0, \quad \frac{1}{C_0}\int_0^t i_1 dt = U_0, \qquad (1)$$

$$R_2(T_2)\cdot i_2 + L_2\frac{di_2}{dt} + M_{21}(z)\frac{di_1}{dt} + i_1 v(t)\frac{dM_{12}}{dz} = 0, \quad (2)$$

where n = 1, 2 are the indexes of inductor and armature, respectively; R_n, L_n, T_n, i_n are the active resistance, inductance, temperature and current of the n-th element, respectively; C_0 is the capacity of CES charged on the voltage U_0; $M_{12}(z)$ is the mutual inductance between inductor and armature moving along the z-axis with speed v_z.

We denote

$$R_1 = R_1(T_1); R_2 = R_2(T_2); M_{12} = M_{12}(z); \; v_z = v_z(t).$$

The system of equations (1,) (2) after a series of transformations is reduced to the equation:

$$a_3\frac{d^3 i_1}{dt^3} + a_2\frac{d^2 i_1}{dt^2} + a_1\frac{di_1}{dt} + a_0 i_1 = 0, \qquad (3)$$

where

$$a_3 = \upsilon; \; a_2 = \chi - 2Mv_z\frac{dM_{12}}{dz}; \; a_1 = R_1R_2 + \frac{L_2}{C_0} - v_z^2\left(\frac{dM_{12}}{dz}\right)^2;$$

$$a_0 = \frac{R_2}{C_0}; \; \upsilon = L_1L_2 - M_{12}^2; \; \chi = R_1L_2 + L_1R_2.$$

The characteristic equation of the differential equation (3) is represented in the canonical form

$$x^3 + r_* x^2 + s_* x + t_* = 0, \qquad (4)$$

where $r_* = a_2/a_3$; $s_* = a_1/a_3$; $t_* = a_0/a_3$.

Using the substitution $y = x + r_*/3$, equation (4) is reduced to the form

$$y^3 + p_* y + q_* = 0, \qquad (5)$$

where $p_* = s_* - r_*^2/3$; $q_* = 2(r_*/3)^3 - r_* s_*/3 + t_*$.

The roots of equation (5) are found using the Cardano formula:

$$y_1 = u_* + v_*; \quad y_2 = \varepsilon_1 u_* + \varepsilon_2 v_*; \quad y_3 = \varepsilon_2 u_* + \varepsilon_1 v_*, \quad (6)$$

where $u_* = \sqrt[3]{D^{0.5} - 0.5q_*}$; $v_* = \sqrt[3]{-D^{0.5} - 0.5q_*}$; $\varepsilon_{1,2} = 0.5\left(-1 \pm j\sqrt{3}\right)$; $D = (p_*/3)^3 + (q_*/2)^2$ is the discriminant of equation (5).

If D<0, then the cubic equation (5) has three real roots:

$$y_p = 2\sqrt[6]{-p_*^3/27}\cos\left[\frac{1}{3}\arccos\left(-\frac{q_*}{2\sqrt{-p_*^3/27}}\right) + \frac{2}{3}\pi(p-1)\right], \quad (7)$$

where p = 1, 2, 3.

The solution of the system of equations (1), (2) is found in the form:

$$i_1(t) = A_{11}\exp(x_1 t) + A_{12}\exp(x_2 t) + A_{13}\exp(x_3 t) - $$

$$- v_z\frac{i_2}{R_1}\frac{dM_{12}}{dz}; \qquad (8)$$

$$i_2(t) = A_{21}\exp(x_1 t) + A_{22}\exp(x_2 t) + A_{23}\exp(x_3 t) -$$

$$- v_z\frac{i_1}{R_2}\frac{dM_{12}}{dz}, \qquad (9)$$

where A_{11},…, A_{23} are the constant determined at the moment of time t_k.

After finding the constants A_{11}, …, A_{23}, the expressions for the currents of the inductor and the armature are represented in a recurrent form:

$$i_n(t_{k+1}) = \delta^{-1}\left\{\left[i_n(t_k) - \frac{i_m(t_k)v_z^2}{R_1R_2}\left(\frac{dM_{12}}{dz}\right)^2\right]\times\right.$$

$$\times(\alpha_1\beta_2\beta_3 + \alpha_2\beta_1\beta_3 + \alpha_3\beta_1\beta_2) + \left(\Omega_n - \frac{v_z\Omega_m}{R_n}\frac{dM_{12}}{dz}\right)[\alpha_1(\beta_2+\beta_3) +$$

$$\left. + \alpha_2(\beta_1+\beta_3) + \alpha_3(\beta_1+\beta_2)] + \left(\Lambda_n - \frac{v_z\Lambda_m}{R_n}\frac{dM_{12}}{dz}\right)(\alpha_1+\alpha_2+\alpha_3)\right\}\times$$

$$\times\left[1 - \frac{v_z^2}{R_1R_2}\left(\frac{dM_{12}}{dz}\right)^2\right]^{-1}, \qquad (10)$$

where n = 1, 2 at m = 2, 1;

$$\delta = \beta_1\beta_2(\beta_2 - \beta_1) + \beta_1\beta_3(\beta_1 - \beta_3) + \beta_2\beta_3(\beta_3 - \beta_2);$$

$$\alpha_1 = (\beta_3 - \beta_2)\exp(\beta_1\Delta t); \; \alpha_2 = (\beta_1 - \beta_3)\exp(\beta_2\Delta t);$$

$$\alpha_3 = (\beta_2 - \beta_1)\exp(\beta_3\Delta t);$$

$$\beta_p = \left\{2\left(a_2^2 - 3a_1a_3\right)^{0.5}\cos[2\pi(p-1)/3 + \varsigma] - a_2\right\}/3a_3;$$

$$p = 1, 2, 3;$$

$$\varsigma = \arccos\left[\left(a_2^2 - 3a_1a_3\right)^{-1.5}\left(4.5a_1a_2a_3 - a_2^3 - 13.5a_0a_3^2\right)\right];$$

$$\Omega_n = B_n + \frac{B_m v_z}{R_n}\frac{dM_{12}}{dz}; \; \Lambda_n = E_n + \frac{E_m v_z}{R_n}\frac{dM_{12}}{dz};$$

$$\gamma_1 = L_2; \; \gamma_2 = -M_{12};$$

$$B_n = \upsilon^{-1}\left[i_n(t_k)\left(M_{12} v_z \frac{dM_{12}}{dz} - R_n L_m \right) + i_m(t_k) \times \right.$$
$$\left. \times \left(R_m M - L_m v_z \frac{dM_{12}}{dz} \right) - \gamma_k u_c(t_k) \right];$$

$$E_1 = \upsilon^{-2}\left\{ i_1(t_k)\left[R_1\left(R_2 M_{12}^2 + R_1 L_2^2 - C^{-1} L_2 \upsilon\right) - v_z M_{12} \frac{dM_{12}}{dz}(\chi + 2R_1 L_2) + \right.\right.$$
$$\left. + v_z^2\left(L_1 L_2 + M_{12}^2\right)\left(\frac{dM_{12}}{dz}\right)^2 \right] + i_2(t_k)\left[v_z\left(L_2\chi + 2R_2 M_{12}^2\right)\frac{dM_{12}}{dz} - M_{12} R_2 \chi - \right.$$
$$\left.\left. - V^2 M_{12} L_2 \left(\frac{dM_{12}}{dz}\right)^2 \right] + u_c(t_k)\left(R_2 M_{12}^2 + L_2^2 R_1 - 2L_2 V M_{12} \frac{dM_{12}}{dz} \right) \right\};$$

$$E_2 = \upsilon^{-2}\left\{ i_1(t_k)\left[M_{12}\left(C^{-1}\upsilon - R_1\chi\right) + v_z\left(2R_1 M_{12}^2 + L_1\chi\right)\frac{dM_{12}}{dz} - 2v_z^2 L_1 M_{12} \times \right.\right.$$
$$\left. \times \left(\frac{dM_{12}}{dz}\right)^2 \right] + i_2(t_k)\left[R_2\left(R_1 M_{12}^2 + R_2 L_1^2\right) - M_{12} v_z (2L_1 R_2 + \chi)\frac{dM_{12}}{dz} + \left(L_1 L_2 + \right.\right.$$
$$\left.\left. + M_{12}^2\right) v_z^2 \left(\frac{dM_{12}}{dz}\right)^2 \right] + u_c(t_k)\left[v_z\left(L_1 L_2 + M_{12}^2\right)\frac{dM_{12}}{dz} - M_{12}\chi \right] \Bigg\},$$

where $u_c(t_k)$ is the CES voltage at the moment of time t_k.

If the discriminant $D<0$ of the characteristic equation (5), then one of its roots is real $x_1 = d$, and the other two are complex conjugate $x_{2,3} = f \pm jg$. The solution of the system of equations (1), (2) is found in the form:

$$i_1(t) = B_{11}\exp(dt) + \exp(ft)\left[B_{12}\cos(gt) + B_{13}\sin(gt)\right] - v_z \frac{i_2}{R_1}\frac{dM_{12}}{dz}; \quad (11)$$

$$i_2(t) = B_{21}\exp(dt) + \exp(ft)\left[B_{22}\cos(gt) + B_{23}\sin(gt)\right] - v_z \frac{i_1}{R_2}\frac{dM_{12}}{dz}; \quad (12)$$

where B_{11}, …, B_{23} are the constant determined at the moment of time t_k.

In the final form, the currents of the inductor and the armature can be represented in the form of recurrence relations:

$$i_n(t_{k+1}) = \left(\xi_n - \frac{\xi_m v_z}{R_n}\frac{dM_{12}}{dz} \right) \Bigg/ \left[1 - \frac{v_z^2}{R_1 R_2}\left(\frac{dM_{12}}{dz}\right)^2 \right], \quad (13)$$

where

$$\xi_n = g^{-1}\left[g^2 + (f-d)^2\right]^{-1}\Big\langle g\cdot\exp(d\Delta t)\left[\left(g^2 + f^2\right)\Theta_n - 2f\Omega_n + \Lambda_n\right] +$$
$$+ \exp(f\Delta t)\{\sin(g\Delta t)d\left(f^2 - g^2 - fd\right)\Theta_n + \left(g^2 + d^2 - f^2\right)\Omega_n +$$
$$+ (f-d)\Lambda_n\right] + g\cdot\cos(g\Delta t)\left[d(d-2f)\Theta_n + 2f\Omega_n - \Lambda_n\right]\}\Big\rangle;$$

$$\Theta_n = i_n(t_k) + \frac{v_z i_m(t_k)}{R_n}\frac{dM_{12}}{dz}.$$

Mechanical processes in the LPIEC can be described by equation:

$$i_1(t) i_2(t)\frac{dM}{dz} = (m_a + m_2)\frac{dv_z}{dt} + K_P \Delta z(t) + K_T v_z(t) + 0.125\pi\gamma_a\beta_a D_{2m}^2 v_z^2(t), \quad (14)$$

where m_2, m_a are the mass of the armature and AE, respectively; K_P is the coefficient of elasticity of the return spring; $\Delta z(t)$ is the displacement of the armature with AE; K_T is the coefficient of the dynamic friction; γ_a is the density of the medium; β_a is the coefficient of aerodynamic resistance; D_{2m} is the AE outer diameter.

The efficiency of the axial force action on the armature will be estimated by the value of the EDF impulse:

$$F_z = \int f_z(z,t)dt, \quad (15)$$

where $f_z(z, t)$ is the instantaneous value of axial EDF acting on the armature.

On the basis of equation (14), the value of the displacement of the armature with AE can be represented as a recurrence relation:

$$\Delta z(t_{k+1}) = \Delta z(t_k) + v_z(t_k)\Delta t + \vartheta\cdot\Delta t^2 / (m_a + m_2), \quad (16)$$

where $v_z(t_{k+1}) = v_z(t_k) + \vartheta\cdot\Delta t/(m_a + m_2)$ is the speed of the armature with AE along the z-axis;

$$\vartheta = i_1(t_k) i_2(t_k)\frac{dM}{dz}(z) - K_P\Delta z(t_k) - K_T v_z(t_k) - 0.125\pi\gamma_a\beta_a D_{2m}^2 v_z^2(t_k).$$

Thermal processes. In the absence of moving the armature which occurs either before the start of the direct stroke or after the return stroke, there is thermal contact between the active elements through the insulating gasket. The temperatures of the n-th active elements of the LPIEC can be described here by the recurrence relation [10]:

$$T_n(t_{k+1}) = T_n(t_k)\xi + (1-\xi)\left[\pi^{-1} i_n(t_k) R_n(T_n)\left(D_{en}^2 - D_{in}^2\right)^{-1} + \right.$$
$$\left. + 0.25\pi T_0 D_{en} H_n \alpha_{Tn} + T_m(t_k)\lambda_a(T) d_a^{-1}\right]\left\{0.25\pi\alpha_{Tn} D_{en} H_n + \right. \quad (17)$$
$$\left. + \lambda_a(T) d_a^{-1}\right\}^{-1},$$

where $\xi = \exp\left\{ -\frac{\Delta t}{c_n(T_n)\gamma_n}\left(0{,}25 D_{en}\alpha_{Tn} + \frac{\lambda_a(T)}{d_a H_n} \right) \right\}$;

$\lambda_a(T)$ is the thermal conductivity of the insulation gasket; d_a is the gasket thickness; D_{en}, D_{in} are the outer and inner diameters of active elements, respectively; α_{Tn} is the heat transfer coefficient of the n-th active element; c_n is the heat capacity of the n-th active element.

The temperatures of the n-th active elements when moving the armature and the absence of thermal contact between the armature and the inductor can be described by the recurrence relation:

$$T_n(t_{k+1}) = T_n(t_k)\chi + (1-\chi)\left[T_0 + 4\pi^{-2} i_n(t_k) R_n(T_n)\alpha_{Tn}^{-1} \times \right.$$
$$\left. \times D_{en}^{-1} H_n^{-1}\left(D_{en}^2 - D_{in}^2\right)^{-1}\right], \quad (18)$$

where $\chi = \exp\left\{ -0.25\Delta t D_{en}\alpha_{Tn} c_n^{-1}(T_n)\gamma_n^{-1} \right\}$.

Initial conditions for the system of equations (1)–(18): $T_n(0)=T_0$ is the temperature of the n-th active element; $i_n(0)=0$ is the current of the n-th active element; $\Delta z(0)= \Delta z_0$ is the initial axial distance between armature and inductor winding; $u_c(0)=U_0$ is the CES voltage; $v_z(0)=0$ is the armature speed along the z-axis.

The LPIEC efficiency will be estimated by the relation:

$$\eta = 100\frac{(m_2 + m_e)v_z^2 + K_P\Delta z^2}{C_0 U_0^2}\ \%. \quad (19)$$

The main parameters of the LPIEC. Let us consider the LPIEC of a coaxial configuration in which the armature is made in the form of a flat disc one side of

which faces the inductor, and the other interacts with the AE. Main parameters of LPIEC:

Inductor: outer diameter D_{ex1}=100 mm, inner diameter D_{in1}=10 mm, height H_1=10 mm, section of copper bus $a \times b$ = 1.8×4.8 mm^2, the number of turns of the bus N = 46. The inductor is made in the form of a double-layer winding with external electrical terminals.

Armature: outer diameter D_{ex2}=100 mm, inner diameter D_{in2}=6 mm, height H_2=2.5 mm. Armature is made of technical copper.

CES: capacitance C_0 = 1 mF, voltage U_0 = 1 kV.

The initial distance between the inductor and the armature is Δz_0 = 1 mm. Coefficient of elasticity of the return spring K_P = 25 kN/m. Weight of the AE m_e = 0.25 kg.

We suppose that in the circuits of the LPIEC inductor power supply, the resistance of the diodes and the thyristor in the forward direction is negligible, and in the opposite direction their conductivity is just as low.

Power supply circuit of the LPIEC inductor forming an unipolar current excitation pulse. The simplest is the power supply circuit of the inductor of the LPIEC which forms an unipolar current excitation pulse in which only the starting thyristor *VS* is used (Fig. 2).

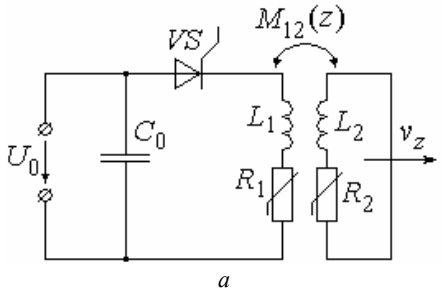

a

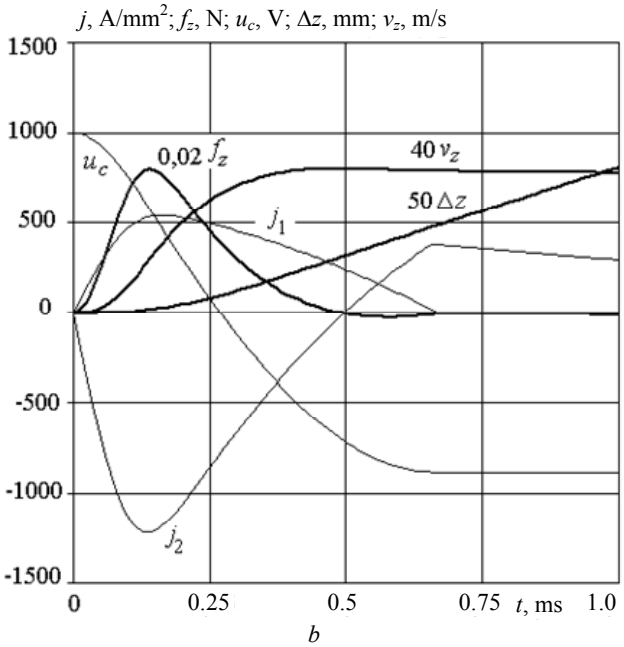

b

Fig. 2. The electric circuit of the LPIEC forming an unipolar current pulse of the inductor, (*a*) and the electromechanical characteristics of this LPIEC (*b*)

The current pulse in the inductor has a relatively short duration of the leading edge and a longer duration of the trailing edge. This form of the current pulse of the inductor is due to the induction effect of the armature current, which shifts the maximum to the beginning of the excitation process. Note that in the absence of the armature, the inductor current pulse is close in half-sine wave. The maximum values of armature current and inductor due to magnetic coupling occur almost at the same instant of time. The induced current in the armature changes the polarity after 0.5 ms, which causes the appearance of minor brake EDF which act until the current pulse in the inductor passes. The maximum values of current density are: in the inductor j_{1m} = 538.7 A/mm^2, in the armature j_{2m} = 1218.5 A/mm^2. At the instant of the maximum of the current densities, a maximum of the EDF arises, reaching the value f_{zm} = 39.8 kN. The LPIEC considered creates a force impulse F_z = 7.6 Ns, under which the armature, together with the AE, reaches a speed v_z = 17.9 m/s. At the end of the operating cycle, the inductor temperature rise is θ_1 = 0.5 °C, and the temperature rise of the armature is θ_2 = 2 °C. The efficiency of this LPIEC is η = 16.66 %.

The power supply circuit of the LPIEC inductor which forms a vibrationally damped current excitation pulse. The power supply circuit of the LIIEP inductor which forms a vibrationally damped current excitation pulse is realized by shunting the starting thyristor *VS* with a reverse diode VD_1 (Fig. 3).

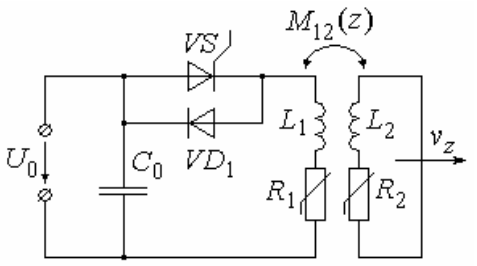

a

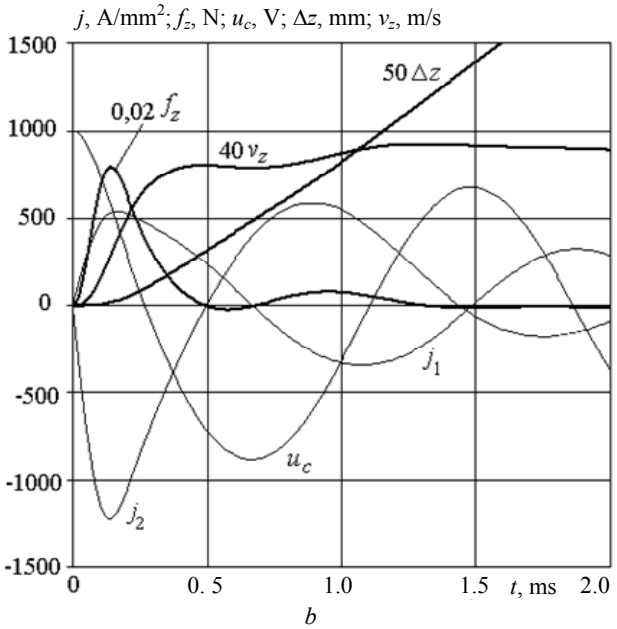

b

Fig. 3. The electric circuit of the LPIEC which forms the oscillating-damped current pulse of the inductor, (*a*) and electromechanical characteristics of this LPIEC (*b*)

The excitation of the LPIEC inductor by a vibrationally-suppressed current pulse leads to a significant change in its electromechanical characteristics. Because of the non-synchronous change in the polarities of the inductor currents and the armature between them, there are both EDF of repulsion, moving the armature with the AE along the *z*-axis, and the EDF of the attraction, which retard the armature. We can note the presence of the main (up to 0.5 ms) and additional (in the interval 0.7-1.3 ms) EDF of repulsion. The additional EDF of repulsion is much less than the main forces, primarily because of the weakened magnetic coupling between the inductor and the armature removed from it.

In the power supply circuit of the LPIEC inductor which forms a vibrational-damped current excitation pulse, an increased EDF impulse F_z = 9.46 Ns acts on the armature, so that together with AE it reaches the speed v_z = 22.3 m/s. At the end of the operating cycle, the inductor temperature rise is θ_1 = 1 ºC, and the temperature rise of the armature θ_2 = 2.4 °C. The efficiency of this LPIEC is increased to the value η = 24.88 %.

However, in the inductor supply circuits that form an unipolar and oscillating-damped excitation current pulses, the voltage of the CES u_c changes its polarity which requires the use of special nonpolar capacitors.

Power supply circuit of the LPIEC inductor forming an aperiodic current excitation pulse. The power supply circuit of the LPIEC inductor which forms an aperiodic current excitation pulse is realized by shunting the inductor with an inverse diode VD_0. This circuit allows the use of electrolytic capacitors with increased specific energy parameters (Fig. 4).

Until the voltage on the CES becomes zero, the currents in the inductor and armature are described by the relations (10) and (13). In the following, currents are described by a system of equations [11]:

$$R_n(T_n)i_n(t) + L_n\frac{di_n}{dt} + M_{nm}(z)\frac{di_m}{dt} + i_m(t)v_z(t)\frac{dM_{nm}}{dz} = 0 \,, \quad (20)$$

where m = 1, 2 at n = 2, 1.

After a number of transformations, this system is reduced to the equation:

$$\left(1-K_{12}^2\right)\frac{d^2i_1}{dt^2} + \left(\gamma_1+\gamma_2-2\xi_1\chi_2\right)\frac{di_1}{dt} + \left(\gamma_1\gamma_2-\chi_1\chi_2\right)i_1 = 0 \,, \quad (21)$$

where

$$\gamma_n = \frac{R_n}{L_n};\ \xi_n = \frac{M_{nm}(z)}{L_n};\ \chi_n = \frac{v_z(t)}{L_n}\frac{dM_{nm}}{dz};\ K_{12} = \frac{M_{nm}(z)}{(L_nL_m)^{0,5}}.$$

The characteristic equation of the differential equation (21) has two real roots

$$x_{1,2} = \frac{1}{1-K_{12}^2}\left\langle \xi_1\chi_2 - 0.5\cdot\left(\gamma_1+\gamma_2\right) \pm \left\{\left[0.5\left(\gamma_1+\gamma_2\right)-\xi_1\chi_2\right]^2 + \left(K_{12}^2-1\right)\left(\gamma_1\gamma_2-\chi_1\chi_2\right)\right\}^{0.5}\right\rangle. \quad (22)$$

Expressions for currents in the final form are described by recurrence relations:

$$i_n(t_{k+1}) = \frac{1}{x_1-x_2}\left\{i_n(t_k)\left[x_1\exp\left(x_2\Delta t\right)-x_2\exp\left(x_1\Delta t\right)\right] + \frac{\exp\left(x_1\Delta t\right)-\exp\left(x_2\Delta t\right)}{1-K_{12}^2}\left[i_n(t_k)\left(\xi_n\chi_m-\gamma_n\right)+i_m(t_k)\left(\gamma_m\xi_n-\chi_n\right)\right]\right\}. \quad (23)$$

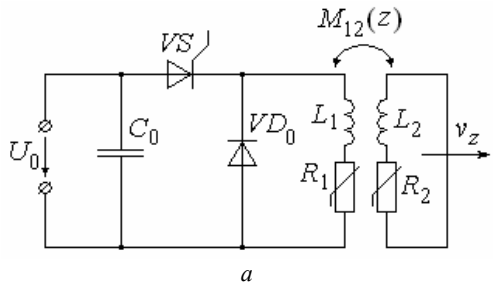

a

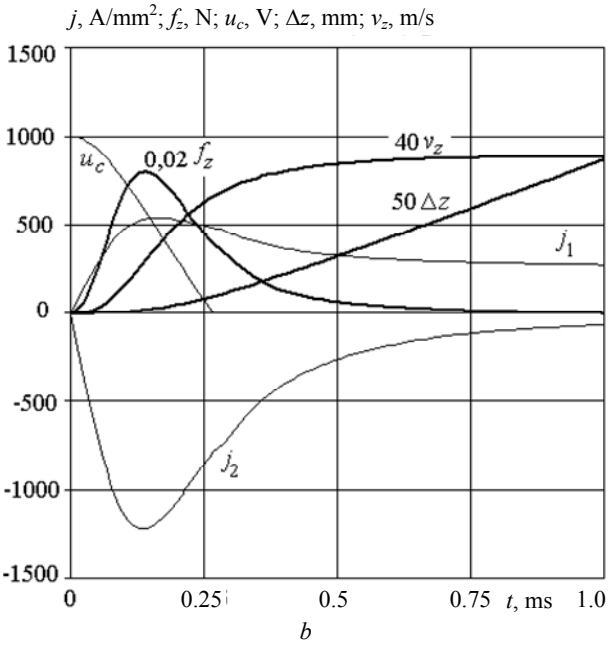

b

Fig. 4. The electrical circuit of the LPIEC which forms the aperiodic current pulse of the inductor, (*a*) and the electromechanical characteristics of this LPIEC (*b*)

At an aperiodic current pulse of an inductor, the LPIEC retains both the polarity of the CES voltage u_c and the polarity of the inductor and armature currents (Fig. 4). After reaching the CES voltage u_c = 0, the current in the inductor starts to flow through the inverse diode VD_0. Due to the preservation of the polarity of the currents, only the repulsion EDF act on the armature, the value of the impulse being F_z = 8.85 Ns. The armature, together with AE, reaches the speed v_z = 20.8 m/s. At the end of the operating cycle, the inductor temperature rise θ_1 is 1.1 °C, and the temperature rise of the armature θ_2 is 1.7 °C. The efficiency of the LPIEC η is 22.23 %.

Electromechanical indices of LPIEC with aperiodic current pulse of inductor are better than in LPIEC with excitation of inductor by unipolar current pulse, but worse than in LPIEC with excitation of inductor by oscillating-damped current pulse. In the converter with an aperiodic current pulse of the inductor, the inductor is heated more warmly and the armature heating is lowered.

Power supply circuit of the LIIEP inductor forming an aperiodic current excitation pulse with the connection of an additional CES. The preservation of the polarity of the voltage u_c in the power circuit of the LIIEP inductor forming an aperiodic current excitation pulse opens up prospects for improving this circuit, for example, by connecting an additional CES-1 during the

discharge of the initial CES-0 with the parameters C_0 and U_0 [12]. The additional CES-1 with capacity C_1 is pre-charged to voltage U_1 which is less than the voltage U_0 of the original CES-0 (Fig. 5). During the discharge of the CES-0, when the voltage $u_c<U_1$, the CES-1 is connected via the diode VD_1, increasing the discharge capacitance to the value C_0+C_1.

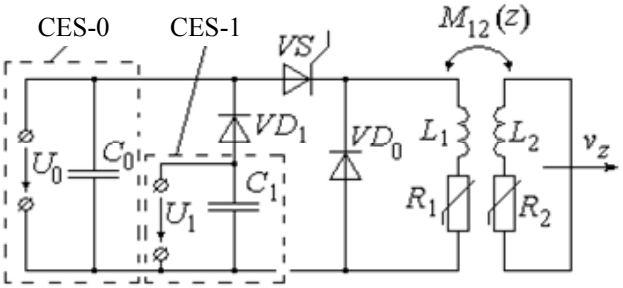

Fig. 5. The electrical circuit of the LPIEC which forms an aperiodic current pulse of the inductor with the connection of an additional CES-1

Since this circuit has not been practically studied, let us consider the effect of the parameters of the additional CES-1 on the electromechanical parameters of the LPIEC. First, consider the effect of the value of the voltage U_1 of the additional CES-1 on the LPIEC indicators, since its value determines the moment of connection to the initial CES-0. Let us consider three options for connecting an additional CES-1: before (U_1=0.7U_0), at the time (U_1=0.6U_0) and after (U_1=0.5U_0) reaching the maximum EDF acting on the armature. We will use an additional CES-1 for which $C_1 = C_0$.

The efficiency of the LPIEC with this circuit of the inductor supply will be estimated by the relation

$$\eta = 100\frac{(m_2 + m_e)v^2 + K_P\Delta z^2}{C_0U_0^2 + C_1U_1^2}\ \%. \qquad (24)$$

At the moment of connection of the additional CES-1, up to the maximum of the EDF (U_1=0.7U_0) at the leading edge of the current pulses of the inductor and the armature, perturbations are observed (Fig. 6,*a*). This gives rise to a corresponding perturbation at the leading edge of the EDF curve. After connecting the additional CES-1, the voltage u_c begins to decrease more slowly. Compared with the use of only the original CES-0, the maximum values of the current densities have increased: in the inductor, up to 603.6 A/mm^2, in the armature up to 1324.6 A/mm^2. This led to an increase in the EDF maximum to 47.2 kN, the EDF impulse to 11.5 Ns, and the armature speed with AE to 27.1 m/s. However, due to the energy of the additional CES-1, the efficiency of the LPIEC is reduced to 18.8 %. In addition, when the LPIEC operates with this inductor feed circuit, higher temperature rises ($\theta_n = T_n - T_0$) of the inductor θ_1 = 2.1 °C and an armature θ_2 = 2.2 °C are observed, in comparison with the previously considered circuits.

When connecting the additional CES-1 at the time of the appearance of the maximum of the EDF (U_1 = 0.6U_0), local growth of the values of the current pulses of the inductor and the armature is observed (Fig. 6,*b*).

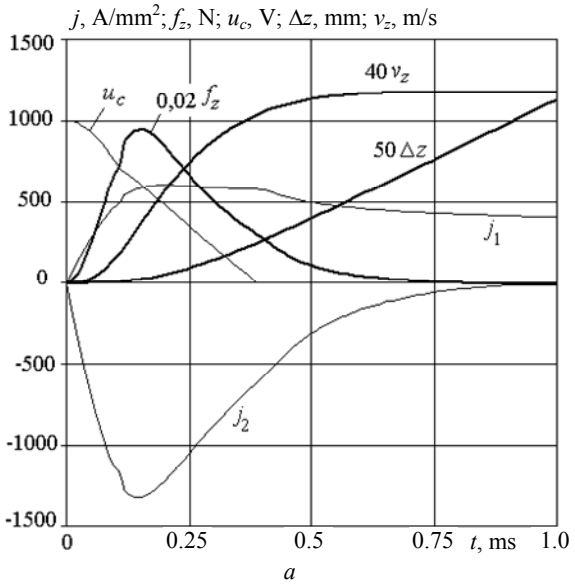

Fig. 6. Electromechanical characteristics of LPIEC when connecting an additional CES-1 charged to voltage U_1: 0.7U_0 (*a*); 0.6U_0 (*b*); 0.5U_0 (*c*)

At that moment, a corresponding increase in EDF occurs. Despite a certain change in electromechanical characteristics, on the whole, the indicators of the LPIEC remained virtually unchanged compared to the previous version ($U_1 = 0.7U_0$). When CES-1 is connected, after the appearance of the maximum of the EDF ($U_1 = 0.5U_0$), a local increase in the values of the current pulses of the inductor and the armature on their trailing edge is observed (Fig. 6,*c*).

After connecting the ENE-1, the current in the inductor begins to decrease more slowly until the instant $u_c = 0$.

Thus, the additional CES-1 and with small and high values of voltages U_1, which are connected, respectively, on the back and front edges of the EDF, allow increasing the electromechanical performance of the LPIEC. For example, when connecting CES-1 with low voltage ($U_1 = 0.15U_0$), the armature speed increases by 27 %, the value of the EDF impulse increases by 27 %, and the efficiency decreases by 25 %. When connecting CES-1 with high voltage ($U_1 = 0.75U_0$), the armature speed increases by 29.7 %, the value of the EDF impulse increases by 29.6 %, and the efficiency decreases by 18.7 %.

With this power circuit, all electromechanical parameters of the LPIEC are higher in comparison with the LPIEC with the circuit of the inductor supply forming a vibrationally damped current excitation pulse. So, when using CES-1 with voltage $U_1 = 0.6U_0$, the maximum value of the EDF f_{zm} is increased by 20 %, and the value of the EDF impulse F_z and the speed of the armature v_z by 21.6 %. In this case, the temperature rise of the inductor θ_1 increases by 2.12 times, and the temperature rise of the armature θ_2 decreases by 11.3 %. The efficiency of the LPIEC η is reduced by 32.2 %.

We note that the electromechanical indicators of the LPIEC using an additional CES-1 with voltage $U_1 = 0.6U_0$ are higher than in the LPIEC with a power circuit that forms an aperiodic current excitation pulse of the inductor with initial capacitance $C_0 = 2$ mF.

LPIEC indicators also depend on the capacitance C_1 of the additional CES-1 (Fig. 7).

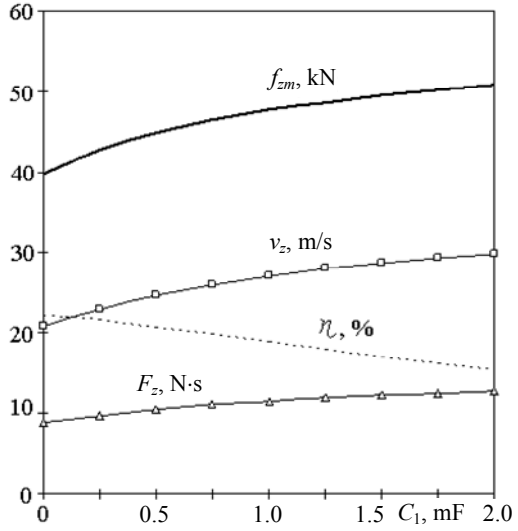

Fig. 7. Dependence of electromechanical indicators of LPIEC on capacitance C_1 at $U_1 = 0.6U_0$

With increasing this capacity, all main electromechanical indicators of the LPIEC grow. Thus, as the capacitance C_1 increases from zero to 2 mF, the maximum current density of the inductor j_{1m} increases by 24.3 %, the armature current density j_{2m} by 12.8 %, the maximum EDF value F_z by 27.6 %, the EDF impulse value F_z and the armature speed v_z by 43.6 % . However, in this case, the temperature rise of the inductor θ_1 increases by 2.7 times, the armature temperature rise θ_2 by 40.7 %. The efficiency of the LPIEC η is reduced by 45.2 %.

Thus, LPIEC with the power circuit of the inductor which forms an aperiodic current excitation pulse with connection of an additional CES-1 provides increased electromechanical parameters. However, it should be borne in mind that the additional CES-1 leads to increased heating of the inductor and armature, as well as to a decrease in the efficiency of the LPIEC.

Conclusions.

1. With the use of the developed circuit mathematical model, recurrence relations were obtained for calculating the interrelated electromagnetic, mechanical, and thermal parameters of the LPIEC with different inductor power circuits.

2. It is established that the electromechanical indicators of the LPIEC with the power supply circuit of the inductor forming the aperiodic current excitation pulse are better than in the LPIEC with the excitation of the inductor by a unipolar current pulse, but worse than in the LPIEC with excitation of the inductor by a vibrationally damped current pulse. In the converter with an aperiodic current excitation pulse, the inductor is heated most strongly, and the armature is least strongly heated.

3. It is established that in the LPIEC with the power supply circuit of the inductor forming an aperiodic current excitation pulse with the connection of an additional CES, all electromechanical parameters are higher in comparison with the LPIEC with the power circuit forming the oscillating-damped current excitation pulse of the inductor. However, in this LPIEC there is an increased heating of active elements, especially an inductor, and a decrease in efficiency occurs.

REFERENCES

1. Balikci A., Zabar Z., Birenbaum L., Czarkowski D. Improved performance of linear induction launchers. *IEEE Transactions on Magnetics*, 2005, vol.41, no.1, pp. 171-175. **doi: 10.1109/tmag.2004.839283.**

2. D.-K. Lim, D.-K. Woo, I.-W. Kim, D.-K. Shin, J.-S. Ro, T.-K. Chung, H.-K. Jung. Characteristic Analysis and Design of a Thomson Coil Actuator Using an Analytic Method and a Numerical Method. *IEEE Transactions on Magnetics*, 2013, vol.49, no.12, pp. 5749-5755. **doi: 10.1109/tmag.2013.2272561**.

3. Tomashevsky D.N., Koshkin A.N. Modeling of linear impulse electric motors. *Russian Electrical Engineering*, 2006, no.1, pp. 24-27. (Rus).

4. Bolyukh V.F., Oleksenko S.V., Shchukin I.S. Comparative analysis of linear pulse electromechanical converters electromagnetic and induction types. *Technical Electrodynamics*, 2016, no.5, pp. 46-48. (Rus).

5. Bissal A., Magnusson J., Engdahl G. Comparison of two ultra-fast actuator concept. *IEEE Transactions on Magnetics*, 2012, vol.48, no.11, pp. 3315-3318. **doi: 10.1109/tmag.2012.2198447.**

6. Young-woo Jeong, Seok-won Lee, Young-geun Kim, Hyun-wook Lee. High-speed AC circuit breaker and high-speed OCD. *22nd International Conference and Exhibition on Electricity Distribution (CIRED 2013)*, 2013, 10-13 June, Stockholm, Paper 608. **doi: 10.1049/cp.2013.0834.**

7. Li W., Koh C.S. Parametric analysis of Thomson-coil actuator using adaptive equivalent circuit method. *Digests of the 2010 14th Biennial IEEE Conference on Electromagnetic Field Computation*, May 2010, pp. 1-9. **doi: 10.1109/cefc.2010.5481673.**

8. Bolyukh V.F., Oleksenko S.V., Katkov I.I. The use of fast cryogenic cooling and ferromagnetic core greatly increases efficiency of a linear induction-dynamic converter. *Proceedings of the 13th cryogenics 2014 IIR int. conf.* Praha, Czech Republic, 7-11 April, 2014, Paper ID: 012, pp. 268-275.

9. Bolyukh V.F., Shchukin I.S. *Lineinye induktsionno-dinamicheskie preobrazovateli* [Linear induction-dynamic converters]. Saarbrucken, Germany, LAP Lambert Academic Publ., 2014. 496 p. (Rus).

10. Bolyukh V.F., Markov A.M., Luchuk V.F., Shchukin I.S.. Energy processes and efficiency of a dynamic induction percussion converter. *Electrical engineering and electromechanics*, 2009, no.2, pp. 9-14. (Rus). **doi: 10.20998/2074-272X.2009.2.02.**

11. Bolyukh V.F., Markov A.M., Luchuk V.F., Shchukin I.S. Theoretical and experimental studies of an induction-dynamic motor excited from a polar capacitive reservoir. *Technical electrodynamics. Thematic issue «Problems of modern electrical engineering»*. 2006, part 2, pp. 65-70. (Rus).

12. Ivashin V.V., Ivannikov N.A. *Induktsionno-dinamicheskiy privod* [Induction-dynamic drive]. Patent Russian Federation, no. 2485614, 2013. (Rus).

Received 10.11.2017

V.F. Bolyukh[1], *Doctor of Technical Science, Professor,*
A.I. Kocherga[1], *Postgraduate Student,*
I.S. Schukin[2], *Candidate of Technical Science, Associate Professor,*
[1] National Technical University «Kharkiv Polytechnic Institute»,
2, Kyrpychova Str., Kharkiv, 61002, Ukraine,
phone +380 57 7076427,
e-mail: vfbolyukh@gmail.com
[2] Firm Tetra, LTD,
2, Kyrpychova Str., Kharkiv, 61002, Ukraine,
phone +380 57 7076427,
e-mail: tech@tetra.kharkiv.com.ua

How to cite this article:
Bolyukh V.F., Kocherga A.I., Schukin I.S. Investigation of a linear pulse-induction electromechanical converter with different inductor power supply circuits. *Electrical engineering & electromechanics*, 2018, no.1, pp. 21-28. **doi: 10.20998/2074-272X.2018.1.03.**

UDC 621.316.761.2; 621.316.728 **doi: 10.20998/2074-272X.2018.1.04**

R.V. Vlasenko, O.V. Bialobrzeski

LIMITATIONS OF CURRENT OF THE THREE-PHASE ACTIVE POWER FILTER IN THE CONDITIONS OF OVERLOAD AND SHORT CIRCUIT

Purpose. The purpose of the work is to develop a method of limiting the maximum allowable level of current of a three-phase active power filter in conditions of overload or short circuit and a system for the implementation of the method. Methodology. For research purposes, the provisions of the pq-theory of instantaneous power, the method of the theory of automatic control in systems with relay controllers, and the methods of simulation in the visual programming environment were used. Results. Both the overloading mode and the short circuit emergency mode, using the proposed solution, do not lead to significant changes in the voltage level on the accumulation capacitor, thus maintaining the stability of the power part of the active power filter. Originality. In the case of temporary overloads of current and short circuits at the network node to which a active power filter is connected, the current's limiting is performed by scaling the current to the level allowed by normal operation of the semiconductor elements of the device, which allows the basic operating algorithm to be implemented in the specified modes. Practical value. The proposed solution can be used as a mean to protect the power part of the device in case of overload, which, in the event of emergencies, and their elimination will automatically restore the normal mode of the device. References 11, tables 2, figures 5.

Key words: **active power filter, pq-theory of instantaneous power, relay current control, effective current value, hysteresis zone**.

Цель. Целью работы является разработка методики ограничения до предельно допустимого уровня тока трехфазного силового активного фильтра (САФ) в условиях перегрузки или короткого замыкания и системы для реализации методики. Методика. Для проведения исследований использовались положения pq-теории мгновенной мощности, метод теории автоматического управления в системах с релейными регуляторами, методы моделирования в среде визуального программирования. Результаты. Как режим перегрузки, так и аварийный режим короткого замыкания, с использованием предлагаемого решения, не приводят к существенным изменениям уровня напряжения на накопительном конденсаторе, соответственно поддерживая стабильность работы силовой части силового активного фильтра. Научная новизна. При временных перегрузках по току и коротких замыканий в узле сети, к которому присоединяют силовой активный фильтр, ограничения его тока выполняют путем масштабирования действующего тока до уровня допустимого в условиях нормальной работы полупроводниковых элементов устройства, позволяет в указанных режимах реализовывать основной алгоритм работы. Практическое значение. Предложенное решение может быть использовано как средство защиты силовой части устройства в случае перегрузки, или в случае возникновения аварийных ситуаций, а их устранение обеспечит автоматическое обновление нормального режима устройства. Библ. 11, табл. 2, рис. 5.

Ключевые слова: **силовой активный фильтр, pq-теория мгновенной мощности, релейное регулирование тока, действительное значение тока, зона гистерезиса.**

Introduction. In industry, frequency converters, thyristor converters, inverters, rectifiers are widely used designed to control the flow of energy of electromechanical and electrical devices. These converters by the operation principle of their power unit have a significant impact on the quality of electrical energy. Thus, they negatively affect the electromechanical and electrical engineering devices, electric machines and apparatus. The compensation of resulting from the operation of such converters the reactive power and the filtration of higher harmonics of current generated by the above devices is at present a topical task. The use of harmonic filters and compensating capacitor batteries in the case of controlled converters does not lead to the desired result in ensuring the quality of electric energy [1].

Innovation in the issue of compensation of reactive power and filtration of higher harmonics of current is the use of active compensating devices - active power filters (APF) [2, 3]. APF have the ability, thanks to the algorithm, to perform compensation of reactive power and filtering of higher harmonics of current. The APF current is formed on the basis of active filtering algorithms based on one of the theories of power: the theory of full power Frise [4], *pq*-theory of instantaneous power [5], *pqr*-theory of instantaneous power [6], and others. It depends on the neutral mode of the network node to which APF is connected which in turn affects the structure of its power unit.

Analysis of previous research. The APF current is formed on the basis of the load current and the network voltage in accordance with the existing methods for determining the components of power or current [4-6].

In the nodes of the system of electric consumption there are modes caused by overloads of technological mechanisms. This is possible, both in the technological process, and in case of emergency. A critical case of an overload of a network node is the emergence of a short circuit in the current or adjacent area. Taking into account the algorithm of operation, in the event of emergencies or overload, the control system of the APF will attempt to form a current that is likely to exceed the calculated current of the power unit. Definitely at the design stage of the industrial sample, elements of protection will be introduced into the power part of the APF but the problem of protection may be resolved in another way.

Elements of the APF power unit are selected based on the calculation mode: switching frequency, operating (nominal) current and operating (nominal) voltage, voltage of the accumulation capacitor in the circuit of constant sign voltage [7, 8].

Thus, the problem arises of limiting the given current of the APF in the part of the active filtering algorithm under the following conditions:

1) in the case of overloading of the APF –at a load current, the effective value of which exceeds the maximum permissible level for which the power part of the APF is calculated;

2) in the conditions of the short circuit of the load circuit of the APF in the current or adjacent areas of the power supply system for a period sufficient to trigger the emergency automatics.

The goal of the work is the development of a method for limiting up to the maximum permissible level of three-phase active power filter current in conditions of overload or short circuit and a system for the implementation of the technique.

Main material. APF provides the formation of a given current i^*_{apf} which during the operation of the device is compared with the actual current of the APF (current received from the sensors), the adjustment of the output parameter by the deviation. On the principle of relay regulation, the current error, or rather its sign, is a sign for the formation of pulses of control transistors of upper or lower arm of the converter [11].

Execution of the limitation by applying an appropriate line of limitation will lead to a change in the shape of the current, accordingly, it will lead to a violation of the procedure of formation of current and, as a consequence, of the principle of compensation. Thus, as a rational solution, the idea of scaling the current to a value that does not exceed the permissible actual value of the current of semiconductor valves of the power part $I_{\max}$ is proposed.

On the basis of the above, the following method of APF current limitation is proposed:

1. Set the value of the maximum current $I_{\max}$ due to the properties of the valves of the converter of the APF.

2. Determine the actual value of the given current of the APF for the period of the basic harmonic (T = 0.02 s):

$$I_{RMS} = \left\| i^*_{apf} \right\| = \sqrt{\frac{1}{T}\int_{t_0}^{t_0+T} \left(i^*_{apf}\right)^2 dt} \,. \qquad (1)$$

3. Determine the ratio of the determined actual current value to the given maximum.

$$k = \frac{I_{\max}}{I_{RMS}} \,. \qquad (2)$$

4. In the event that the actual value of the APF current is below the maximum, no limitations are required, that is, the scale factor must be equal to one. In case if the actual value of current of the APF is above the maximum, it is necessary to comply with the limit on the value of the excess, in this way, the scale factor:

$$K = \begin{cases} 1, & for\ k \ge 1 \\ k, & for\ k < 1 \end{cases} . \qquad (3)$$

Such conditions may be fulfilled using the limitation block.

5. The set actual current values of the APF is scaled:

$$i^{*`}_{apf} = K \cdot i^*_{apf} \,. \qquad (4)$$

To implement the developed technique, a block diagram of the subsystem of the current limitation of the active power filter shown in Fig. 1 is proposed.

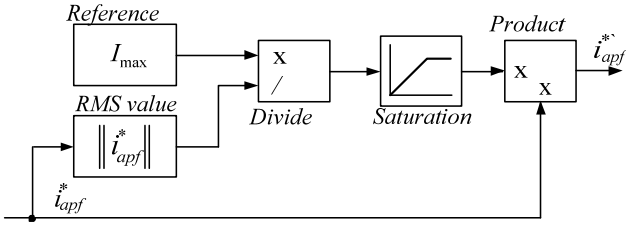

Fig. 1. Block diagram of the subsystem of the current limitation of the APF

The proposed block diagram (Fig. 1) is implemented in the subsystem of current formation (*pq-theory power control*), the control system of the APF in the composition of the electric power complex whose model (Fig. 2) is constructed in a graphical environment of simulation modeling and described in [9]. To determine the current of the compensation of the APF, the *pq*-theory of instantaneous power [4] was chosen, and as the method of pulse control of transistors of the converter - the method of relay current control (RCC) [11], the block (*Relay current control*) (Fig. 2).

The nonlinear load is represented by a three-phase thyristor converter (*Thyristor converter*) with an active-inductive load (*RL-load*) with parameters R_{ld} = 0.666 Ω and L_{ld} = 0.0386 H which at a control angle of 45° in a thyristor converter corresponds to calculated power P_{ld} = = 66 kW, Q_{ld} = 135 kVAr. By the load parameters, taking into account the permissible deviation of the voltage, the three-phase source of electric energy [10] (*Three-phase source*) with the following parameters is calculated and introduced to the circuit: the current value of the interphase voltage U_s = 380 V, frequency f_s = 50 Hz, active and reactive resistances respectively R_s=0.1 Ω and L_s=1.3·10^{-5} H.

Elements of the power part of the three-phase APF are calculated according to the method [7]: reactor inductance L=0.0054 H; capacitor voltage U_{dc} = 2000 V; capacitor capacitance C = 20·10^{-3} F [9]. The value of the hysteresis zone (current tube) in the RCC method is HB = 10 which corresponds to 5% of the nominal load current [11].

The operation of the model was studied in the mode of exceeding the maximum operating current in the case of overload (Fig. 3, 4) and in the emergency short circuit mode (Fig. 5, 6) using the *Three-Phase Fault* block (Fig. 2).

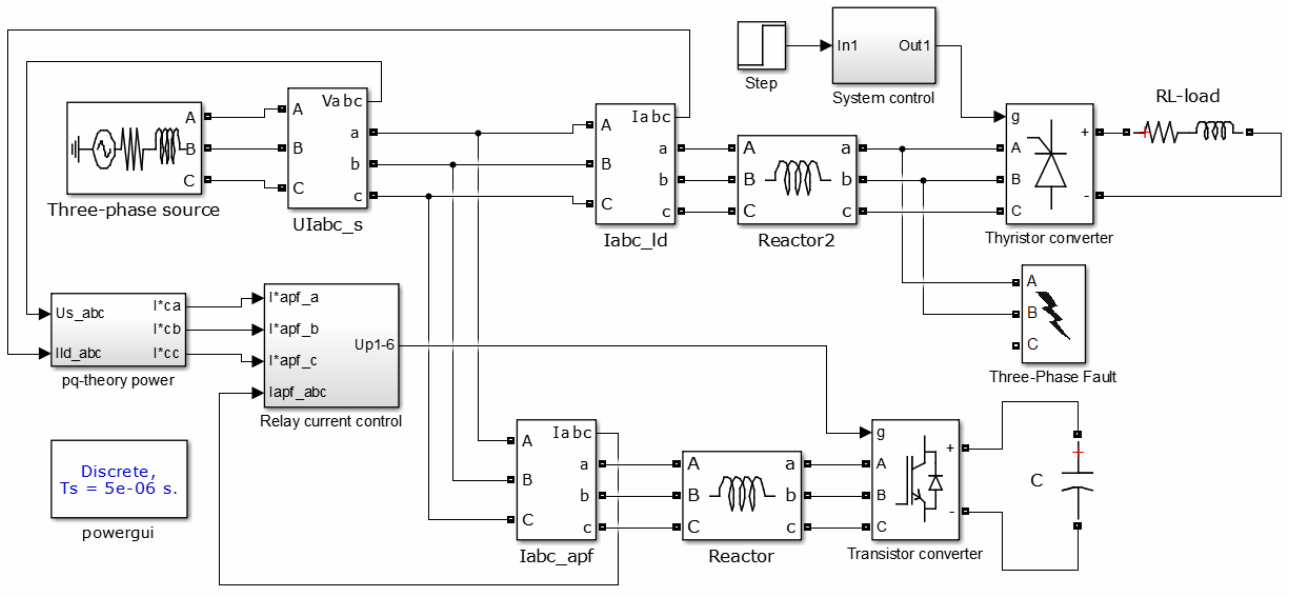

Fig. 2. Matlab Simulink model of the electric power system with three-phase APF

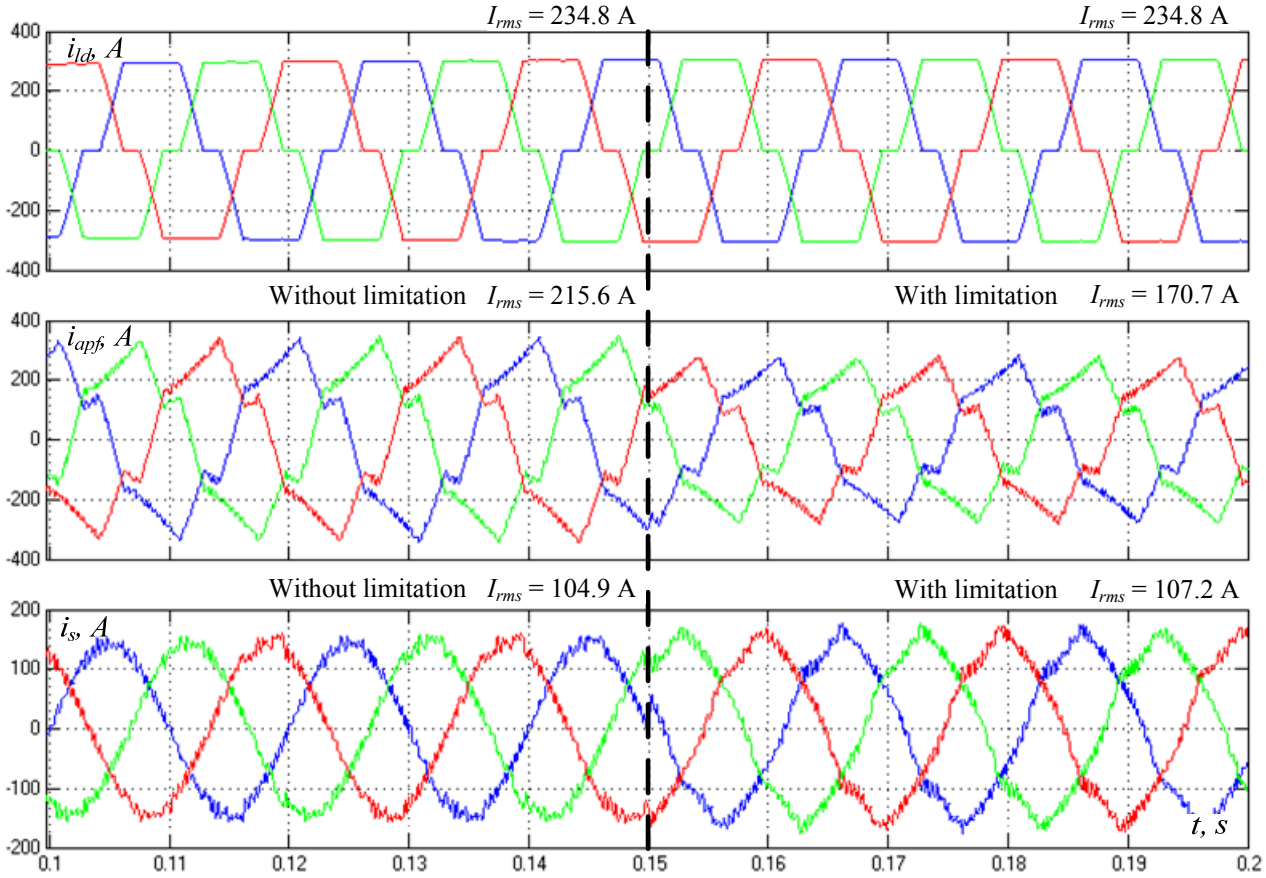

Fig. 3. Oscillograms of currents: of load current i_{ld}, actual of the APF i_{apf} and of the network i_s without and with limitation by maximum current value

Overload mode. The study was conducted with current limitation and without limitation. The given maximum actual value of current is set at the level I_{max} = 170 A. The results of simulation with the specified conditions are shown in Fig. 3. At the time interval (0.1-0.15 s) the current limiting subsystem is not active, there is an overload of the APF converter by working current of 215.6 A, while the compensation efficiency can be estimated by the integral indicators - Table 1 (without limitation). At the time interval (0.15-0.2 s), the current limiting subsystem is activated and the actual value of the APF current is reduced to the established maximum level, while the compensation indicators deteriorate – Table 1 (with limitations), but the device provides a reduction in reactive power and a coefficient of distortion of current.

Table 1

Summary results of study of the overload mode

Parameter	Without APF	Without limitation	With limitation
P, W	21300	21870	20630
Q, VAr	44270	–275.5	8621
I_{rms}, A	234.8	104.9	107.2
THD_I, %	13.96	6.24	7.94
I_{apf}, A	–	215.6	170.7
THD_{Iapf}, %	–	15.2	16.23

Based on the diagram of the change in the voltage of the accumulation capacitor (Fig. 4), the voltage deviation does not exceed 1 %. At the same time reducing the value of the current causes an increase in the energy reserve of the capacitor.

Short circuit mode (SC). The SC research was performed by simulating the phase-to-phase short circuit of two phases to the ground at the load node. In the system model a block is additionally introduced that implements the mode of short circuit in Fig. 2 (*Three-Phase Fault*) by closing the two phases to resistance R = 0.001 Ω, at the interval of time (0.1-0.2 s).

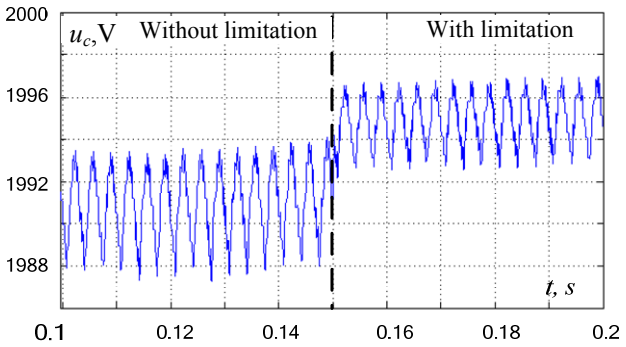

Fig. 4. Capacitor voltage with limitation and without limitation by the maximum current value

Due to the fact that the short circuit is realized using the ohmic resistance (Fig. 5), at the interval of the short circuit current caused by the active power significantly exceeds the current due to reactive power and distortion power.

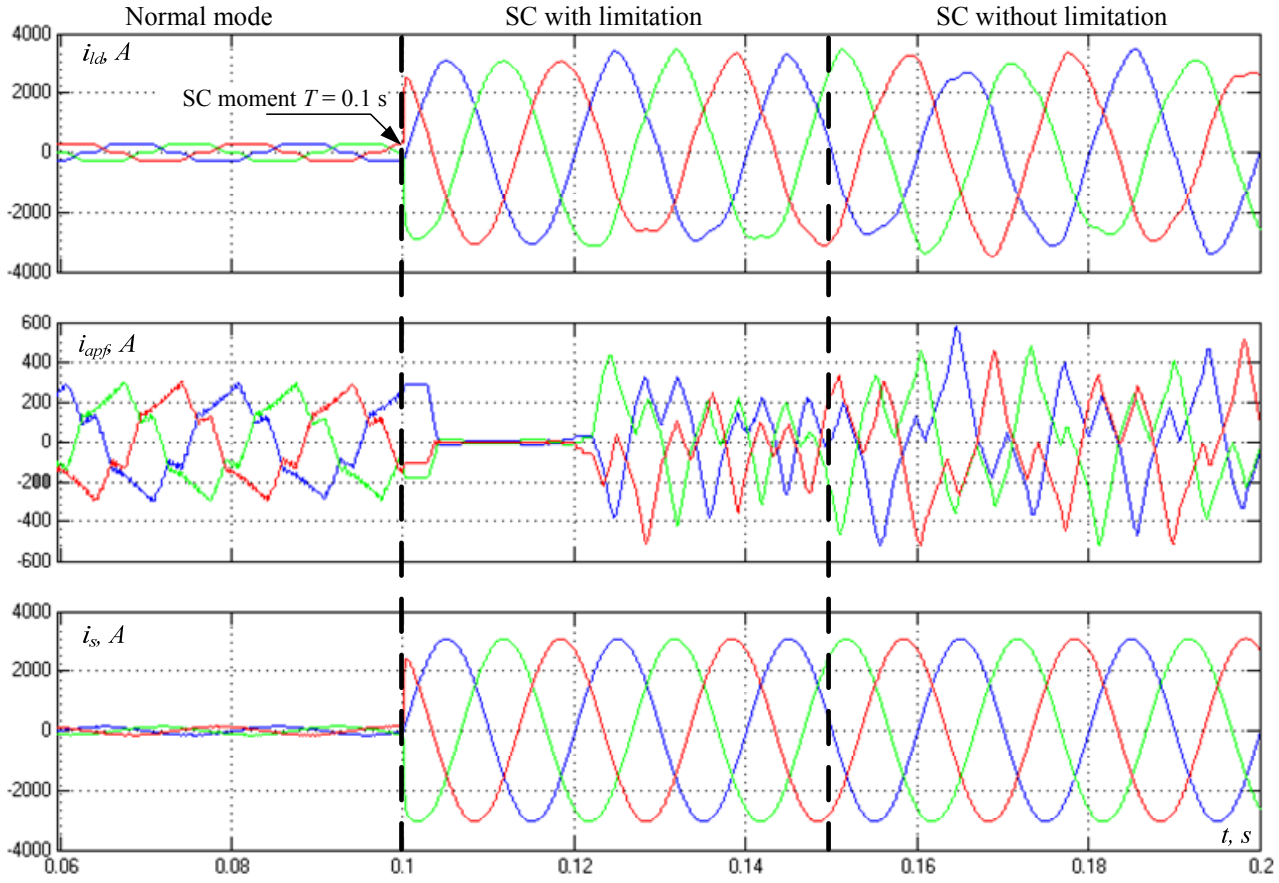

Fig. 5. Oscillograms of currents: of load current i_{ld}, actual of the APF i_{apf} and of the network i_s in the short circuit mode without and with limitation by maximum current value

Under the conditions of the short circuit mode, the operation of the block (*pq-theory power control*) is violated due to a significant decrease in the network voltage. In this case, the APF continues to provide compensation of the load current (Table 2 without limitation) and current limitation in the interval 0.1-0.15 s (Table 2 with limitation). Additionally, it should be noted that the use of the limitation leads to a decrease in overcompensation of reactive power.

The analysis of the voltage of the accumulation capacitor during the implementation of the short circuit mode shows, as in the previous case, a slight increase in the amplitude of the voltage pulses, which does not exceed 3 %.

Thus, the implementation of the proposed method, where the limitation up to the maximum allowable level of current of a three-phase APF in conditions of overload or short circuit is performed by scaling the current value of SAF to the level acceptable in the normal operation of semiconductor elements, allows, in the specified modes, to implement the basic algorithm of the operation of the APF, which is confirmed by the presented results of the research of the computer model of the system (Fig. 3-6).

Table 2

Summary results of study of the three-phase short circuit mode

Parameter	Without APF	Without limitation	With limitation
P, W	21300	4418	4671
Q, VAr	44270	–490	16,29
I_{rms}, A	234.8	2172	2171
THD_I, %	13.96	0.8	0.8
I_{apf}, A	–	317.8	161.8
THD_{Iapf}, %	–	60.9	70.6

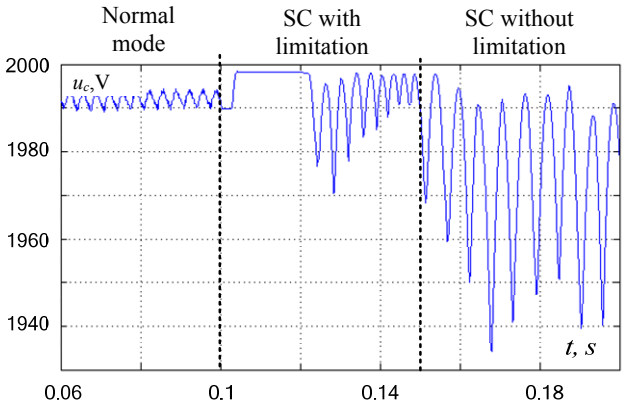

Fig. 6. Capacitor voltage at steady state without limitation by the maximum value and with limitation in the short circuit mode

Conclusions.

1. A method of limiting up to the maximum permissible level of current of a three-phase APF and a block diagram of the current limiting subsystem of the APF are proposed which allows to realize the basic algorithm of operation of the APF in the modes of its overload or short circuit.

2. Implementation of the proposed method allows to protect the power part of the APF in the case of emergency overload and short-circuit modes as well as provides automatic updating of the normal operating mode of the APF after the elimination of emergency modes by the system of emergency automatics.

REFERENCES

1. Zhezhelenko I.V., Saenko Yu.L. *Pokazateli kachestva elektroenergii i ikh kontrol' na promyshlennykh predpriiatiiakh: Ucheb. posobie dlia vuzov. 3-e izd* [Indicators of quality of the electric power and their control at the industrial enterprises. Educational manual for students of higher educational institutions, 3rd ed.]. Moscow, Energoatomizdat Publ., 2000. 252 p. (Rus).

2. Davydov A.Y., Bialobrzeski A.V. Analysis of facilities of indemnification of reactive-power is in electrical engineerings systems. *Transactions of Kremenchuk Mykhailo Ostrohradskyi National University*, 2010, no.3(62), part 1, pp. 132-136. (Ukr).

3. Alekseev B.A. Active harmonic filters. *ELEKTRO. Electrical engineering, power industry, electrical industry*, 2007, no.3, pp. 28-32. (Rus).

4. Zhemerov G.G., Ilina O.V. Fryze power theory and modern power theories. *Electrical engineering & electromechanics,* 2007, no.6, pp. 63-65. **doi: 10.20998/2074-272X.2007.6.14.**

5. Akagi H., Watanabe E.H., Aredes M. *Instantaneous Power Theory and Applications to Power Conditioning*. Wiley-IEEE Press, April 2007. 379 p. ISBN 978-0-470-10761-4.

6. Vlasenko R.V., Bialobrzeski O.V. Using active power filter to compensate the current component of asymmetrical non-linear load in the four wire network. *Reporter of the Priazovskyi State Technical University. Section: Technical sciences*, 2015, no.31, pp. 156-165. (Ukr).

7. Zakis J., Rankis I. Comparison of flexible systems of reactive power compensation. *5th International symposium «Topical problems in the field of electrical and power engineering». Doctoral school of energy and geotechnology*. Kuressaare, Estonia. 14-19 January, 2008, pp. 99-102.

8. Byalobrzheskii O.V., Vlasenko R.V. Interrelation of electric-power parameters of the single-phase active power filter mode with parameters of the stores attached. *Naukovyi Visnyk Natsionalnoho Hirnychoho Universytetu*, 2015, no.4, pp. 79-84. (Ukr).

9. Vlasenko R.V., Bialobrzeski O.V. Comparison of inactive power compensation methods by three-phase active power filter with adaptive relay current controller. *Electrical Engineering and Power Engineering*, 2014, no.2, pp. 20-27. (Ukr).

10. Segeda M.S. *Elekrychni merezhi ta systemy* [Electric grids and systems]. Lviv, Lviv Polytechnic National University Publ., 2007. 488 p. (Ukr).

11. Dixon J.W., Tepper S., Moran L. Analysis and evaluation of different modulation techniques for active power filters. *Proceedings of 1994 IEEE Applied Power Electronics Conference and Exposition – ASPEC'94*. pp. 894–900. **doi: 10.1109/APEC.1994.316303**.

Received 24.11.2017

R.V. Vlasenko[1], *Assistant Lecturer,*
O.V. Bialobrzeski[1], *Candidate of Technical Sciences, Associate Professor,*
[1] Kremenchuk Mykhailo Ostrohradskyi National University, 20, Pershotravneva Str., Kremenchuk, Poltava region, 39600, Ukraine,
phone +380 97 1902815, +380 66 7197298,
e-mail: ruslan.vlasenko@i.ua, seemAl@kdu.edu.ua

How to cite this article:
Vlasenko R.V., Bialobrzeski O.V. Limitations of current of the three-phase active power filter in the conditions of overload and short circuit. *Electrical engineering & electromechanics*, 2018, no.1, pp. 29-34. **doi: 10.20998/2074-272X.2018.1.04.**

UDC 621.365.5 **doi: 10.20998/2074-272X.2018.1.05**

V.M. Zolotaryov, M.A. Shcherba, R.V. Belyanin, R.P. Mygushchenko, O.Yu. Kropachek

COMPARATIVE ANALYSIS OF ELECTRICAL AND THERMAL CONTROL OF THE LINING STATE OF INDUCTION APPARATUS OF COPPER WIRE MANUFACTURE

Aim. ***This article is intended to develop a technique for monitoring the lining state of induction channel furnaces for melting oxygen-free copper by monitoring changes in the distribution of thermal fields in their lining and carrying out a comparative analysis of the developed technique with the existing one that controls the electrical resistance of the melting channel of the furnaces.*** ***Technique.*** ***For carrying out the research, the theories of electromagnetic field, thermodynamics, mathematical physics, mathematical modeling based on the finite element method were used.*** ***Results.*** ***A technique for diagnosing the lining state of the induction channel furnaces for melting oxygen-free copper has been developed, which makes it possible to determine the dislocation and the size of the liquid metal leaks by analyzing the temperature distribution over the body surface both the inductor and the furnace.*** ***Scientific novelty.*** ***The connection between the temperature field distribution on the surface of the furnace body and the dislocation and dimensions of the liquid metal leaks in its lining is determined for the first time.*** ***Practical significance.*** ***Using the proposed technique will allow to conduct more accurate diagnostics of the lining conditions of the induction channel furnaces, as well as to determine the location and size of the liquid metal leaks, creating the basis for predicting the working life of the furnace.*** References 10, tables 3, figures 4.

Key words: **induction heating, diagnostics and control, interconnected electromagnetic and thermal processes, thermal field distribution, three-dimensional mathematical modeling, finite element method.**

Цель. ***Целью статьи является разработка методики контроля состояния футеровки индукционных канальных печей для плавки бескислородной меди путем мониторинга изменений распределения тепловых полей в их футеровке и проведение сравнительного анализа разработанной методики с существующей, которая контролирует электрическое сопротивление плавильного канала печей.*** ***Методика.*** ***Для проведения исследований использовались положения теории электромагнитного поля, термодинамики, математической физики, математического моделирования с применением метода конечных элементов.*** ***Результаты.*** ***Разработана методика диагностики состояния футеровки индукционной канальной печи для плавки бескислородной меди, которая позволяет определять дислокацию и размер протеканий жидкого металла путем анализа распределения температуры по поверхности корпуса индуктора и печи.*** ***Научная новизна.*** ***Впервые установлена связь между распределением температурного поля на поверхности корпуса печи и дислокацией и размерами протеканий жидкого металла в ее футеровке.*** ***Практическое значение.*** ***Использование предложенной методики позволит проводить более точную диагностику состояния футеровки индукционных канальных печей, а также определять расположение и размеры протеканий жидкого металла, создавая основы для прогнозирования ресурса работы печи.*** Библ. 10, табл. 3, рис. 4.

Ключевые слова: **индукционный нагрев, диагностика и контроль, взаимосвязанные электромагнитные и тепловые процессы, распределение теплового поля, трехмерное математическое моделирование, метод конечных элементов.**

Introduction. Taking into account the constant increase in energy prices and imported components of industrial induction apparatus, the urgency of increasing their resource and energy efficiency, as well as import substitution of the component equipment, is increasing. [3, 8]. All these tasks need to be addressed during the melting of ultrapure oxygen-free copper in induction channel furnaces, in particular in the UPCAST furnaces [6], the application of which is expanded due to a number of technological advantages.

The resource of the UPCAST induction channel furnaces depends on the duration of the failure-free operation of the inductor, which heats the liquid metal channel (0.3 tons), and the furnace, which is above the inductor and contains most of the liquid melt (up to 10 tons). At present, there is a problem of matching the resources of the inductor and the furnace. If the predicted working life of the furnace is 4-6 years, then working life of the inductor is only 1-2 years, i.e. the technology includes a planned 2-3-fold replacement of the inductor design with unchanged furnace design [6, 10].

However, joint experimental studies of PJSC Yuzhcable Works (Kharkiv) and the Institute of Electrodynamics of the National Academy of Sciences of Ukraine (Kiev) using UPCAST line US20X-10 as an example on the continuous casting of oxygen-free copper wire have showed that the replacement procedure of the inductor significantly reduces the working life of the furnace [8]. Due to the temperature drop from 1150 °C (the temperature of the copper melt and the furnace lining surface) up to 300-400 °C (the temperature of furnace lining after the copper draining during its heating with gas burners), the lining inevitably cracks. After re-commissioning the furnace with a new inductor and an old lining, liquid metal leaks occur in cracks.

The most expedient solution to this problem is to increase working life of the inductor to working life of the furnace and use them as a single system during the entire continuous cycle lasting 4-6 years. As a consequence, the line resource is expected to increase beyond 4-6 years due to the lack of planned inductor replacements. The first step to achieve this goal is to improve the system for diagnosing the lining thermal state of the inductor and the furnace.

Now the diagnostics is based on monitoring the active and reactive inductor resistance by measuring the impedance of the melting channel and the water temperature as it passes through the cooling system pipes [6]. The furnace lining is monitored visually and copper leaks through lining are inaccessible for inspection and it

is made by measuring the temperature of the furnace body. This method of diagnostics is indirect, since it does not allow revealing the location and size of the leaks areas of liquid metal, and the actual state of the furnace and inductor is determined by inspection only after they are completely stopped and cooled.

Therefore, there is a need to develop a new technique for diagnosing the lining state, which would allow estimating the direct location and dimensions of the liquid metal leaks into the lining cracks and thus predicting working life of the furnace.

The aim of the paper is to develop a technique for monitoring the lining state of induction channel furnace for melting oxygen-free copper by monitoring changes in the distribution of thermal fields in it using a three-dimensional mathematical model.

Three-dimensional mathematical model. According to the physical formulation, the problem of induction heating of a metal consists of electromagnetic and thermal problems with strong mutual relations [1, 2, 5, 9].

To calculate the distribution of the magnetic field and the current density, the system of Maxwell equations with respect to the vector potential $\vec{A}$ is solved.

$$\mathrm{rot}\vec{H} = \vec{J}, \quad \vec{B} = \mathrm{rot}\vec{A}, \qquad (1, 2)$$

$$\vec{J} = \sigma(T)\vec{E} + \vec{J}_{ext}, \quad \vec{E} = -\mathrm{grad}\varphi - \frac{\partial \vec{A}}{\partial t}, \qquad (3, 4)$$

where $\vec{B}$, $\vec{H}$, $\vec{E}$ are vectors of magnetic induction, magnetic and electric fields intensity, $\vec{J}$, $\vec{J}_{ext}$ are the density vectors of the total current and current in the inductor busbars, φ is the electric scalar potential, σ(T) is electric conductivity of copper, which is a function of temperature T and is described by the following expression:

$$\sigma(T) = \frac{1}{\rho_0(1+\alpha(T-T_{ref}))}, \qquad (5)$$

where $\rho_0 = 1.72\cdot10^{-8}$ Ohm·m is specific electric resistance of copper, $\alpha = 3.9\cdot10^{-8}$ K^{-1} is its temperature resistance coefficient, $T_{ref} = 273.15$ ºK is reference temperature.

The ferromagnetic properties of the magnetic core of the inductor are described by the magnetization curve:

$$\vec{H} = f(B)\vec{B}/B. \qquad (6)$$

The inductor is connected to a 50 Hz sine voltage transformer and consumes from 14 to 616 kW. Simulated processes of continuous heating, especially with primary starts, can last more than 18 hours. Since the scales of the electromagnetic and thermal processes on the time axis differ significantly (20 ms period of electromagnetic oscillations and more than 64,800 with the heating duration), then while solving the general interrelated problem, the electromagnetic subtask is solved in the frequency domain using the actual values for the magnetization curve, and the thermal subtask is solved in the time domain [4].

The calculation equations for various elements of the inductor are:

- for a copper template:

$$\mathrm{rot}\left[\frac{1}{\mu_0}\mathrm{rot}\,\dot{\vec{A}}\right] + j\omega\sigma(T)\dot{\vec{A}} = 0, \qquad (7)$$

- for copper inductor busbars:

$$\mathrm{rot}\left[\frac{1}{\mu_0}\mathrm{rot}\,\dot{\vec{A}}\right] - \dot{\vec{J}}_{ext} = 0, \qquad (8)$$

- for steel core:

$$\mathrm{rot}\left[\frac{1}{\mu_0\mu_{ef}}\mathrm{rot}\,\dot{\vec{A}}\right] = 0, \qquad (9)$$

- for lining mixture, steel casing, water cooling system and ambient air:

$$\mathrm{rot}\left[\frac{1}{\mu_0}\mathrm{rot}\,\dot{\vec{A}}\right] = 0. \qquad (10)$$

The solutions of equation (7) – (10) were joined on the boundaries of the elements and were supplemented by the Dirichlet conditions $\vec{n}\cdot\vec{A} = 0$ on the boundaries of the computational domain.

To calculate the heat distribution, the thermal balance equation is solved:

$$\rho C_p \frac{\partial T}{\partial t} - k\,\Delta T = Q_{eddy} + Q_{water}, \qquad (11)$$

where ρ, C_p, k are density, heat capacity and thermal conductivity of materials, Q_{eddy}, Q_{water} are heat sources, including the heating of the template by eddy currents Q_{eddy} (the time average over one period) and cooling of busbars and lining in the course of water flowing through the tubes of the cooling system Q_{water}.

The heat removal through the water was calculated taking into account the heat capacity of the water, its temperature and the mass flow:

$$Q_{water} = M_t \cdot C_p (T_{in} - T)/V, \qquad (12)$$

where M_t is water flow in kilograms, passing through the cross section of the tubes per unit time, T_{in} is the temperature of incoming water, V is the internal volume of the system pipes.

The multi-physical relationship between the problems of calculating the distributions of magnetic and thermal fields was realized by using the eddy currents as a source of heat induced by the magnetic field and determined according to the solution of the electromagnetic problem:

$$Q_{eddy} = 0.5\cdot\sigma(T)\,|\,\vec{E}\,|^2 = 0.5\cdot\sigma(T)\,|\,\partial\vec{A}/\partial t\,|^2. \qquad (13)$$

Equation (11) was supplemented by conditions on the boundaries of the computational domain and on the boundaries of various materials. The convective heat removal from the inductor and the furnace bodies through the ambient air was determined at a given heat transfer coefficient h according to the equation:

$$-k\frac{\partial T}{\partial n} = h(T - T_{ext}), \qquad (14)$$

where T_{ext} is the ambient temperature, n is the normal vector to the outer boundary.

According to the engineering drawings of the channel furnace used at PJSC Yuzhcable Works, a three-dimensional model was constructed in the software

package Comsol Multiphysics [4], for which the solution of the system of differential equations (7) – (11) was found by the finite elements method.

Comparative analysis of electrical and thermal control. Lining furnace is formed by four layers of brick, where the first and second layers serve as «armor» and keep the metal melt from leaks. In this case, the temperature difference at the boundaries of these layers is 119 °C (from 1150 to 1031 °C). The third and fourth layers perform the functions of the heat insulator and the main temperature drop at 899 °C (from 1031 to 132 °C) occurs on their boundaries [6]. However, because of the porous structure, the third and fourth layers of brick after penetration of the metal melt through the «armor» actively absorb it, which eventually leads to the metal flow to the outer steel body of the furnace. As a result, even drops of liquid copper may appear, emerging through its technological holes. Because of this, areas of high temperature rise appear on the body. Such processes increase the power consumption, i.e. reduce the energy efficiency of the entire production process and significantly reduce working life of the furnace.

At the moment, the diagnostics of its resource is carried out by monitoring and recording the active R and reactive X of the inductor resistance. Fig. 1,*a* shows black dots which are the results of measuring the impedance Z of the melting channel of the inductor at PJSC Yuzhcable Works for the period from 01.2013 to 09.2017.

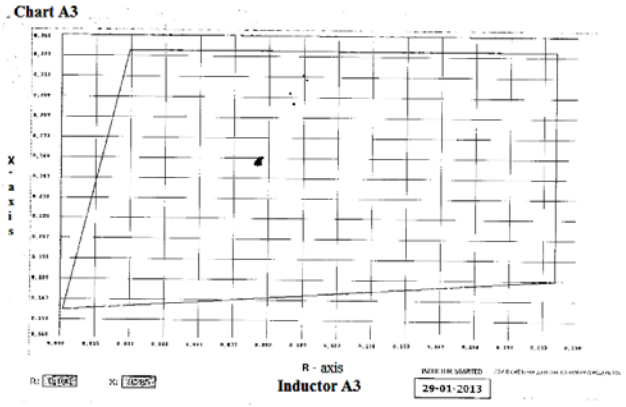

a

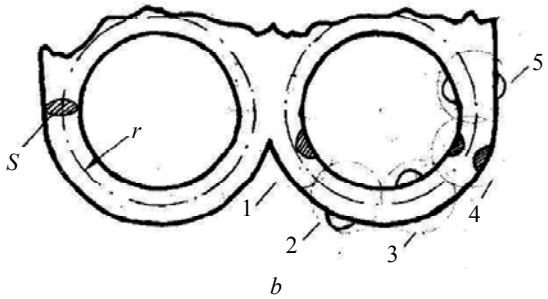

b

Fig. 1. Measurements of impedance Z of the melting channel of the inductor at PJSC Yuzhcable Works (*a*); the shape of the melting channel and its possible defects (*b*)

The active resistivity of the R channel is plotted in ohms along the ordinate axis and its reactive resistance X. The value of R varies inversely with the cross-sectional area of the channel S in Fig. 1,*b* ($R \sim 1/S$). The value X has an inductive character and is proportional to the channel radius ($X \sim r$). The region bounded by the quadrilateral in Fig. 1,*a* is the region of values of the impedance Z of the channel during normal operation of the inductor. The deviation of the measured values of Z beyond the limits of the quadrilateral indicates the emergency operation of the induction apparatus, which is connected with the flow of the melt into the lining of the furnace or vice versa by the entrapment of the melting channel slags in the inductor.

Table 1 shows the change in the parameters R, X, and Z for each of the five types of melting channel defects shown in Fig. 1,*b*.

Table 1

The change of the parameters R, S and Z of the melting channel for each of the five types of its defects

	$R \sim 1/S$	$X \sim r$	Z
1	↑	↑	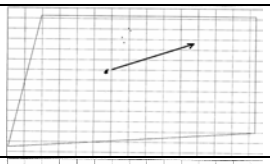
2	↓	↑	
3	↓	↓	
4	↑	unchanged	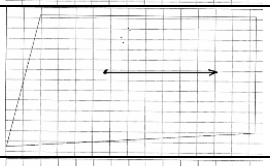
5	↓	unchanged	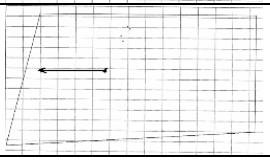

Also, the existing diagnostics system includes monitoring the change in the temperature T of the running water in the cooling system. The system has 4 water-cooled circuits, the tubes of this circuit pass along the surface of the furnace adjoining to the inductor, along the surface of the cylindrical inductor holes for the magnetic circuit, inside the copper busbars and the inductor body base. According to the technical documentation, if the difference in ΔT across all circuits remains within 5 °C, then the line condition is considered normal.

To improve the diagnostics system, it was suggested to monitor not only the system-specific parameters (impedance Z and temperature difference ΔT), but also the temperature distribution along the inductor and furnace bodies. The task was to develop a mathematical model and a technique for calculating the temperature distributions both on the body surface and inside the lining of the inductor and furnace in nominal and emergency operation modes. The verification of the model was carried out by comparing the isotherms

calculated on the body with the real ones measured on the operating casting line.

According to the developed method, with a non-uniform temperature distribution on the surface of the metal casings of the furnace and inductor, temperature changes in local areas and sizes of such areas are monitored. Then, the model determines the shape and size of the melt flowing in the furnace lining and inductor to obtain isotherms that coincide with the experimental ones. With the help of this approach, the instantaneous state of the furnace is diagnosed.

Table 2

The measurement results of the values T_{min}, T_{max} and ΔT in the cathode loading zone

	The cathode loading zone, T_{min}, °C								
	1	2	3	4	5	6	7	8	9
1	70	95	75	78	115	115	70	70	71
2	101	89	105	105	105	105	70	70	56
3	92	96	95	130	124	99	79	79	60
4	70	85	85	95	95	99	80	80	74
	The cathode loading zone, T_{max}, °C								
	1	2	3	4	5	6	7	8	9
1	95	78	77	96	95	95	98	65	95
2	105	90	105	105	105	105	70	69	64
3	105	91	135	152	124	120	79	80	68
4	95	96	91	108	90	88	83	82	79
	The cathode loading zone, ΔT, °C								
	1	2	3	4	5	6	7	8	9
1	25	0	2	18	0	0	1	0	24
2	4	1	0	0	0	0	0	0	8
3	13	5	45	22	0	21	0	1	8
4	25	11	6	13	0	0	3	2	5

Table 3

The measurement results of the values T_{min}, T_{max} and ΔT in the wire drawing zone

	The wire drawing zone, T_{min}, °C								
	1	2	3	4	5	6	7	8	9
1	75	72	77	81	101	87	91	95	95
2	62	62	75	119	119	11	129	118	105
3	71	88	143	127	115	115	128	145	117
4	92	109	124	75	122	120	101	99	71
	The wire drawing zone, T_{max}, °C								
	1	2	3	4	5	6	7	8	9
1	105	105	110	110	102	105	130	110	115
2	106	118	130	226	150	151	160	163	125
3	120	148	242	215	180	190	199	201	141
4	140	200	254	170	202	170	182	154	108
	The wire drawing zone, ΔT, °C								
	1	2	3	4	5	6	7	8	9
1	30	45	33	29	20	18	39	15	5
2	44	56	55	107	31	40	31	45	20
3	49	60	99	88	65	75	71	56	24
4	48	91	130	95	80	50	81	55	37

To predict working life of the furnace, a study was made on the change in the isotherms on the furnace body after a long operating time. An experiment with duration of 3.5 years (from 04.2014 to 09.2017) was planned and conducted to measure the temperature T on the inductor body and the line furnace. The main attention was paid to the furnace, since it contains the bulk of the melt.

The furnace body was divided into 72 control zones (36 in the section for loading copper cathodes for melting and 36 for the stretching of the copper wire), in which the temperature T was measured by an optical pyrometer.

Table 2 for the cathode loading zone and Table 3 for the wire drawing zone show the measurement results of the minimum temperature T_{min} (measured in 2014), the maximum temperature T_{max} (observed from 2014 to 2017) and the temperature difference ΔT reflecting the increase in the average operating temperatures in the zones due to the melt flowing into the lining.

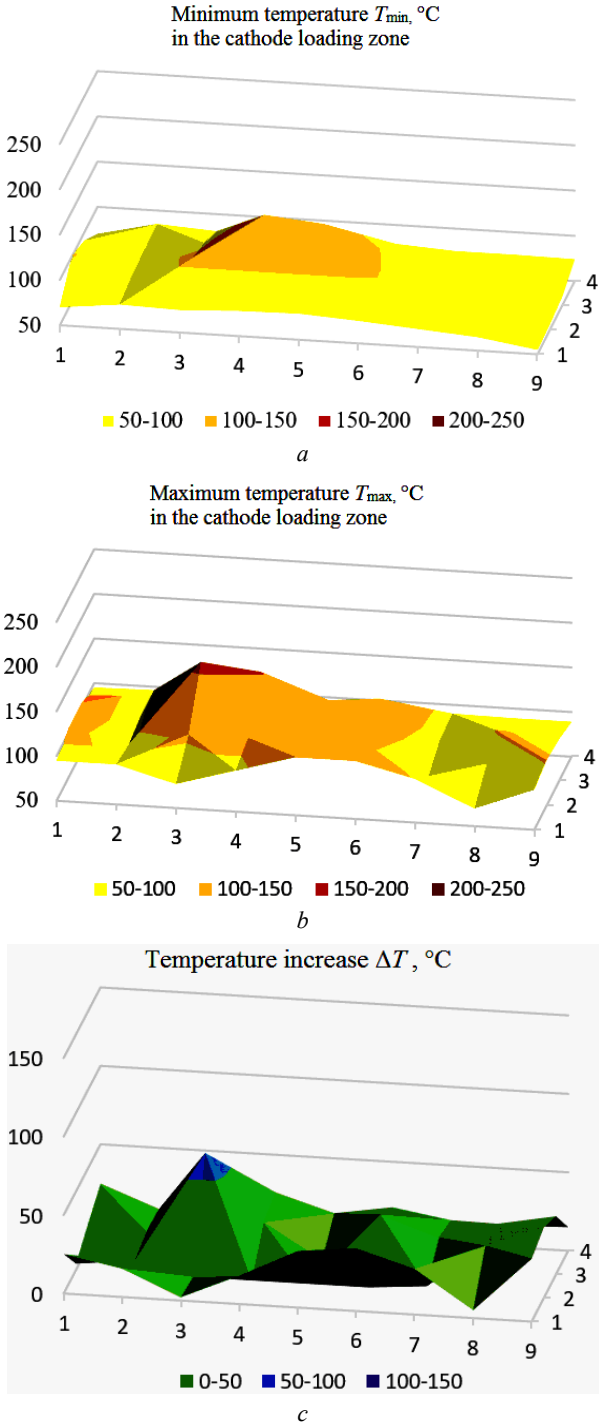

Fig. 2. The measurement results of the values T_{min}, T_{max} and ΔT in the cathode loading zone

The measurement results are plotted accordingly in the diagrams in Fig. 2 and Fig.3, where the height and color of the peaks demonstrate the location and temperature of the zones of the furnace body. Fig. 2,*a* and Fig. 3,*a* show the temperature distribution measurements T_{min} according to measurements made in 2014, when the furnace lining had a small number of defects. Fig. 2,*b* and Fig. 3,*b* show the distribution of the maximum temperature T_{max}, which was observed for 3.5 years of industrial operation of the furnace. Fig. 2,*c* and Fig. 3,*c* reflect the temperature increase over the body ΔT due to the lining degradation.

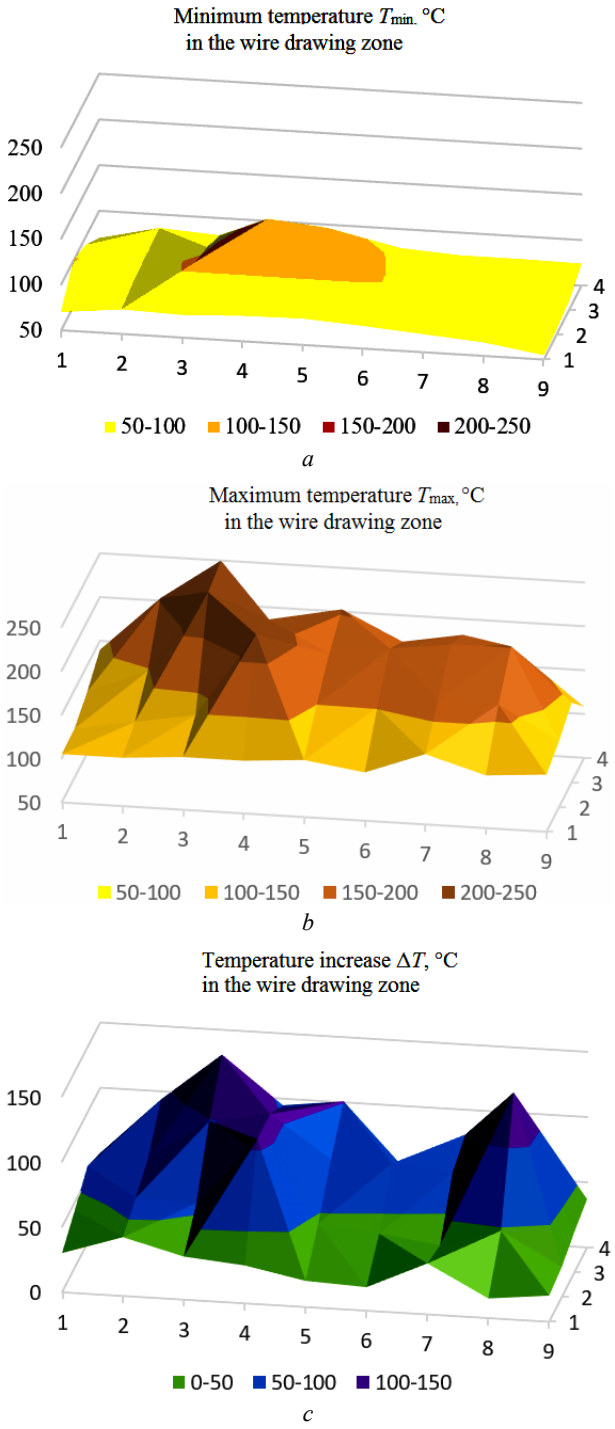

Fig. 3. The measurement results of the values T_{min}, T_{max} and ΔT in the wire drawing zone

Fig. 4 shows graphs of temperature increase T in time in the four hottest control points.

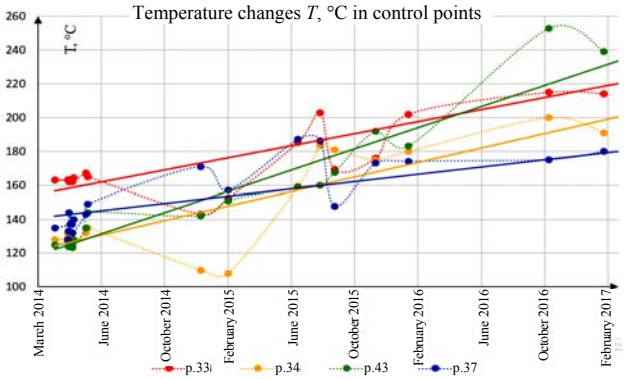

Fig. 4. Temperature increase T in time in the four hottest control zones

Comparing the experimental results in Fig. 2 and Fig. 3, we note that in the wire drawing zone higher temperatures are observed, and this can be seen in both minimum and maximum values. If in the cathode loading zone the average values are $T_{min\ av1}$ = 82 °C and $T_{max\ av1}$ = = 101 °C, then in the wire drawing zone these values are $T_{min\ av2}$ = 96 °C and $T_{max\ av2}$ = 154 °C.

It was determined that during the operation of the furnace, the average temperature on its body increased by 58 °C (from 96 °C to 154 °C). At the same time, in the wire drawing zone, the maximum temperature is 254 °C, as shown by the peak in Fig. 3,*b*, and three zones of the greatest temperature increase (to 130, 107, and 81 °C), which is shown by the three peaks in Fig. 3,*c*. Such an increase in temperature indicates the presence of several zones of liquid metal flowing into the furnace lining and its degradation in the future.

Conclusions.

1. The method of monitoring the lining state of induction channel furnaces for melting oxygen-free copper is well-reasoned by monitoring changes in the distribution of thermal fields in their lining. According to the proposed method, the temperature and location of the hottest areas are measured on the furnace body, according to which, using a three-dimensional mathematical model, the shape and size of the metal melt flowing into the lining is determined.

2. As a result of the planned experiment (lasting 3.5 years) and controlling the change in temperature T in 72 control zones of the furnace casing and inductor of the casting line of the copper wire UPCAST US20X-10 at PJSC Yuzhcable Works, regions of greatest temperature, temperature gradients on the body, and also their variations with time are detected.

3. It was determined that during the operation of the furnace, the average temperature on its body increased by 58 °C (from 96 °C to 154 °C). At the same time, in the wire drawing zone, the maximum temperature was 254 °C, as shown by the peak in Fig. 3b, and three zones of the greatest temperature increase (to 130, 107, and 81 °C), which indicates the presence of several zones leaks in lining furnace

4. The use of the proposed technique allows more accurate diagnostics of the lining state of the induction

channel furnaces, as well as determining the location and size of the liquid metal flow, creating the basis for predicting the working life of the furnace.

REFERENCES

1. .Bermúdez A., Gómez D., Muñiz M.C., Salgado P., Vázquez R. Numerical simulation of a thermo-electromagneto-hydro-dynamic problem in an induction heating furnace. *Applied Numerical Mathematics*, 2009, vol.59, no.9, pp. 2082-2104. **doi: 10.1016/j.apnum.2008.12.005.**

2. Gleim T., Schröder B., Kuhl D. Nonlinear thermo-electromagnetic analysis of inductive heating processes. *Archive of Applied Mechanics*, 2015, vol.85, no.8, pp. 1055-1073. **doi: 10.1007/s00419-014-0968-1.**

3. Lucia O., Maussion P., Dede E.J., Burdio J.M. Induction heating technology and its applications: past developments, current technology, and future challenges. *IEEE Transactions on Industrial Electronics*, 2014, vol.61, no.5, pp. 2509-2520. **doi: 10.1109/TIE.2013.2281162**.

4. Pepper D.W., Heinrich J.C. *The Finite Element Method: Basic Concepts and Applications with MATLAB, MAPLE, and COMSOL*. CRC Press, 2017. 610 p.

5. Stegmueller M.J.R., Schindele P., Grant R.J. Inductive heating effects on friction surfacing of stainless steel onto an aluminum substrate. *Journal of Materials Processing Technology*, 2015, vol.216, pp. 430-439. **doi: 10.1016/j.jmatprotec.2014.10.013**.

6. *UPCAST, Finland*. Available at: http://www.upcast.com (accessed 10 May 2017).

7. Hadad Y., Kochavi E., Levy A. Inductive heating with a stepped diameter crucible. *Applied Thermal Engineering*, 2016, vol.102, pp. 149-157. **doi: 10.1016/j.applthermaleng.2016.03.151**.

8. Zolotaryov V.M., Belyanin R.V., Podoltsev O.D. Analysis of electromagnetic processes in the induction channel furnace used in the cable industry. *Works of the Institute of Electrodynamics of the National Academy of Sciences of Ukraine*, 2016, vol.44, pp. 110-115. (Rus).

9. Shcherba A.A., Podoltsev O.D., Kucheriava I.M., Ushakov V.I. Computer modeling of electrothermal processes and thermo-mechanical stress at induction heating of moving copper ingots. *Technical Electrodynamics*, 2013, no.2, pp. 10-18. (Rus).

10. Zolotaryov V.M., Shcherba M.A., Belyanin R.V. Three-dimensional modeling of electromagnetic and thermal processes of induction melting of copper template with accounting of installation elements design. *Technical Electrodynamics*, 2017, no.3, pp. 13-21. (Rus).

Received 07.11.2017

V.M. Zolotaryov[1]*, Doctor of Technical Science,*
M.A. Shcherba[2]*, Candidate of Technical Science,*
R.V. Belyanin[1]*,*
R.P. Mygushchenko[3]*, Doctor of Technical Science,*
O.Yu. Kropachek[3]*, Candidate of Technical Science,*
[1] Private Joint-stock company Yuzhcable works,
7, Avtogennaya Str., Kharkiv, 61099, Ukraine,
phone +380 57 7545228, e-mail: zavod@yuzhcable.com.ua
[2] The Institute of Electrodynamics of the NAS of Ukraine,
56, prospekt Peremogy, Kiev-57, 03680, Ukraine,
phone +380 44 3662460, e-mail: m.shcherba@gmail.com
[3] National Technical University «Kharkiv Polytechnic Institute»,
2, Kyrpychova Str., Kharkiv, 61002, Ukraine,
phone +380 57 7076116, e-mail: mrp1@ukr.net

How to cite this article:
Zolotaryov V.M., Shcherba M.A., Belyanin R.V., Mygushchenko R.P., Kropachek O.Yu. Comparative analysis of electrical and thermal control of the lining state of induction apparatus of copper wire manufacture. *Electrical engineering & electromechanics*, 2018, no.1, pp. 35-40. **doi: 10.20998/2074-272X.2018.1.05.**

UDC 621.3.01 **doi: 10.20998/2074-272X.2018.1.06**

B.I. Kuznetsov, T.B. Nikitina, A.V. Voloshko, I.V. Bovdyj, E.V. Vinichenko, B.B. Kobilyanskiy

SINGLE-CIRCUIT ACTIVE SCREENING OF MAGNETIC FIELD GENERATED BY SEVERAL OVERHEAD TRANSMISSION LINES IN RESIDENTIAL AREA

Purpose. ***The synthesis of active screening system of magnetic field, generated by several high voltage overhead transmission lines, with the help of single compensation cables is presented.*** ***Methodology.*** ***The initial parameters for the synthesis of active screening system parameters are the location of the high voltage overhead transmission lines with respect to the protected transmission line space, geometry and number of cables, operating currents, as well as the size of the protected space and normative value of magnetic flux density, which should be achieved as a result of screening. The objective of the synthesis of the active screening system is to determine their number, configuration, spatial arrangement, wiring diagrams and compensation cables currents, setting algorithm of the control systems as well as the resulting value of the induction magnetic field at the points of the protected space. Synthesis of active screening system is reduced to the problem of multi objective nonlinear programming with constraints in which calculation of the objective functions and constraints are carried out on the basis of the Maxwell equations solutions in the quasi-stationary approximation. The problem is solved by a stochastic multi swarm multi agent particles optimization, which can significantly reduce the time to solve it.*** ***Results.*** ***Active screening system synthesis results for reduction of a magnetic field generated by several high voltage overhead transmission lines are presented. The possibility of a significant reduction in the level of source magnetic flux density within a given.*** ***Originality.*** ***For the first time the synthesis of the active screening systems of magnetic field generated by the several high voltage overhead transmission lines within a given region of space is carried out.*** ***Practical value.*** ***Practical recommendations on reasonable choice of the number and spatial arrangement of compensating cables of active screening systems of the magnetic field generated by the several high voltage overhead transmission lines is given.*** References 10, figures 7.

Key words: **high voltage overhead transmission lines, power frequency technogenic magnetic field, active screening system, multiobjective synthesis.**

Получил дальнейшее развитие метод синтеза систем активного экранирования магнитного поля, генерируемого несколькими воздушными ЛЭП, на основе многокритериального подхода. При синтезе используется упрощенная математическая модель магнитного поля, генерируемого несколькими воздушными ЛЭП, идентификация которой выполнена по экспериментальным значениям индукции магнитного поля в заданных точках на основе решения задачи оптимизации. Приведены результаты синтеза одноконтурной системы активного экранирования магнитного поля, генерируемого несколькими воздушными ЛЭП. Показана возможность уменьшения индукции магнитного поля с помощью синтезированной системы до уровня санитарных норм Украины. Библ. 10, рис. 7.

Ключевые слова: **воздушные линии электропередачи, магнитное поле промышленной частоты, система активного экранирования, многокритериальный синтез.**

Introduction. Ukrainian electricity networks are characterized by high density, and especially near high-voltage power substations. There is usually a group of overhead transmission lines (TL), in the immediate vicinity of which can be located residential buildings. In this case, the level flux density of the magnetic field (MF) created by a group of TL in residential areas may exceed sanitary standards [1], which creates a threat to public health and requires the adoption of appropriate measures to normalize the MF.

For Ukraine, the method of active circuit screening of MF is economically the most acceptable method of reducing the MF in a residential area of operating overhead TL [2].

Analysis of existing active screening systems. At present, in many countries, active screening systems (ASS) for MF generated by overhead TL [3-7] have been developed and implemented. In such systems with different control algorithms [8, 9], special compensation windings – active cables, the number of which is determined by the specific nature of the problem being solved – are used as the executive body of the ASS.

The simplest single-circuit ASS with one compensating winding are the most widely used [3], however, the synthesis methods of such ASS are currently developed only for single TL [10].

In connection with this, the problem arises of synthesizing single-circuit ASS for efficient screening of MF generated by a group of overhead TL.

The goal of the work is synthesis and investigation of single-circuit active screening systems of the magnetic field of the power frequency created in a residential area by several overhead TL.

Problem definition. Let us consider the construction of an ASS for protection against MF created by several TL the layout of which is shown in Fig. 1.

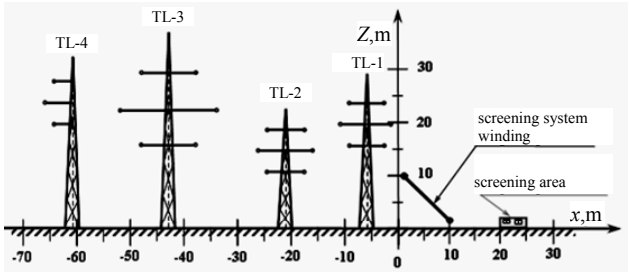

Fig. 1. The layout of several TL and protected area

In the immediate vicinity of the screening are there are two double-circuit TL 110 kV (TL-1 and TL-2), a two-circuit TL 330 kV (TL-3) and a single-circuit TL 330 kV (TL-4).

Method of synthesis. We synthesize the ASS of MF generated by several TL on the basis of the method developed in [10]. In this case, the synthesis of the ASS is reduced to solving the problem of multicriterion nonlinear programming with constraints in which the calculations of objective functions and constraints are performed on the basis of the solution of the Maxwell equation in the quasi-stationary approximation [1]. This problem is solved on the basis of constructing Pareto-optimal solutions with the help of algorithms of stochastic multi-agent optimization by multiswarm of particles [10].

For the synthesis of ASS, in addition to the geometrical dimensions of the TL, the location of the residential zone, where it is necessary to shield the MF, it is necessary to determine the complex values of the currents in the wires of the TL. Moreover, when the currents in different power lines change, not only the level of the total MF generated by several TL changes, but also the space-time electromagnetic field characteristics (STC) of the MF due to the relative redistribution of the vertical and horizontal components of the magnetic flux density vector created by different TL.

The complexity of solving the problem of synthesizing the ASS is determined by the number of wires of the TL. Naturally, taking into account all the wires of the TL creating the MF in the screening zone, the problem of synthesizing the ASS is complicated.

Let us consider an approach to the synthesis of the ASS which makes it possible to simplify the solution of the synthesis problem on the basis of taking into account a smaller number of wires compared with the original problem. To this end, we first carry out experimental studies of the MF level both in the screening zone and near the TL. On the basis of the data obtained, we solve the problem of identifying the currents in the wires of the TL under which the sum of the squared errors of the measured and model values of the flux density of the MF at the given points is minimized.

In fact, this approach solves the problem of approximating the initial MF measured as a result of experimental studies, with the help of several TL. Depending on the required accuracy of the approximation, the number of TL taken into account can be reduced to two or even one which makes it possible to substantially simplify the solution of the problem of synthesis of the ASS.

On the basis of the obtained simplified model of MF created by several TL the problem of synthesis of ASS can be solved on the basis of the method described in [10].

Mathematical model of the initial MF generated by several TL. Mathematical model of MF created by several TL on the basis of a quasi-stationary solution of Maxwell equation [1] can be represented in the following form

$$\vec{B}_o(P_i,t)=\sum_{k=1}^{K}\sum_{l=1}^{L_k}\vec{B}_{lk}(P_i,I_{lk}(t)), \qquad (1)$$

where $\vec{B}_o(P_i,t)$, $\vec{B}_{lk}(P_i,I_{lk}(t))$ are the instantaneous values of the flux density vectors of the resultant magnetic field at the point of space P_i and the magnetic field created at the same point in space by k-th current line of lk-th TL, K is the number of TL; L_k is the number of wires in k-th TL; $I_{lk}(t)$ is the instantaneous current in k-th wire of the lk-th TL.

Fig. 2 shows the lines of the same level of the magnetic flux density calculated for the rated currents of the TL.

Experimental studies of the MF created by these several TL in a residential area in which it is necessary to reduce the level of the magnetic field to sanitary standards have shown that the flux density values of the MF calculated at the rated values of the currents of the TL and the measured values are very different.

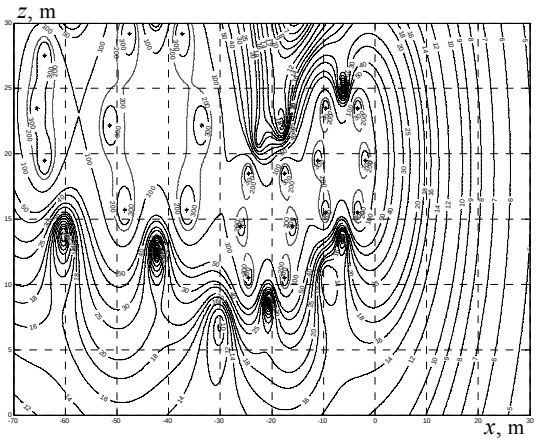

Fig. 2. The distribution of the flux density of the initial magnetic field generated by several TL at rated currents

Simulation of the MF created by individual TL in the screening zone was carried out. Fig. 3 shows the results of calculating the distribution of the flux density of the magnetic field in the screening zone at the operation: *a*) of one TL-4; *b*) at the operation of two TL-3 and TL-4; *c*) when three TL-2, TL-3 and TL-4 are operating; and *d*) when four TL-1, TL-2, TL-3 and TL-4 are operating. In this case, the currents in the wires of all TL were assumed the same and equal to 500 A.

Based on the analysis of the dependencies shown in Fig. 3 it can be seen that as the TL is removed from the screening, the level of the flux density of the magnetic field created by this TL in the screening zone decreases. However, in the system under consideration, the rated currents in the TL-3 and TL-4 wires are 2000 A, and the rated currents in the TL-1 and TL-2 wires are 1000 A. Therefore, despite the fact that TL-3 and TL-4 are removed from the screening zone for a longer distance than TL-1 and TL-2, the effect of TL-4 and especially TL-3 on the level of the flux density of MF in the screening zone can be significant.

Let us now consider the construction of a simplified mathematical model of the initial MF generated by several TL, and its identification from experimental data. In order to determine the required number of TL wires to be considered and the current values in these wires, we construct a simplified model of the magnetic field based on the simulation of the MF distribution in the screening zone, taking into account the different number of wires and the results of experimental studies.

We define the current $I_{lk}(t)$ in the k-th wire of the lk-th TL in the following form

$$I_{lk}(t) = A_{lk}\sin(\omega t + \varphi_{lk}). \quad (2)$$

To determine the amplitudes A_{lk} of the currents $I_{lk}(t)$ we introduce the vector of the required parameters $\vec{Z} = \{A_{lk}\}$, the components of which are the amplitudes A_{lk} of the currents $I_{lk}(t)$ in the k-th wire of the lk-th TL.

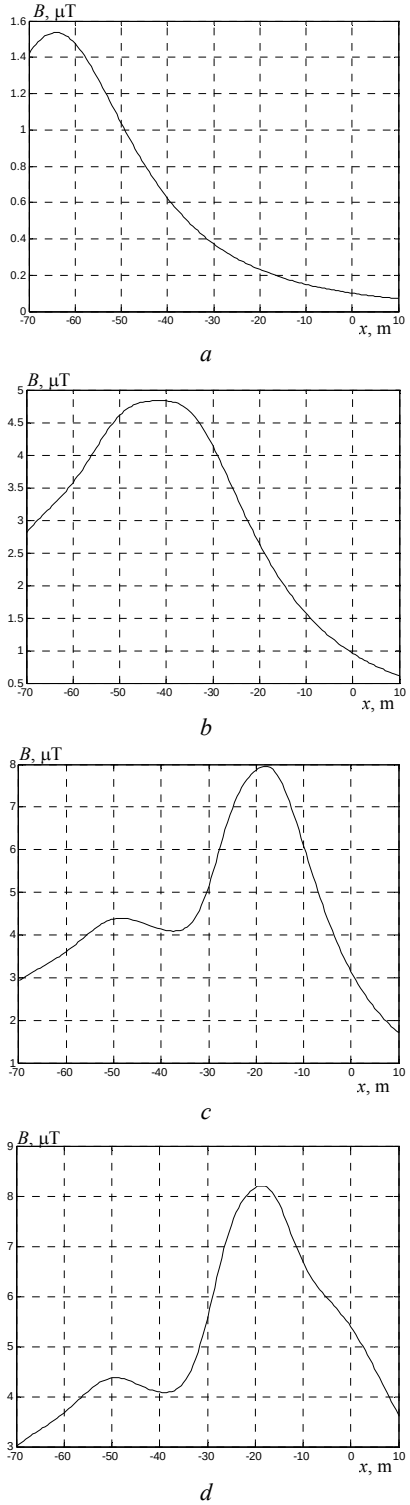

Fig. 3. Distribution of the magnetic flux density in the screening zone during operation: *a*) one TL-4; *b*) two TL-3 and TL-4; *c*) three TL-2, TL-3 and TL-4; *d*) four TL-1, TL-2, TL-3 and TL-4

Then the identification of the mathematical model (1) can be reduced to minimizing the quadratic criterion

$$\vec{Z}^* = \arg\min \sum_{i=1}^{I} \left| \vec{B}_0(P_i) - \vec{B}_e(P_i) \right|^2, \quad (3)$$

where $\vec{B}_e(P_i)$ is the measured magnetic flux density vector in the point P_i.

For the problem under consideration, an approximated mathematical model of the initial MF is constructed, in which the influence of only two 110 kV L on the MF is taken into account. Fig. 4 shows the flux density distribution of the MF of this approximated model.

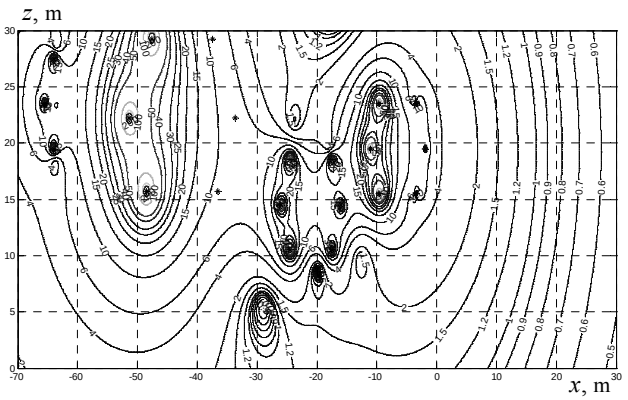

Fig. 4. Flux density distribution of the approximated model of the magnetic field created by several TL

Fig. 5 shows the dependence of the flux density of the MF of *1* – approximated model and *2* – measured values. Comparison of simulation results and experimental studies of the MF distribution in the screening zone showed that when only the first two TL-1 and TL-2 of voltage of 110 kV are taken into account, the error between such an approximated model and the experimental values of the MF level does not exceed 4 %.

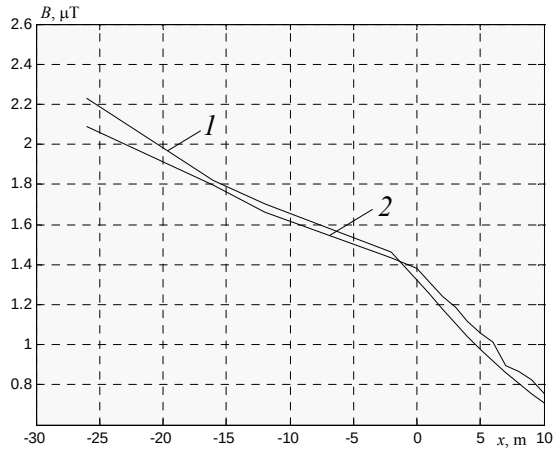

Fig. 5. Dependencies of the MF flux density: *1* – calculated and *2* – measured values

Results of synthesis of ASS. We consider the synthesis of the ASS of the MF created by several TL the layout of which is shown in Fig. 1. This figure also shows the residential area in which the MF screening is required, and the location of the compensation winding. Based on

experimental studies, it was found that in the screening zone, the MF generated by these TL has a negligible polarization, which makes it possible to construct a single-circuit ASS with one compensation winding. It should be noted that such systems have become most widespread in the world practice [3-7].

Fig. 6 shows the lines of equal level of the magnetic flux density module: *a*) of the initial MF created by several TL and *b*) with the active screening system turned on. The initial flux density of the MF in the residential space under consideration is 1.8 μT which is 3.6 times higher than the sanitary norms of 0.5 μT [1]. When the active screening system is turned on, the flux density level of the MF does not exceed 0.4 μT.

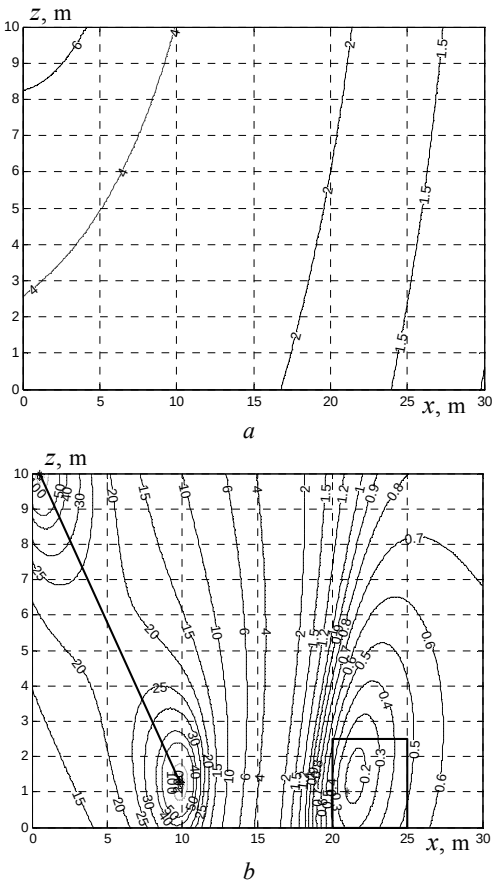

Fig. 6. Flux density distribution: *a*) of the initial MF created by several TL and *b*) of the MF with the ASS turned on

Fig. 7 shows the STC of the MF created: *1* – by several TL; *2* – by compensating winding and *3* – total MF with the system turned on. As can be seen from this figure, in the space under consideration, the initial MF created by several TL has a negligible polarization, so that its STC represents a strongly elongated ellipse, and the ellipse coefficient (ratio of the smaller semi-axis of the ellipse to the larger semi-axis) is about 0.4, that is confirmed by experimental research. Naturally, such a MF can be effectively compensated with a single-circuit ASS. With the help of one winding, the lager semi-axis of the STC ellipse of the original MF is compensated, so that the STC of the resultant MF remaining after the operation of the ASS is an ellipse with an ellipse coefficient equal to 0.8.

In conclusion, we note that the calculated screening efficiency of the synthesized ASS in a residential zone has been experimentally confirmed in the field on its full-scale model and is more than four.

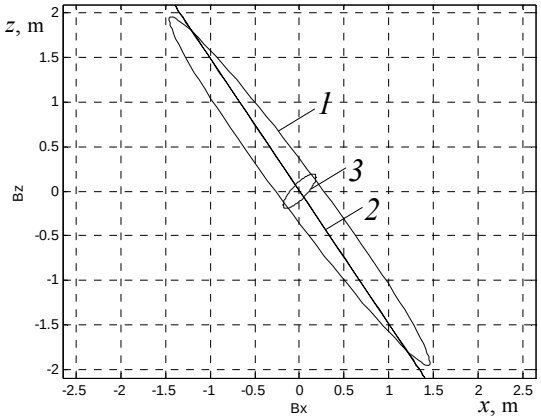

Fig. 7. Space-time characteristics of the flux density vector of MF created: *1* – by TL; *2* – by compensating winding and *3* – of total MF with ASS turned on

Conclusions.

1. Methods for the synthesis of active screening systems of the MF generated by several TL on the base of multicriteria approach and methods for constructing a mathematical model of the MF generated by several TL based on the experimental values of the flux density of the MF at given points of space, based on solving the optimization problem, have been further developed.

2. On the basis of the proposed methods, a single-circuit active screening system for the MF created by several overhead TL in a residential zone was first synthesized.

3. The possibility of a significant (by 4 or more time) reduction of the flux density of the MF with the help of a synthesized single-circuit screening system and achieving the sanitary standards for the MF in the residential zone located near the TL group is shown.

REFERENCES

1. Rozov V.Yu., Grinchenko V.S., Pelevin D.Ye., Chunikhin K.V. Simulation of electromagnetic field in residential buildings located near overhead lines. *Technical electrodynamics*, 2016, no.3, pp. 6-8. (Rus).

2. Voloshko O.V. Synthesis of active shielding systems of power transmission lines magnetic field. *Visnyk of the National Academy of Sciences of Ukraine*, 2017, no.7, pp. 64-73. (Ukr). **doi: 10.15407/visn2017.07.064**.

3. Active Magnetic Shielding (Field Cancellation). Available at: http://www.emfservices.com/afcs.html (accessed 10 September 2012).

4. Beltran H., Fuster V., García M. Magnetic field reduction screening system for a magnetic field source used in industrial applications. *9 Congreso Hispano Luso de Ingeniería Eléctrica (9 CHLIE)*, Marbella (Málaga, Spain), 2005, pp. 84-99.

5. Celozzi S., Garzia F. Active shielding for power-frequency magnetic field reduction using genetic algorithms optimization. *IEE Proceedings – Science, Measurement and Technology*, 2004, Vol.151, no.1, pp. 2-7. **doi: 10.1049/ip-smt:20040002**.

6. Shenkman A., Sonkin N., Kamensky V. Active protection from electromagnetic field hazards of a high voltage power line. *HAIT Journal of Science and Engineering. Series B: Applied Sciences and Engineering*, Vol. 2, Issues 1-2, pp. 254-265.

7. Celozzi S. Active compensation and partial shields for the power-frequency magnetic field reduction. *Conference Paper of IEEE International Symposium on Electromagnetic Compatibility*. Minneapolis (USA), 2002, Vol.1, pp. 222-226. **doi: 10.1109/isemc.2002.1032478.**

8. Rozov V.Yu., Assyirov D.A., Reytskiy S.Yu. Technical objects magnetic-field closed loop compensation systems with different feed-backs forming. *Technical electrodynamics. Thematic issue «Problems of modern electrical engineering»*, 2008, chapter 4, pp. 97-100. (Rus).

9. Rozov V.Y., Assyirov D.A. Method of external magnetic field active shielding of technical objects. *Technical electrodynamics. Thematic issue «Problems of modern electrical engineering»*, 2006, chapter 3, pp. 13-16. (Rus).

10. Kuznetsov B.I., Turenko A.N., Nikitina T.B., Voloshko A.V., Kolomiets V.V. Method of synthesis of closed-loop systems of active shielding magnetic field of power transmission lines. *Technical electrodynamics*, 2016, no.4, pp. 8-10. (Rus).

Received 15.12.2017

B.I. Kuznetsov[1], *Doctor of Technical Science, Professor,*
T.B. Nikitina[2], *Doctor of Technical Science, Professor,*
A.V. Voloshko[1], *Candidate of Technical Science,*
I.V. Bovdyj[1], *Candidate of Technical Science,*
E.V. Vinichenko[1], *Candidate of Technical Science,*
B.B. Kobilyanskiy[1], *Candidate of Technical Science, Associate Professor,*
[1] State Institution «Institute of Technical Problems of Magnetism of the NAS of Ukraine»,
19, Industrialna Str., Kharkiv, 61106, Ukraine,
phone +380 50 5766900,
e-mail: kuznetsov.boris.i@gmail.com
[2] Kharkov National Automobile and Highway University,
25, Yaroslava Mudrogo Str., Kharkov, 61002, Ukraine,
e-mail: tatjana55555@gmail.com

How to cite this article:
Kuznetsov B.I., Nikitina T.B., Voloshko A.V., Bovdyj I.V., Vinichenko E.V., Kobilyanskiy B.B. Single-circuit active screening of magnetic field generated by several overhead transmission lines in residential area. *Electrical engineering & electromechanics*, 2018, no.1, pp. 41-45. **doi: 10.20998/2074-272X.2018.1.06.**

UDC 621.3.022: 621.316.9: 537.311.8 **doi: 10.20998/2074-272X.2018.1.07**

M.I. Baranov

NEW HYPOTHESIS AND ELECTROPHYSICS NATURE OF ADDITIONAL MECHANISMS OF ORIGIN, ACCUMULATION AND DIVISION OF ELECTRIC CHARGES IN THE ATMOSPHERIC CLOUDS OF EARTH

Purpose. Development of new hypothesis about the possible additional mechanisms of origin, accumulation and division of electric charges in atmospheric clouds, containing shallow dispersible drops of water, shallow particulate dielectric matters and crystals of ice. Methodology. Electrophysics bases of technique of high voltage, theoretical bases of the electrical engineering, theoretical electrophysics, theory of the electromagnetic field, technique of the high electric and magnetic fields. Results. Pulled out and grounded new scientific supposition, related to possible existence in earthly troposphere of additional mechanisms of origin, accumulation and division of electric charges in the atmospheric clouds of Earth, being based on electrization in the warm ascending currents of air of shallow round particulate dielectric matters, getting in an air atmosphere from a terrene and from the smoke extras of industrial enterprises. By a calculation a way it is shown that the offered additional electrophysics mechanisms are able to provide achievement in the atmospheric clouds of such values of volume closeness of charges, total electric charge and tension of the electrostatic field stocked in them inwardly and on the external border of storm clouds which correspond modern experimental information from an area atmospheric electricity. The calculation estimations of levels of electric potential and stocked electric energy executed on the basis of the offered hypothesis in storm clouds specify on possibility of receipt in them of ever higher electric potentials and large supplies of electric energy. The obtained results are supplemented by the known approaches of forming and development in earthly troposphere of the electric charged atmospheric clouds, being based on electrization in the warm ascending streams of air the masses of shallow round aquatic drops. Originality. First on the basis of the well-known theses of technique and electrophysics of high voltage the important role of shallow round particulate dielectric matters, electrifiable in the warm ascending currents of air of troposphere is scientifically grounded, in the processes of origin, accumulation and division of electric charges in the stratified-rain, heap rain and storm clouds of Earth. Practical value. Application of in practice findings will allow to deepen scientific and technical knowledge of humanity in area of nature of atmospheric electricity, will be instrumental in further development of physics of linear lightning, decision of global problem of lightning protection of earthly technosphere, and also development of the specified approaches at description of the scantily explored people electrophysics phenomena and theories of thunderstorm at sandy storms in the numerous deserts of the world and powerful smoke eruptions of volcanoes on Earth. References 13, figures 2.

Key words: **atmospheric electricity, new mechanisms of origin, accumulation and division of electric charges in atmospheric clouds, hypothesis, calculation, experimental data.**

Выдвинуто новое научное предположение, связанное с возможностью существования дополнительных механизмов возникновения, накопления и разделения электрических зарядов в слоисто-дождевых, кучево-дождевых и грозовых атмосферных облаках, формируемых в тропосфере планеты Земля. В основу новой гипотезы положены электрофизические процессы в воздушной атмосфере, базирующиеся на присутствии в ней электризуемых в теплых восходящих воздушных потоках мелких твердых диэлектрических частиц сферической формы, имеющих объемную плотность по порядку величины равную объемной плотности в атмосфере мелких водяных капель. Путем расчетных оценок обоснованно показано, что предлагаемые дополнительные механизмы формирования и развития атмосферных облаков способны обеспечивать достижение в них экспериментально подтвержденных уровней объемной плотности облачных зарядов, суммарного запасаемого электрического заряда и напряженности электрического поля. Полученные результаты будут способствовать дальнейшему развитию природы атмосферного электричества, физики линейной молнии и решению глобальной проблемы молниезащиты земной техносферы. Библ. 13, рис. 2.

Ключевые слова: **атмосферное электричество, новые механизмы возникновения, накопления и разделения электрических зарядов в атмосферных облаках, гипотеза, расчет, экспериментальные данные.**

Introduction. Despite the great progress achieved so far in unraveling the secrets of the origin of atmospheric electricity, which are rooted in the fundamental scientific ideas and pioneer works of the 18th century by the outstanding physicists of the world – the Russian M.V. Lomonosov [1] and the American B. Franklin [2] in this field of human knowledge, according to the authoritative electrophysics of our time, electrophysical processes associated with the formation and development of thunderclouds in the Earth atmosphere can not be considered as reliably described and finally studied [3]. It should be noted that under the atmospheric cloud is meant the accumulation of small water droplets (supersaturated water vapor), small ice crystals and small solid particles raised up from the surface of the earth and from the smoke emission zones of operating industrial enterprises (for example, powerful thermal power stations) into the troposphere the lower part of the

terrestrial atmosphere up to 11 km high in temperate latitudes, which contains 4/5 of the entire mass of the atmosphere, almost all the water vapor and clouds develop [4]) by warm ascending air currents [3]. As for the concept of an atmospheric lightning cloud, it becomes one of a cumulonimbus cloud in the fulfillment of a number of critical conditions formulated in [3]. It is known that the above processes include [3]: various mechanisms of electrization of liquid and solid particles of clouds; the processes of generation, existence, accumulation and separation of electric charges in a large-scale cloud region with inhomogeneous local temperature and velocity regimes; processes of formation of electric fields in the fine-dispersed medium of clouds; electric discharge phenomena in thunderclouds and the surrounding air atmosphere, which significantly affect the functioning of the electronics of technical means, the human habitat and its vital activity. Without studying these scientific processes that are difficult from the scientific point of view, characteristic for all territories of our planet, further development of physics of lightning, lightning protection and understanding of the role of charged clouds in the global electric circuit of the Earth is impossible.

It should be noted that since the establishment of the electrical nature of linear lightning (a long spark discharge in the air atmosphere [5-8]), about 80 theories have been proposed in the world [3], describing this global natural phenomenon in one or another approximation. Nevertheless, today there is not a single theory of this complex electrophysical phenomenon, which reliably explains many experimental data known to observing specialists. Therefore, further development and improvement of not only these theories, but also individual moments, as well as mechanisms in describing the course of these processes in the atmospheric storm cloud, are urgent scientific problems in the world.

According to [3, 7, 8], the main attention of electrophysicists when considering the initial stage of charge formation in the clouds was turned to the electrification of shallow water droplets in the warm ascending air currents of the atmosphere. For reasons unknown to the author, small solid particles moving in the above air streams were simply forgotten. But they, like water droplets, are capable of electrifying in ascending air currents and further participation in the processes of accumulation and separation of electric charges in atmospheric storm clouds. The natural processes of active electrification of small solid particles in warm airflows are clearly evidenced by the often observed thunderstorms occurring during sandstorms in the deserts of the world and powerful eruptions of volcanoes on the Earth (Fig. 1) [9]. In the author's opinion, only an integrated and multifaceted approach to the problem of the origin of atmospheric electricity can help to solve it.

The goal of the paper is the development of a new hypothesis on possible additional mechanisms for the formation, accumulation and separation of electric charges in atmospheric clouds containing finely dispersed water droplets, small solid dielectric particles, and ice crystals. Let us emphasize that the term «*hypothesis*» used is derived from the Greek word «*hypothesis*» – «*assumption*» [4] and in the case under consideration is a scientific suggestion made to explain these electrophysical processes in an atmospheric cloud.

Fig. 1. General view of lightning discharges occurring in the volcanic hot smoke zone of an eruption containing fine solids in the ashes [9]

1. Problem definition. Let us consider the large-scale region of the air atmosphere (troposphere) of the Earth in the warm spring-summer period of the year, in which formation of stratus-rain, cumulonimbus and storm clouds is possible. To this end, we believe that in this area there are: firstly, water vapor and small drops of water; second, small solid dielectric particles (for example, silica – quartz); third, the ascending warm and descending cold air currents; fourth, small ice crystals in the form of snowflakes and granules. Possible mechanisms of electrification in the considered region of the earth's atmosphere of small drops of water are considered in detail in [3, 7]. In this paper, the main emphasis will be placed on the possible role of these solid particles in the formation, accumulation and separation of electrical charges of both polarities, initially in a cumulonimbus cloud, and then in a thunderstorm cloud. To this end, we assume that the small solid particles moving in the warm ascending air stream have the form of a sphere of radius r_0. We assume that the average concentration (density) of these solid particles in the atmospheric air is N_0. Calculated estimates of the electrization processes of the solid dielectric particles under consideration and the accumulation of a volume electric charge with them in the atmospheric cumulonimbus cloud can be performed for the case of

normal atmospheric conditions (air pressure is $1{,}013\cdot10^5$ Pa, and its absolute temperature T_0 is 273.15 K [10]). These conditions are close to the lower boundary of the level of the isotherm, in the zone of which cloud charges begin to be created [3]. It is required, in the approximation considered, to consider possible additional mechanisms for the formation, accumulation and separation of electric charges in the cumulonimbus and then in a thunderstorm cloud, due to the presence of these solid dielectric particles moving in the warm upward airflow.

2. Calculation estimation of the process of electrification of solid particles in an ascending warm air stream. The results of the studies presented in [3, 7] indicate that the processes of electrification in the air atmosphere of our planet have a bipolar nature. In addition, according to the data of [3], the ionic mechanism of electrization of cloudy particles is characteristic for the initial stage of cloud development in the terrestrial atmosphere. The contact mechanism of particle electrification is the main mechanism leading to the appearance of unipolarly charged regions in atmospheric clouds. The mechanism of electrification of particles in an external electric field can substantially manifest itself in atmospheric cumulonimbus and storm clouds. Proceeding from the results of the influence of these mechanisms of electrization of cloud particles, described in detail in [3, 7], on the finely dispersed dielectric inclusions of a spherical shape moving in the ascending heat, we limit ourselves to the case where the received solid particle of radius r_0 received a free electric charge q_0 of negative polarity, uniformly distributed over its outer spherical surface. We assume that the negatively charged particle of radius r_0, when moving in an ascending warm air flow, is capable of pulling polarized water molecules radially oriented along this field due to the action of its own radial electric field to its outer spherical surface (Fig. 2). As a result, a solid spherical particle with a charge q0 will be surrounded from the outside by a cluster (micro-cloud) of water vapor and, accordingly, covered with a thin water film. Such a state of the investigated charged solid particle of radius r0 will not contradict any of the known physical positions.

And, as in a charged water spherical droplet [3], the outer part of the «particle – water film» system will also have a negative electric charge, but not free, but bound (see Fig. 2). At the molecular level, the electric charges of each water dipole of this system are bound and held intramolecular Coulomb forces [10]. Therefore, there is no neutralization of the free charge q_0 of a solid dielectric particle of radius r_0 due to the presence of electrically neutral molecules near the water. In accordance with the fundamental principles of electrophysics, a double electric layer (DEL) of thickness Δ_e (see Fig. 2) between the electrons of a solid particle of radius r_0 and the first layer of molecular dipoles of water will form on the inner boundary of the «particle – water film» system. The associated positive charge q_+ of each such molecular dipole of water in the DEL zone will be $10e_0$, where $e_0=1.602\cdot10^{-19}$ C is the module of the electric charge of the electron [10]. It is known that the thickness Δ_e of the DEL in the resulting «particle – water film» system will be determined in the form [10]:

$$\Delta_e=\left[\varepsilon_0 kT_0/(n_0q_+^2)\right]^{1/2}=\left[10^{-2}\varepsilon_0 kT_0/(n_0e_0^2)\right]^{1/2}, \quad (1)$$

where $\varepsilon_0 = 8.854\cdot10^{-12}$ F/m is the electrical constant; $k = 1.38\cdot10^{-23}$ J/K is the Boltzmann constant; n_0 is the concentration (density) of molecular dipoles of water.

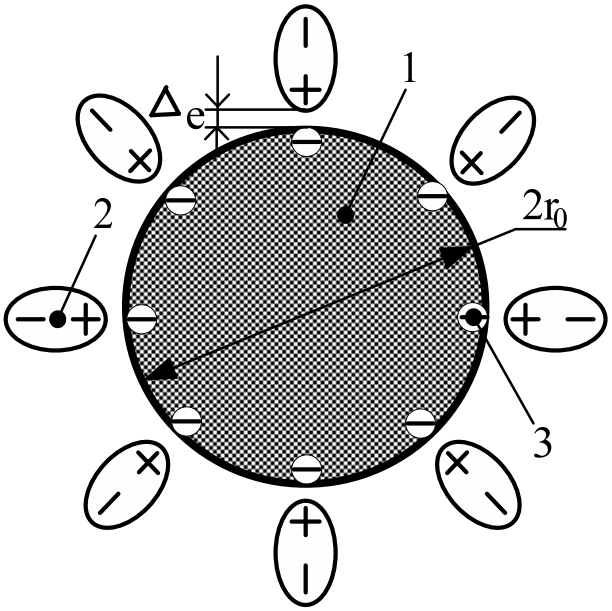

Fig. 2. Simplified view of a negatively charged solid spherical particle surrounded by electrically neutral polarized water molecules (1 is a solid particle, 2 is a molecular dipole of water, and 3 is an electron)

In the case when the molecular dipoles of water suspended in the atmospheric vacuum satisfy the state of an ideal gas, their density n_0 under the normal atmospheric conditions used in the first approximation can be taken equal to the Loschmidt number numerically equal to $N_L=2.68\cdot10^{25}$ m^{-3} [10] . Then it follows from (1) at T_0=273.15 K, $n_0\approx2.68\cdot10^{25}$ m^{-3} and the above-mentioned world constants (ε_0, k and e_0) that $\Delta_e\approx0.22\cdot10^{-10}$ m that even a rough numerical estimation of the thickness Δ_e of the DEL in the system «particle – water film» does not go beyond the reasonable values commensurate with the radius of the atom of a solid dielectric particle [10]. In addition, we note that the Debye shielding radius (length) Δ_D is the same as for a low-temperature plasma containing electrons, ions and neutral atoms (molecules), and a solid-state «metal plasma» (an electrically neutral substance consisting of a negatively charged «electron gas» and ionized positively charged metal atoms) corresponds in order of magnitude to the value of Δ_e found [10, 11]. In order

to be more convincing in the correctness of the estimated estimate Δ_e by (1), we indicate that the Debye radius Δ_D characterizes the distance (linear dimension) at which the Coulomb field of any charge of the plasma is screened by a charge of the opposite sign. It is precisely this situation that is observed in the indicated DEL of the «particle – water film» system under investigation (see Fig. 2).

Now, using the «particle – water film» electrostatic system formed in an ascending warm air stream with its DEL, it is possible to return to the estimated evaluation of the negative electric charge q_0 that appears on the outer spherical surface of a moving solid dielectric particle of radius r_0 due to its electrification in the air atmosphere. Applying the provisions of the well-known theory of DES [3, 10], for the electric charge q_0 of a solid particle in the «particle – water film» system, we find:

$$q_0 = 4\pi\varepsilon_0 r_0 \varphi_0 , \qquad (2)$$

where φ_0 is the Helmholtz electrokinetic potential of (in the case of pure water in the electrostatic system being considered, $\varphi_0 = 0.25$ V [3]).

It can be seen from (2) that for the calculated estimation of the charge q_0 on the outer surface of the earth's atmosphere of the solid dielectric particle, which is electrified in the ascending heat, it is necessary to specify the numerical value of its radius r_0. According to [3], in the layered rain and cumulonimbus clouds, solid particles with a radius r_0 of (5-10) μm can be present. At $r_0 \approx 10 \cdot 10^{-6}$ m and φ_0=0.25 V, we obtain from (2) that the charge of electrification of a solid dielectric particle in an ascending warm air atmospheric flow is numerically equal to approximately $q_0 \approx 2.78 \cdot 10^{-16}$ C. Such a value of the negative electric charge q_0 of solid dielectric particles of radius $r_0 \approx 10$ μm is in good agreement with the data given in [3] and typical for the contact mechanism of the charge of drops of pure water in the ascending warm air stream of the Earth atmosphere. Assuming that in the first approximation the volume density N_0 of solid dielectric particles in the atmospheric cloud is of the order of magnitude of the concentration of water droplets in it and is numerically about 10^8 m^{-3} [3], for the volume density σ_V of the electric charge in a thundercloud due to the presence in it electrified solid dielectric particles of radius r_0, we use the following calculation relation:

$$\sigma_V = q_0 N_0 . \qquad (3)$$

From (3) for $q_0 \approx 2.78 \cdot 10^{-16}$ C and $N_0 \approx 10^8$ m^{-3} it follows that in the case under consideration $\sigma_V \approx 2.78 \cdot 10^{-8}$ C/m^3. This numerical value σ_V obtained with allowance for (2) and (3) corresponds to the experimental data for the mean value of the space charge density in a thunderstorm cloud [3, 7]. For example, with an average overall size of a thunderstorm cloud of 1 km × 1 km × 4 km (horizontal dimensions and size in height) and its corresponding volume $V_0 \approx 4 \cdot 10^9$ m^3, the specified value $\sigma_V \approx 2.78 \cdot 10^{-8}$ C/m^3 causes appearance in the given cloud of the total electric charge $q_\Sigma \approx \sigma_V V_0$, by modulus equals about 111 C. This charge indicator q_Σ correlates well with known probabilistic experimental data characterizing the electric power of such a cloud [3, 5-7].

From (2), for the surface density σ_S of a charge on a solid dielectric particle of radius $r_0$which is electrified in the air atmosphere, we have:

$$\sigma_S = q_0 / (4\pi r_0^2) = \varepsilon_0 r_0^{-1} \varphi_0 . \qquad (4)$$

At $r_0 \approx 10 \cdot 10^{-6}$ m и φ_0=0.25 V, we find from (4) that the value of σ_S for a solid spherical dielectric particle under study assumes a numerical value equal to approximately $2.21 \cdot 10^{-7}$ C/m^2. Note that this calculated value of σ_S is almost two orders of magnitude higher than the average surface density of the negative charge of the planet Earth, which is about 10^{-9} C/m^2 [3]. Taking into account (4) and [10], for the intensity E_0 of the electrostatic field near the surface of a solid dielectric particle of radius r_0 that is electrified in the warm ascending air stream of the Earth, we find:

$$E_0 = \sigma_S / \varepsilon_0 = \varphi_0 / r_0 . \qquad (5)$$

From (5), at φ_0 = 0.25 V for a solid dielectric particle of radius $r_0 \approx 10 \cdot 10^{-6}$ m which has undergone atmospheric electrification, we find that near its negatively charged spherical surface, the electrostatic field strength E_0 can be numerically equal to approximately 25 kV/m. It is likely that such an electric field is capable of pulling the dipoles of polarized water molecules to the surface of the particle under study. With regard to the mean electric field strength in layered rain and cumulonimbus clouds, according to direct experimental measurements by flying directly in the clouds of the electrophysical laboratory, it can reach the level (20-30) kV/m in the pre-threat period (before the transition of these clouds into thunderstorms) [3, 7]. These data may indicate the validity of the estimated estimate from (5) of the value of E_0 near the particle to the formation of a «particle – water film» system.

The probable numerical values of the intensity E_e of the electrostatic field in the DEL zone of the «particle – water film» system can be approximately determined from the following calculated expression:

$$E_e = \varphi_0 / \Delta_e . \qquad (6)$$

Then from (6) at φ_0=0.25 V and $\Delta_e \approx 0.22 \cdot 10^{-10}$ m, which follows from the approximate calculation by (1) with the accepted initial data (T_0=273.15 K; $n_0 \approx 2.68 \cdot 10^{25}$ m^{-3} [10]), it follows that in the zone of the DEL under consideration the intensity E_e of the electrostatic field will reach a huge numerical value of about $1.13 \cdot 10^{10}$ V/m. This level of E_e indicates that an extremely high electric field arises in the zone of the DEL of the «particle – water film» system under

investigation, which determines the electric energy W_e accumulating by the atmospheric thunder cloud.

3. Phenomenological description of the processes of accumulation and separation of electric charges in an atmospheric cloud with solid particles. Raised in the terrestrial troposphere by an ascending warm air flow, charged solid dielectric particles of radius r_0 shielded from the outside by a protective thin water film and simultaneously forming a DEL with its superhigh electrostatic field will contribute to the volumetric accumulation of electric charges in the stratified rain and cumulonimbus clouds under consideration with their volumetric density σ_V. In the author's opinion, in the absence of the protective electrically neutral microspectra surrounding them from the molecular dipoles of water in the absence of charged particles with the same name, physical difficulties in their directed concentrated collection in the troposphere are possible. One of their manifestations may be premature intra-cloud electric discharges (as in volcanic smoke eruptions), leading to partial neutralization of electrification charges for small solid particles. This circumstance will also be facilitated by the fact that, taking into account the previously noted bipolar character of the electrization of solid dielectric particles in the air atmosphere [3], large-scale regions with excessive negative (with an excess of electrons) and positive (with a lack of electrons) by electric charges. On the one hand, it is known from the theory and practice of atmospheric electricity that the upper part of these clouds is in the zone of action of low isotherms (up to –40 °C) [3, 7]. Naturally, in this part of the clouds under consideration, there will be processes of water crystallization (including a thin water film covering a charged solid dielectric particle). And if this is so, then this freezing water film will collapse (due to its volumetric expansion during the crystallization process) (almost explode, like the freezing drop of water [3]) and leave the outer surface of a solid dielectric particle that previously had an excessive negative electric charge q_0. On the other hand, it is also known from the theory and practice of atmospheric electricity that ice crystals formed of electrically neutral pure water with its molecular polarized dipoles (including a thin water film covering the investigated charged solid dielectric particle) have a negative electrical potential and, accordingly, excess negative charge (excess of electrons) with respect to water (Workman-Reynolds effect) [3, 10]. On the appearance of this electrical potential, when a liquid and solid phase of a substance is transformed in the freezing water, the upper layers of the troposphere perform certain work. Proceeding from the fundamental law of nature on the conservation of electric charge [10], it can reasonably be assumed that in the described process of separation of electric charges in the upper supercooled part of the atmospheric cloud, the example of one electrostatic system «particle – water film» is the spherical surface of a solid dielectric particle released from the water film remains negatively charged with charge q_0. All this together (the disappearance of the negative charge q0 from the charged solid particle and the presence of the negative charge q_0 on this particle, and the presence of negatively charged snowflakes and granules due to the crystallization of water vapor in the supercooled part of the cloud) will contribute to an increase in the electric field strength in considered part of the atmospheric cloud.

From applied electrophysics, connected with the study of atmospheric electricity, it is known that at the stage of transition of the cumulonimbus cloud to the thundercloud in its middle and lower parts processes must actively occur, accompanied by the movement of warm ascending and cold descending air masses, as well as the presence of precipitation of rainfall [3]. It is under these conditions that there is a significant increase in the intensity of the electric field inside the thunderstorm cloud, reaching a level of about 0.4 MV/m and more [3], at which it is possible to develop electric discharge processes both inside and outside the cloud, including of the earth's surface. Considered within the framework of the proposed hypothesis on the nature of additional mechanisms for the development of electrophysical processes in atmospheric clouds, the electrostatic system «particle – water film» can justify physically the significant increase in the electric field strength inside and outside the thunderstorm cloud in the case of active release of accumulated moisture vapor in it precipitation from it rainfall. It is in this case that there is a violation of the screening of charged solid dielectric particles by the dipole layers of water vapor (a kind of screening of the electric field of these particles), which carry an excess charge of the cloud q_Σ and provide, with the average volumetric density σ_V, over the atmospheric cloud, in their totality, the formation of the electrostatic field of a thunderstorm cloud.

4. Calculation estimation of the electric field strength inside and outside the thunderstorm cloud with solid particles. For this ion let us use a simplified computational model of a thunderstorm cloud having the form of a sphere of radius R_0 inside which are uniformly distributed with volume density $\sigma_V \approx 2.78 \cdot 10^{-8}$ C/m^3 electric charges $q_0 \approx 2.78 \cdot 10^{-16}$ C of individual little solid dielectric particles with radius $r_0 \approx 10 \cdot 10^{-6}$ m. We assume that the total electric charge of these particles $q_\Sigma \approx 111$ C, as in section 2, is concentrated in a thunderstorm cloud with the volume $V_0 = 4\pi R_0^3/3 = 4 \cdot 10^9$ m^3 and corresponding to a radius of approximately $R_0 \approx 985$ m. Proceeding from the application of the Ostrogradsky-Gauss theorem [10], for the intensity E_r of the electrostatic field inside the assumed

computational model of a thunderstorm cloud of spherical shape at the current value of the radius $r<R_0$, we find:

$$E_r = q_\Sigma r /(4\pi\varepsilon_0 R_0^3). \quad (7)$$

From (7) at R_0≈985 m, r≈R_0/2≈492.5 m and q_Σ≈111 C, we obtain that in the investigated case E_r≈0.514 MV/m. It can be seen that within a thunderstorm cloud containing solid precipitates of electrically neutral water vapor (films) previously electrified in a warm ascending air stream, solid dielectric particles of radius r_0≈10 μm with their volume density N_0≈10^8 m^{-3} in the Earth atmosphere, it is possible to reach critical values of the strength E_r of the electrostatic field, which are characteristic in accordance with [3, 7] for electric discharge processes in the investigated clouds.

For the strength E_R of the electrostatic field at the outer boundary (r=R_0) of the calculated storm cloud model from the theory of electrostatics, we have:

$$E_R = q_\Sigma /(4\pi\varepsilon_0 R_0^2). \quad (8)$$

Substituting in (8) the accepted initial data (q_Σ≈111 C; R_0≈985 m), for the required electric field strength E_R on the outer boundary (edge) of the considered thunderstorm cloud model, we obtain a numerical value equal to approximately 1.03 MV/m. The quantitative calculation data for E_R obtained with the help of (8) and proposed additional mechanisms for the formation and flow of electrophysical processes in atmospheric clouds, indicate the possibility of development from the outer boundary of the described model of a thundercloud of avalanche clouds [3] which are a precursor of a spark breakdown in an atmosphere of a long air gap (lightning).

5. Calculation estimation of the electric potential of a thunderstorm cloud with solid particles. It is known from electrostatics that the electric potential φ_R outside the considered simplified computational model of a thunderstorm cloud of spherical shape (for $r\geq R_0$) with the total electric charge q_Σ containing uniformly distributed over its volume q_0 small fine particles, can be calculated by the following approximate formula [12]:

$$\varphi_R = q_\Sigma /(4\pi\varepsilon_0 r). \quad (9)$$

From (9) at $r \approx R_0 \approx$ 985 m and $q_\Sigma \approx$ 111 C we find that on the outer edge of the lightning cloud under study, φ_R≈$1.01\cdot10^9$ V. It is possible that due to the geometric shape of the calculated region of the thunderstorm cloud and the quantitative of the volumetric density N_0 in it of solid dielectric particles of the order of 10^8 m^{-3}, the numerical values of the electric potential φ_R according to (9) are too high. Thus, according to [13], the difference in electrical potentials between a thundercloud and earth can reach a level of about 100 MV. Assuming in the estimated calculations for (3) the volumetric density σ_V of the electric charge for the lightning cloud under consideration V_0≈$4\cdot10^9$ m^3 (R_0≈985 m) and its total electric charge q_Σ, N_0≈10^7 m^{-3} (an order of magnitude less than the possible volumetric density in an atmospheric cloud of shallow water droplets), it is easy to come according to (9) to the calculated level of the electric potential of a thunderstorm cloud, φ_R≈101 MV, practically indicated in [13]. This value of φ_R appears to the author more plausible for the storm cloud under study. Such a corrected value of N_0will cause, respectively, a tenfold drop in the previously given electrophysical characteristics for the cloud as σ_V, q_Σ, E_r and E_R. In this case, the proposed electrophysical mechanisms for the formation and development of a thundercloud in the terrestrial troposphere are in fact additional to the known mechanisms for the accumulation of electric charges in it, based on the atmospheric electrization of shallow water droplets in warm ascending air currents. Nevertheless, the estimated calculation values of φ_R obtained above indicate that small (r_0≈10 μm) solid dielectric particles electrified in the warm ascending air flow with a volume density of the order of N_0≈(10^7–10^8) m^{-3} and a charge of q_0≈$2.78\cdot10^{-16}$ C, due to the impressive volume of a thunderstorm cloud (of the order of $4\cdot10^9$ m^3) are due to the processes of heat exchange in the atmosphere, the fulfillment of the laws of thermodynamics, which lead to the appearance in the terrestrial troposphere of large zones of various pressures and the movement of huge air mass, forms a quite extended atmospheric electrically charged cloud region carrying ultra high electrical potential and causing the development of lightning.

6. Calculation estimation of the electrical energy stored by a thunderstorm cloud with solid particles. We carry out this estimate proceeding from the assumption that the electric energy W_e of the atmospheric cumulonimbus cloud, before its transition to the stage of a thunderstorm cloud, is stored only in a large number of the electrostatic systems «particle – water film» that we are studying. In this connection, an approximate calculation of the value of W_e for a given volumetric density N_0 of the electrostatic systems under consideration in a pre-threat cloud with a total volume V_0 will be reduced to the determination of the electric energy W_{e0} concentrated in their one DEL with thickness Δ_e. For W_{e0}, we can write the following approximate calculation expression:

$$W_{e0} = 2\pi\varepsilon_0\varphi_0^2 r_0^2 / \Delta_e. \quad (10)$$

Then from (10) at φ_0=0.25 V, r_0≈$10\cdot10^{-6}$ m and Δ_e≈$0.22\cdot10^{-10}$ m we find that in one electrostatic system of spherical form a «particle – water film» (in its DEL with superhigh electric field) the electrical energy of about W_{e0}≈$1.58\cdot10^{-11}$ J is stored. Taking into account (10), for the volume density W_{eV} of electrical energy in a pre-threat cloud with small solid dielectric particles of radius r_0

electrified in the warm ascending air flow of the atmosphere, we have:

$$W_{eV} = W_{e0} N_0 . \quad (11)$$

From (11) at $W_{e0} \approx 1.58 \cdot 10^{-11}$ J and $N_0 \approx 10^7 \text{m}^{-3}$ it follows that in a thunderstorm cloud with small (radius $r_0 \approx 10$ μm) solid charged by atmospheric electrification with dielectric particles, volume density W_{eV} of electric energy, numerically equal to about $1.58 \cdot 10^{-4}$ J/m^3. As a result, for the electric energy W_e stored in the storm cloud under study with a total volume V_0, we can write the following calculation relation:

$$W_e = W_{eV} V_0 . \quad (12)$$

At $W_{eV} \approx 1.58 \cdot 10^{-4}$ J/m^3 and $V_0 \approx 4 \cdot 10^9$ m^3 from (12) we find that in a thundercloud of a given size, during the formation of which, new additional mechanisms for the formation, accumulation and separation of electric charges in atmospheric clouds, the electrical energy W_e can accumulate, which in numerical terms reaches the value of 0.632 MJ. This value of W_e is relatively small. Here it should be emphasized that in the calculation estimation of W_e, we did not take into account the electric charges with their energy, formed in a thundercloud cloud with the known processes of electrization of shallow water droplets and crystallization of cloudy water vapor [3]. At the initially accepted volumetric density in a cloud of small solid particles $N_0 \approx 10^8$ m^{-3}, the stored electric energy W_e in this spherical model of a thunderstorm cloud ($V_0 \approx 4 \cdot 10^9$ m^3), taking into account the proposed hypothesis, will be numerically about 6.32 MJ.

Conclusions.

1. A new hypothesis is presented with the scientific justification for the possible existence of additional mechanisms for the formation, accumulation and separation of electric charges in the atmospheric clouds of our planet based on the electrization in warm ascending air currents of small round solid dielectric particles of radius r_0 falling into the air atmosphere from the Earth surface and from the smoke emissions of industrial enterprises in most countries of the world.

2. It has been shown by calculation that the proposed additional mechanisms for the formation, accumulation and separation of electric charges in atmospheric stratified rain, cumulonimbus and storm clouds are capable of achieving in these types of clouds the values of the volumetric density of σ_V of charges, the total electric charge stored in them q_Σ and the E_r and E_R strengths of the electrostatic field inside and on the outer boundary of similar clouds that correspond to the current experimental data from the atmospheric electricity.

3. Carried out taking into account the proposed hypothesis calculation estimations of the electric potential φ_R in the spherical model of an atmospheric thundercloud with outer radius $R_0 \approx 985$ m and stored in it electrical energy W_e indicate that the atmospheric electrization of small fine solid particles with radius $r_0 \approx 10$ μm with their volumetric density $N_0 \approx 10^7$ m^{-3} in such a cloud is capable of providing an extremely high value of the electric potential φ_R (up to $1.01 \cdot 10^8$ V) on it and the accumulation in it of a very high electric energy W_e (up to $0.632 \cdot 10^6$ J). At $N_0 \approx 10^8$ m^{-3}, the values considered are, respectively, $1.01 \cdot 10^9$ V and $6.32 \cdot 10^6$ J.

4. The considered electrophysical processes and new additional mechanisms of the formation and accumulation of electric charges in atmospheric clouds can be useful in constructing a thunderstorm theory in natural fine-dispersed media with fine solid particles charged by contact electrization, characteristic of sandstorms and volcanic smoke eruptions, when in them the volumetric density N_0 of small solid dielectric particles is not less than 10^8 m^{-3}.

5. The proposed new additional electrophysical mechanisms for the formation of electric charges in the Earth atmospheric clouds, together with known similar mechanisms based on complex electrization in the warm ascending air stream of shallow round water droplets, will contribute to the further development of the nature of atmospheric electricity and the successful solution of the global lightning protection problem on our planet of technical and biological objects.

REFERENCES

1. Radovskiy M.I. Lomonosov and his researches in area of atmospheric electricity. *Electricity*, 1939, no.1, pp. 69-72. (Rus).

2. Kapitza P.L. *Nauchnaja dejatel'nost' V. Franklina* [Scientific activity of V. Franklin]. *Uspekhi Fizicheskih Nauk*, 1956, vol.58, no.2, pp. 169-182. (Rus). **doi: 10.3367/ufnr.0058.195602a.0169**.

3. Bortnik I.M., Beloglovskiy A.A., Vereshchagin I.P., Vershinin Yu.N., Kalinin A.V., Kuchinskiy G.S., Larionov V.P., Monastyrskiy A.E., Orlov A.V., Temnikov A.G., Pintal' Yu.S., Sergeev Yu.G., Sokolova M.V. *Elekrophizicheskie osnovy techniki vysokih naprjazhenij* [Electrophysics bases of technique of high voltage]. Moscow, Publishing house of MEI, 2010. 704 p. (Rus).

4. *Bol'shoj illjustrirovannyj slovar' inostrannyh slov* [Large illustrated dictionary of foreign words]. Moscow, Russkie slovari Publ., 2004. 957 p. (Rus).

5. Bazelyan E.M, Raiser Yu.P. *Fizyka molnii i molnyezashchita* [The physics of lightning and lightning protection]. Moscow, Fizmatlit Publ., 2001. 319 p. (Rus).

6. Uman M.A. Natural and artificially-initiated lightning and lightning test standards. *Proceedings of the IEEE*, 1988, vol.76, no.12, pp. 1548-1565. **doi: 10.1109/5.16349.**

7. Kuzhekin I.P., Larionov V.P., Prohorov E.N. *Molnija i molniezashchita* [Lightning and protection from lightning]. Moscow, Znak Publ., 2003. 330 p. (Rus).

8. Kravchenko V.I. *Molniya. Elektromahnitny faktory i porazhayushchie vozdeystviya na tekhnycheskie sredstva* [Lightning. Electromagnetic factors and their impact on the striking technical objects]. Kharkov, NTMT Publ., 2010. 292 p. (Rus).

9. Available at: http://www.astronet.ru/db/msg/1244664 (accessed 15 July 2012). (Rus).

10. Kuz'michev V.E. *Zakony i formuly fiziki* [Laws and formulas of physics]. Kiev, Naukova Dumka Publ., 1989. 864 p. (Rus).
11. Baranov M.I. Estimation of induction electric charges thickness in a metallic conductor. *Electrical engineering & electromechanics*, 2011, no.4, pp. 56-58. (Rus). **doi: 10.20998/2074-272X.2011.4.11.**
12. Javorskij B.M., Detlaf A.A. *Spravochnik po fizike* [Handbook of physics]. Moscow, Nauka Publ., 1990. 624 p. (Rus).
13. Brzhezitskiy V.A., Isakova A.V., Rudakov V.V. *Tekhnika i elektrofizyka vysokykh napruh* [Technics and Electrophysics of High Voltages]. Kharkov, Tornado Publ., 2005. 930 p. (Ukr).

Received 15.11.2017

M.I. Baranov, Doctor of Technical Science, Chief Researcher,
Scientific-&-Research Planning-&-Design Institute «Molniya»
National Technical University «Kharkiv Polytechnic Institute»,
47, Shevchenko Str., Kharkiv, 61013, Ukraine,
phone +380 57 7076841,
e-mail: baranovmi@kpi.kharkov.ua

How to cite this article:
Baranov M.I. New hypothesis and electrophysics nature of additional mechanisms of origin, accumulation and division of electric charges in the atmospheric clouds of Earth. *Electrical engineering & electromechanics*, 2018, no.1, pp. 46-53. **doi: 10.20998/2074-272X.2018.1.07.**

UDC 621.365.5:537.856 **doi: 10.20998/2074-272X.2018.1.08**

Yu.V. Batygin, E.A. Chaplygin, O.S. Sabokar, V.A. Strelnikova

ANALYSIS OF ELECTROMAGNETIC PROCESSES IN THE SYSTEM «CYLINDRICAL SOLENOID – MASSIVE CONDUCTOR»

Purpose. Defining the key parameters of the inductor geometry, as a long multi-turn solenoid, that influence on the current amplitude induced excited in a massive conductor with a flat boundary surface. Methodology. Performing a mathematical analysis of the electrodynamic problem solution for an area with variable structure by integrating Maxwell's equation within the given boundary and initial conditions and also physical assumptions simplifying the process of solving but not distorting the result and carrying out an experiment that confirms not only the correctly construction considered but also the acceptability of the chosen assumption the opacity applying of the metal blank for these operating fields frequencies. Results. Functional dependencies of the current induced parameters on the metal surface of the heating object have been obtained, along which numerical estimates of the electrodynamic process have been performed, and key parameters influencing the heating efficiency have been determined. The correctness of the solutions obtained was confirmed experimentally. The final form of the solution function of the physical-mathematical problem was shown to be acceptable for performing further engineering and research calculations. Originality. The functional connection of the measured values of the induced surface current and the parameters of the measuring system is determined, the experimental confirmation of which indicates the satisfactory calculation model of the induction heating system and the entire solution as a whole. Practical value. Based on the calculations performed, working samples of inductive systems for induction heating that meet the specified heating rate and area requirements can be constructed. The obtained analytical expressions were transformed and simplified for their further using for engineering calculations with a minimum error value. References 8, tables 1, figures 4.

Key words: **induction heating, Maxwell's equations, sheet metal, electromagnetic field, electrodynamic problem, eddy currents.**

Цель. Определение ключевых параметров геометрии индуктора, как длинного многовиткового соленоида, влияющих на амплитуду индуцированного тока возбуждаемого в массивном проводнике с плоской граничной поверхностью. Методика. Выполнение математического анализа решения электродинамической задачи для среды с переменной структурой путем интегрирования уравнений Максвелла в рамках заданных граничных и начальных условий, а также физических допущений, которые упрощают процесс решения, но не искажают его результат; а также проведение эксперимента подтверждающего не только правильно выполненное построение, но и допустимость применения выбранного допущения о непрозрачности металлической заготовки для данных частот действующих полей. Результаты. Получены функциональные зависимости искомых параметров индуцированного тока на поверхности металла объекта нагрева, по которым были выполнены численные оценки электродинамического процесса, определены ключевые параметры, влияющие на эффективность нагрева. Правильность полученных решений была подтверждена экспериментально. Окончательный вид функции решения физико-математической задачи был приведен к приемлемому для выполнения дальнейших инженерных и исследовательских расчётов. Научная новизна. Определена функциональная связь измеряемых величин индуцированного поверхностного тока и параметров измерительной системы, экспериментальное подтверждение которой свидетельствует об удовлетворительности расчетной модели системы индукционного нагрева и всего решения в целом. Практическая значимость. На основании проведенных расчетов могут быть сконструированы рабочие образцы индуктивных систем для индукционного нагрева, отвечающие заданным требованиям скорости нагрева и его площади. Полученные аналитические выражения были преобразованы и упрощены с целью их дальнейшего использования для инженерных расчётов с минимальной величиной погрешности. Библ. 8, табл. 1, рис. 4.

Ключевые слова: **индукционный нагрев, уравнения Максвелла, листовой металл, электромагнитное поле, электродинамическая задача, вихревые токи**

Introduction. The development proposed by the authors [1] with the use of induction local heating of metal surfaces assumes the fulfillment of research calculations of the field penetration process into sample sheet metal in order to determine its qualitative and quantitative characteristics.

Today, there are large number amount of research material covering the physical processes and the corresponding solutions to the problems of induction heating technologies. The author [2] describes the electrodynamic processes under metal cylinder heating and numerical values obtained coinciding with the experimental data. A similar model of the system is also described in [3] for heating the walls of a cylindrical surface to simulate the process of strips welding. No less significant are research into the microscopic parameters behavior of an object. The author [4], among other things, studied the effect of magnetic permeability and its changes on the efficiency of the metal heating for its heat treatment. The characteristic combining factor of the works analyzed, including similar ones [5, 6], is the orientation to objects of cylindrical geometry and a common mathematical apparatus, namely, the numerical analysis of FEM, by which it is impossible to obtain analytical dependencies suitable for engineering calculations.

Since in most cases induction heating is used for cylindrical objects heating processes, the application of the available recommendations for flat surfaces heating can lead to incorrect technical solutions in practice.

The analysis of the flat surfaces heating is an actual task for the further determination of the induction heating tools optimal parameters.

To obtain a general estimation of the electromagnetic interaction between the field source and

the object, it is advisable to neglect the penetration processes, and to considered the metal of the billet as the ideal conductivity approximation.

To exclude all kinds of circumstances that occur in real constructions of inductor systems and to evaluate precisely the geometry of the relative location of the field source and the object of electromagnetic influence, it is advisable to neglect the penetration processes, and to consider the metal of the sample in the ideal conductivity approximation.

The goal of the paper is to define the key parameters of the inductor geometry, as a long multi-turn solenoid, that influence on the current amplitude induced excited in a massive conductor with a flat boundary surface.

Fields and the eddy currents. The computational model in the cylindrical coordinate system is shown in Fig. 1.

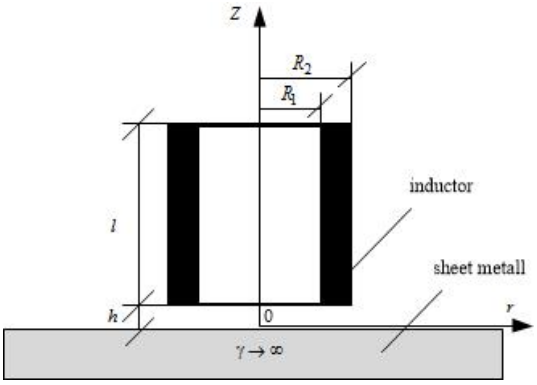

Fig. 1. The model of the inductor system with a long cylindrical inductor, above the ideally conducting blank.

Formulation of the problem:

- the system has an azimuthal symmetry, so that $\frac{\partial}{\partial\varphi}=0$, φ – azimuth angle;
- the current in the winding of the inductor is represented by the azimuthal component with a uniformly distributed spatial density – $j_\varphi(t)$, t – time;
- electromagnetic processes in the system are quasisteady in the Landau sense, so that $\frac{\omega}{c}\cdot l>>1$, ω – cyclic frequency, c – light speed in vacuum, l – the largest characteristic size of the system [7].
- the metal of the inductor winding has not influence the flowing electromagnetic processes.

The solution carrying out of the problem is mannered according to the [7, 8].

The Maxwell's equations for non-zero components of electromagnetic field strengths, been transformed by Laplace taking into account zero initial conditions, at space above the blank, where $z \geq 0$, have a view [7]:

$$\begin{cases}\dfrac{\partial H_r(p,r,z)}{\partial z}-\dfrac{\partial H_z(p,r,z)}{\partial r}=j_\varphi(p,r,z);\\ \dfrac{1}{r}\cdot\dfrac{\partial}{\partial r}\left(r\cdot E_\varphi(p,r,z)\right)=-\mu_0\cdot p\cdot H_z(p,r,z);\\ \dfrac{\partial E_\varphi(p,r,z)}{\partial z}=\mu_0\cdot p\cdot H_r(p,r,z);\end{cases} \quad (1-3)$$

where p – Laplace transform parameter;

$$E_\varphi(p,r,z)=L\{E_\varphi(t,r,z)\},$$
$$H_{r,z}(p,r,z)=L\{H_{r,z}(t,r,z)\},$$
$$j_\varphi(p,r,z)=L\{j_\varphi(t,r,z)\}.$$

In the general case, the current density on the right-hand side of equation (1) is written as:

$$j_\varphi(p,r,z)=(p\cdot\varepsilon_0+\gamma)\cdot E_\varphi(p,r,z)+j_{\varphi_i}(p,r,z), \quad (4)$$

where $j_{\varphi_i}(t,r,z)$ – the inductor outside current density,

$$j_{\varphi_i}(p,r,z)=j(p)\cdot f_1(r)\cdot f_2(z),$$

$j(p)$ – amplitude-time dependence; $f_1(r)$ – the radial current distribution function in the inductor; $f_2(z)$ – the inductor current distribution function by variable – z; ε_0 – the dialectical vacuum permeability.

For a cylindrical inductor in Fig. 1 with a radial and longitudinal number of turns – w_r, w_z accordingly, homogeneous distributions of the exciting current with respect to the spatial variables are described by the following functions.

$$\begin{cases}f_1(r)=[\eta(r-R_1)-\eta(r-R_2)]\\ f_2(r)=[\eta(z-h)-\eta(z-(h+l))]\end{cases}, \quad (5)$$

where $R_2-R_1=w_r\cdot d$, $l=w_z\cdot d$, $d\times d$ – cross-sectional dimension of the square turn.

The amplitude-time dependence of the excitation current density is written as:

$$j(p)=\frac{I(p)}{d^2}, \quad (6)$$

where $I(p)=L\{I(t)\}$, $I(t)$ – the inductor current,

$$I(t)=I_m\cdot\psi(t),$$

I_m, $\psi(t)$ – amplitude and time dependence, respectively.

From the Maxwell system (1) – (3) a differential equation for the azimuthal component of the electric field strength $E_\varphi(p,\lambda,z)$ can be obtained, which after the integral Fourier-Bessel transform takes the form [8].

The unknown constants can be defined from the boundedness conditions of the function $E_\varphi(p,\lambda,z)$ with $z \to \infty$ and its equality to zero on an ideally conducting surface $z = 0$. Intermediate identical transformations are omitted because of its triviality and to avoid excessive unwieldiness in the material presentation.

In the end, it is found that

$$E_\varphi(p,\lambda,z)=-\frac{K(p,\lambda)}{\lambda^2}\cdot e^{-\lambda h}\cdot\left(1-e^{-\lambda l}\right)\cdot sh(\lambda z), \quad (7)$$

where λ – parameter of the Fourier-Bessel integral transformation; $J_1(\lambda\cdot r)$ – the first order Bessel function,

$$K(p,\lambda)=\mu_0\cdot p\cdot j(p)\cdot F(\lambda),$$

where $F(\lambda)=\int_{R_1}^{R_2} rJ_1(\lambda\cdot r)dr$ – the radial current distribution Fourier-Bessel image function in the inductor – $f_1(r)$ from (5).

Using (3) and (7), taking into account the quantities presented in (8), and the Fourier-Bessel image of the tangential component of the magnetic field intensity in the region $z < 0$ is determined as

$$H_r(p,\lambda,z) = -\frac{j(p)}{\lambda}\cdot F(\lambda)\cdot e^{-\lambda h}\cdot\left(1-e^{-\lambda l}\right)\cdot ch(\lambda z). \quad (8)$$

The current density module on the surface of the ideally conducting workpiece – $j_\varphi(p,\lambda)$ is equal to the modulus of the magnetic field strength tangential component [2].

Using (8), taking into account (6) after inverse Fourier-Bessel and Laplace transforms, it is found that

$$j_\varphi(t,r) = -\frac{I_m}{d^2}\cdot\psi(t)\times \\ \times\int_0^\infty F(\lambda)\cdot e^{-\lambda h}\cdot\left(1-e^{-\lambda l}\right)\cdot J_1(\lambda r)d\lambda. \quad (9)$$

The eddy current in the circular region of the radius R is found by integrating expression (9) for $r \in [0; R]$:

$$I_\varphi(t, r\le R) = -I_m\cdot\psi(t)\cdot\int_0^\infty \frac{F(\lambda)}{(\lambda d)}\cdot e^{-\lambda h}\times \\ \times\left(1-e^{-\lambda l}\right)\cdot(1-J_0(\lambda R))d\lambda. \quad (10)$$

We reduce the formula (9), (10) to a form converted for practical estimates. Thus, in terms of the new integration variable, the expressions (9) and (10) are transformed to the form of the following dependencies:

a) relative density of current induced,

$$J_0(r) = \frac{j_{\varphi m}}{\left(\frac{I_m}{d}\right)} = \\ = \int_0^\infty F(x)\cdot e^{-x\cdot\frac{h}{d}}\cdot\left(1-e^{-x\cdot\frac{l}{d}}\right)\cdot J_1\left(x\cdot\frac{R_1}{d}\cdot\left(\frac{r}{R_1}\right)\right)dx, \quad (11)$$

where $F(x) = \frac{1}{x^2}\cdot\int_{\left(x\cdot\frac{R_1}{d}\right)}^{\left(x\cdot\frac{R_2}{d}\right)} y\cdot J_1(y)dy$; $x = \lambda d$, $x \in [0; \infty)$;

b) relative magnitude of the current induced (current transformation ratio),

$$I_0(R) = \frac{I_{\varphi m}}{I_m} = \int_0^\infty \frac{F(x)}{x}\cdot e^{-x\cdot\frac{h}{d}}\cdot\left(1-e^{-x\cdot\frac{l}{d}}\right)\times \\ \times\left(1-J_0\left(x\cdot\frac{R_1}{d}\cdot\left(\frac{R}{R_1}\right)\right)\right)dx. \quad (12)$$

In reality, the turns are separated by dielectric gaps. Let it be the same and equal in the vertical and horizontal directions Δ. Concerning, the geometric parameters of the inductor can be determined by the following relations:

$$\begin{cases} l = w_l\cdot\left[d+\Delta\cdot\left(1-\frac{1}{w_l}\right)\right]; \\ R_2 = R_1 + w_r\cdot\left[d+\Delta\cdot\left(1-\frac{1}{w_r}\right)\right]. \end{cases} \quad (13)$$

Taking into account (13), the expressions (11) and (12) take the next forms:

a) relative density of the current induced,

$$J_0(r) = \frac{j_{\varphi m}}{\left(\frac{I_m}{d}\right)} = \\ = \int_0^\infty F(x)\cdot e^{-x\cdot\frac{h}{d}}\cdot\left(1-e^{-x\cdot\frac{l}{d}}\right)\cdot J_1\left(x\cdot\frac{R_1}{d}\cdot\rho\right)dx. \quad (14)$$

b) relative magnitude of the current induced in the region of radius – R (current transformation ratio respectively),

$$I_0(R_0) = \frac{I_{\varphi m}}{I_m} = \frac{1}{N_m}\cdot\int_0^\infty \frac{F(x)}{x}\times \\ \times e^{-x\cdot\frac{h}{d}}\left(1-e^{-x\cdot\frac{l}{d}}\right)\cdot\left(1-J_0\left(x\cdot\frac{R_1}{d}\cdot R_0\right)\right)dx, \quad (15)$$

where

$$N_m = \left(1+\frac{\Delta}{d}\cdot\left(1-\frac{1}{w_l}\right)\right)\cdot\left(1+\frac{\Delta}{d}\cdot\left(1-\frac{1}{w_r}\right)\right),\ R_0 = \frac{R}{R_1}.$$

Numerical estimations of the excitation processes efficiency for eddy currents are given in the example for the system with the following parameters: R_1 = 0.02 m, d = 0.002 m, Δ = 0.0005÷0.001 m, h = 0.001 m.

There are indices off induction processes for windings with the number of turns in one row equal to $w_{l,r}$ = 10 (Table 1).

Table 1

Numerical estimations

No.	Wire row quantity	Wire turns common quantity	Cylindrical inductor, Relative current	Flat circular inductor, Relative current
1	1	10	4.6	9.35
2	2	20	9.5	16.2
3	3	30	14.6	22.4

Fig. 2 shows the situation with increasing number of turns in one row of winding up to $w_{l,r}$ = 20.

Experiment. To confirm the correctness of the calculations performed, similar experimental measurements for a similar electrodynamic system took place. The purpose of the following experiment is:

- the veracity confirmation about the consideration of the ideal conductor system;
- the veracity confirmation of the graphs obtained for induced current density distribution.

It is necessary to carry out two types of measurements for this. The measurement of the distribution of induced currents using an induction sensor located and moved along the radius of the conductor surface and the direct measurement of the induced current density by the voltage drop at a given gap in the conductor. The assumption about the ideal conductor makes it possible to affirm that the density of induced currents on the ideal conductor surface is equal numerically to the magnetic field strength above the conductor. Its veracity can be confirmed with the following scheme of the experiment.

The Fig. 3 below shows a schematic diagram of a contact measuring method.

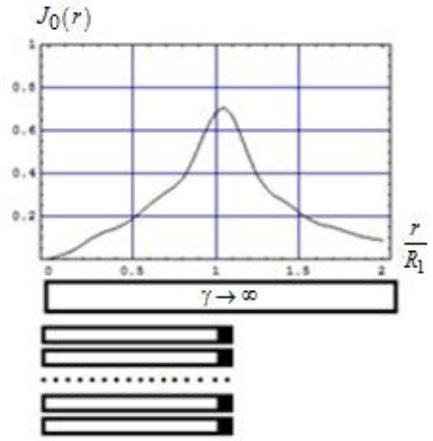

a

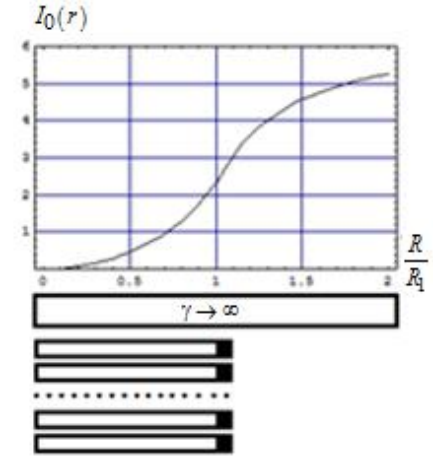

b

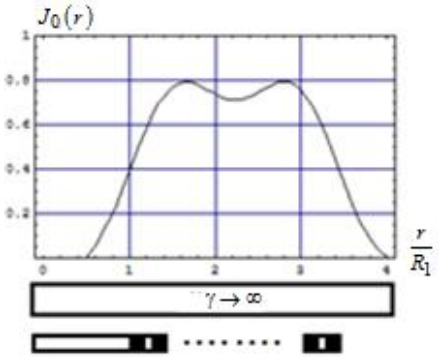

c

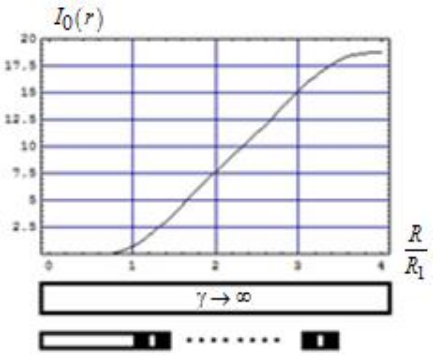

d

Fig. 2. Radial distributions of process efficiency indicators of eddy currents in inductors with single-layer windings, *a, b* – relative density and relative magnitude of the induced current, respectively, for $w_l = 20$, $w_r = 1$; *c*, *d* – relative density and relative magnitude of the induced current, respectively, for $w_l = 1$, $w_r = 20$

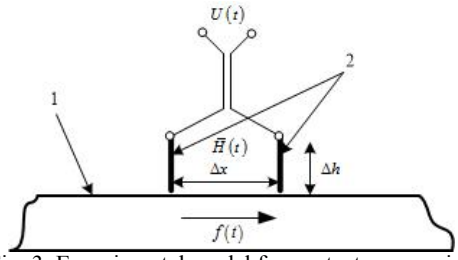

Fig. 3. Experimental model for contacts measuring

- Diameters of inductors used: cylindrical inductor 45 mm, disk inductor 112 mm;
- Height of inductors used: cylindrical inductor – 50 mm, disc inductor – 2 mm;
- Number of turns inductors: 20;
- Inductor current frequency: 20.56 kHz;
- The amplitude of the inductor current: 16.8 A;
- Conductivity of sheet billet: $\gamma = 59.5 \cdot 10^6$ Sm/m;
- The value of the contact gap: $\Delta x = 5$ mm;
- Cross-sectional area of the contact contour and the inductive sensor: $S = 5$ mm^2;
- Number of the inductive sensor coil turns: $N = 100$.

It should be taken into account that the voltage measured at the contacts is the sum of the voltage drop and the induced EMF in the contact contour formed. According to this it's possible to determine the function of the measured voltage by the following formula

$$U(t) = k_1 j(t) + k_2 \frac{dj(t)}{dt}, \qquad (16)$$

where $k_1 = \frac{\Delta}{\gamma} = \frac{5 \cdot 10^{-3}}{59.5 \cdot 10^6} = 0.084 \cdot 10^{-9}$,

$$k_2 = \mu_0 SN = 100 \cdot 4\pi \cdot 10^{-7} \cdot 5 \cdot 10^{-6} = 1.57 \cdot 10^{-10}$$

The solution of the resulting differential equation is the sought-for function of the current density on the metal surface

$$j(t) = \frac{U_m \omega}{k_2(\omega^2 + k_{12}^2)} e^{-k_{12}t} + \frac{U_m}{k_2(\omega^2 + k_{12}^2)} \times \qquad (17)$$
$$\times (k_{12} \sin(\omega t) - \omega \cos(\omega t)),$$

where $k_{12} = k_1 / k_2$.

Taking into account the shape of the exciter current of the inductor and the signal measured, it is fairly to measure the amplitude of the induced current – the maximum of the signal. Neglecting the aperiodic component of the general solution, which eventually tends to zero, the sought-for value can be calculated as

$$j_m = \frac{U_m}{k_2 \sqrt{(\omega^2 + k_{12}^2)}}, \qquad (18)$$

In its turn, the induced current measured by the induction sensor should give the same value as in the case of the contact measurement method.

$$\xi(t) = \mu_0 S_s N \frac{dH(t)}{dt} \approx \mu_0 S_s N \frac{dj(t)}{dt}, \qquad (19)$$

$$j(t) = \frac{1}{\mu_0 S_s N} \int \xi(t) dt = \left| \xi(t) = \xi_m \sin(\omega t) \right| = \qquad (20)$$
$$= \frac{\xi_m}{\mu_0 S_s N \omega} \cos(\omega t)$$

where N – number of sensor coil turns; S_s – sensor cross-sectional area.

Fig. 4 shows the distribution of the induced current and its radial density with two different measurement methods.

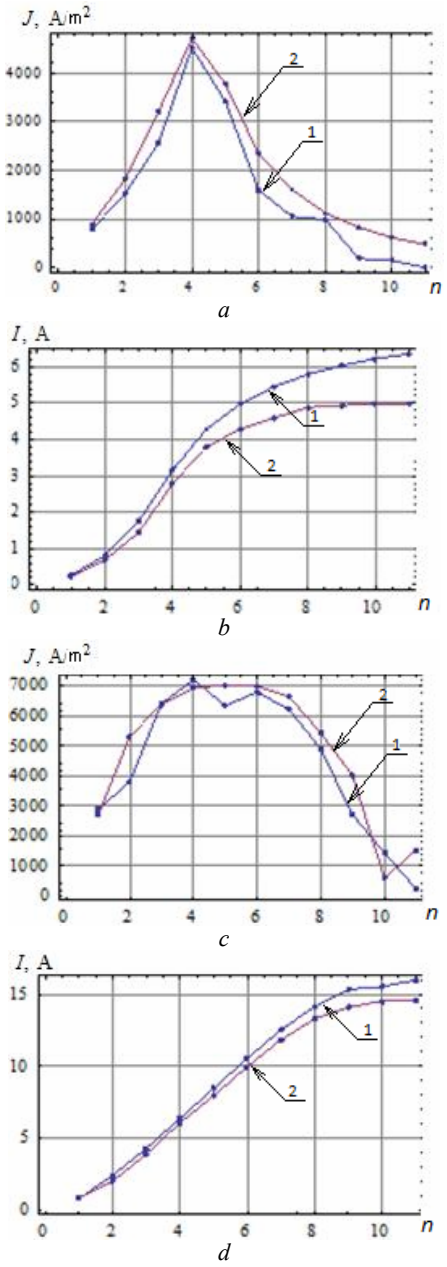

Fig.4. Radial distributions of process efficiency indicators of eddy currents in inductors with single-layer windings: *a*, *b* – density and relative magnitude of the induced current, respectively, for $w_l = 20$, $w_r = 1$; *c*, *d* – density and relative magnitude of the induced current, respectively, for $w_l = 1$, $w_r = 20$; measurements performed by: 1 – induction sensor, 2 – contact method

The qualitative and quantitative coincidence of the current density distributions measured and the calculated currents values for two different measurement methods allow to state the correct representation of the electrodynamic process model and the acceptability of the analytical dependences obtained.

Conclusions. The calculations carried out related for effective systems creation not only for the induction heating of thin-walled metals, but also for a number of electrical devices that represent air current transformers in this case.

The value of the current transformation coefficient depends essentially on the mutual arrangement of the inductor turns.

The most effective is to increase the radial number of turns, with a linear increase in the transmission coefficient. In turn, an increase in the turns along the vertical direction from the surface of the metal does not lead to a substantial transformation coefficient increasing due to the self-shielding effect of the winding.

In the case of a cylindrical inductor, the radial distribution of the excited currents has a pronounced maximum that coincides with the center at the end of the winding. For the practice of induction heating, it means a quadratic dependence of the heat emitting in this region of sheet metal.

The objectivity of the assumption of considering a massive conductor as an ideally conducting surface, as well as the reliability of the graphical dependencies obtained, were confirmed experimentally.

REFERENCES

1. Batygin Yu.V., Gnatov A.V., Chaplygin Ye.O., Sabokar O.S. *Sposib indukcijnogo nagrivu dlja remontu metalevyh elementiv avtomobil'nyh konstrukcij* [Method of induction heating for repair of the metal automobile constructions elements]. Patent UA, no.103494, 2015. (Ukr).

2. Kennedy M.W. *Magnetic fields and induced power in the induction heating of aluminium billets. Licentiate Thesis*. Royal Institute of Technology, Stockholm, 2013.70 p.

3. Wright J. Principles of high frequency induction tube welding. Washington Electronic Heating Equipment Inc., 1997. 8 p.

4. Klonk S. *Modélisation Numérique du Chauffage par Induction de Pièces à Géométrie Complexe.* [Numerical modelling of induction heating for complex geometrical parts]. Thèse pour obtenir le grade de docteur délivré. Doctorat Paris Tech. Paris, 2013. 186 p. (French).

5. Korshikov S.E. *Optimal'noye upravleniye temperaturnymi rezhimami induktsionnogo nagreva tsilindricheskikh slitkov s uchetom tekhnologicheskikh ogranicheniy.* Diss. kand. techn. nauk [Optimum control of temperature modes of cylindrical ingots induction heating taking into account technological limitations. Cand. tech. sci. diss.]. Samara, 2015. 153 p. (Rus).

6. Dershpak N.S. The modes of induction heating of cylindrical parts connected with tension fitting. *Technical electrodynamics*, 2009, no.6, pp. 61-65. (Ukr).

7. Batygin Yu.V., Lavinskiy V.I., Khimenko L.T. *Impul'snyye magnitnyye polya dlya progressivnykh tekhnologiy. Tom 1. Izdaniye vtoroye, pererabotannoye i dopolnennoye*. [Pulsed magnetic fields for advanced technologies. Vol.1. 2nd edition, revised and enlarged.] Kharkov, MOST-Tornado Publ., 2003. 284 p. (Rus).

8. Shneerson G.A. *Polya i perehodnye processy v apparature sverhsilnyh tokov* [Fields and transients in equipment ultra strong currents]. Moscow, Energoatomizdat Publ., 1992, 413 p. (Rus).

Received 03.11.2017

Yu.V. Batygin[1], *Doctor of Technical Sciences, Professor,*
Chaplygin E.A.[1], *Candidate of Technical Sciences, Associate Professor,*
Sabokar O.S.[1], *Postgraduate Student,*
Strelnikova V.A.[1], *Postgraduate Student,*
[1] Kharkiv National Automobile and Highway University,
25, Yaroslava Mudrogo Str., Kharkiv, 61002, Ukraine.
phone +380 57 7073727,
e-mail: yu.v.batygin@gmail.com, chaplygin.e.a@gmail.com,
o.s.sabokar@gmail.com, v.strelnikova91@gmail.com

How to cite this article:
Batygin Yu.V., Chaplygin E.A., Sabokar O.S., Strelnikova V.A. Analysis of electromagnetic processes in the system «cylindrical solenoid – massive conductor». *Electrical engineering & electromechanics*, 2018, no.1, pp. 54-58. **doi: 10.20998/2074-272X.2018.1.08.**

UDC 621.37 **doi: 10.20998/2074-272X.2018.1.09**

N.I. Boyko

POWERFUL GENERATORS OF HIGH-VOLTAGE PULSES WITH NANOSECOND FRONTS

Purpose. ***Purpose of the article is to show the possibility of joint efficient operation of semiconductor switches and spark arresters in high-powerful high-voltage generators for obtaining nanosecond and shorter pulse fronts on a high-voltage load.*** ***Methodology.*** ***The variants of generators of power high-voltage pulses with semiconductor switches in the form of IGBT-transistors, SOS-diodes and spark dischargers as pulse front peaking spark gaps are considered. A scheme is proposed for such a generator of high-voltage pulses with nanosecond front on the basis of a linear pulsed transformer in the Tesla scheme.*** ***Results.*** ***On the complex load of the generator in the form of a serial connection of a gas bubble in water with a discharge in it and a layer of water under the bubble, voltage pulses with an amplitude of 23 kV and current pulses with an amplitude of 15 A were obtained. In this case, the pulse front, both voltage and current, on the levels 0.1-0.9, was approximately 10 ns, and the repetition rate of pulses in the load ranged from 1200 to 5000 pulses per second.*** ***Originality.*** ***A scheme is proposed for a generator of high-voltage pulses with a nanosecond front. The difference of the proposed generator with a nanosecond front, high pulse repetition rate, using its high-voltage and low-voltage circuits in the discharge circuit, is the presence in its composition of a linear pulse transformer and a system of peaking of pulse front using SOS diodes and spark gaps.*** ***Practical value.*** ***These generators considered in this work can find wide application in high-voltage technologies, including decontaminating water treatment, water purification by electric discharges.*** References 11, figures 3.

Key words: **spark gap discharger, generator, switch, transistor, SOS-diode, high-voltage pulse transformer, pulse repetition frequency, capacitive storage, inductance, load resistance.**

Рассмотрены варианты генераторов мощных высоковольтных импульсов с полупроводниковыми коммутаторами в виде IGBT-транзисторов, SOS-диодов и искровыми разрядниками. Предложена схема такого генератора высоковольтных импульсов с наносекундным фронтом. Отличием предложенного генератора с наносекундным фронтом, высокой частотой следования импульсов, с использованием в разрядном контуре его высоковольтных и низковольтных цепей является наличие в его составе линейного импульсного трансформатора и системы обострения фронта импульсов с использованием SOS-диодов и искровых разрядников. Библ. 11, рис. 3.

Ключевые слова: **разрядник, искровой промежуток, генератор, коммутатор, транзистор, SOS-диод, высоковольтный импульсный трансформатор, частота следования импульсов, емкостный накопитель, индуктивность, сопротивление нагрузки.**

Introduction. Modern transistor assemblies with operating voltages up to 10 kV and thyristors as power electronic energy switches in low-voltage circuits of pulse generators make it possible to receive microsecond pulses with an amplitude of 25-500 kV on the load connected to the high-voltage terminals of these generators [1, 2]. Generators with semiconductor switches provide a pulse repetition rate of 50,000 pulses per second [3, 4].

In [3-6], generators are presented on the basis of pulse transformers (PT) and IGBT switches in which PT and reverse diodes in IGBT are used to recover energy not released in the load. In this paper, we present modes in which both the high-voltage and low-voltage PT circuits are involved in the discharge circuits of the generators. IGBT-key can be used both as a closing and as an opening switch. In the figures with the diagrams in this article, L_{lv}, L_{hv} is the inductance of the dispersion and the lead-in conductors in the low-voltage and high-voltage winding of the PT respectively. When the IGBT-key is an opening switch and the magnetization inductance is intermediate energy storage, both the high-voltage and low-voltage circuits of PT participate in the discharge circuit of the high-voltage load.

For peaking of the pulse front, SOS diodes in the high-voltage PT circuit, as well as spark gaps, can be used.

The purpose of the article is to show the possibility of joint efficient operation of semiconductor switches and spark arresters in high-power high-voltage generators for obtaining nanosecond and shorter pulse fronts on a high-voltage load.

Choice of generator scheme. Schemes with SOS-diodes were developed by Russian scientists [1, 7]. But in these generators in the SOS-diodes' pumping circuits, inductance choke with saturation (magnetic keys) are used, which reduce the efficiency of the generators. Fig. 1 shows the circuit diagram of the generator with IGBT switches in the low-voltage circuit of PT in the form of a linear pulse transformer (LPT) and with a SOS switch in the high-voltage circuit of PT without throttles with saturating. The operation of the generator in the case of using T (IGBT) as a closing switch is described in [8]. With a low-resistance load with impedance ≤10 Ohm and the need to allocate in it of all the energy from C_{hv} in each pulse, it is required to minimize inductances of dissipation of high-voltage and low-voltage winding (L_{sh}, L_{sl}) of pulse transformer (PT). This can be done by applying a linear pulse transformer (LPT) as an PT [1]. The replacement circuit of the generator with the lead to the primary winding of the LPT is shown in Fig. 2. Given leaded values are marked with a prime ('). The ferromagnetic magnetic core LPT is divided into sections. Each section is wound with a single-turn primary winding, in the circuit of which there are series-connected capacitive storage C_{lv} and switch T (in Fig.1 IGBT- switch). The total primary winding consists of a series of single-turn primary windings wound each on its own section. The secondary winding is also single-turn, but covers all sections of the magnetic circuit. The design of LPT provides the minimum inductance of leakage L_s and inductance of magnetization L_μ (here $L_s << L_\mu$ as well as in traditional PT).

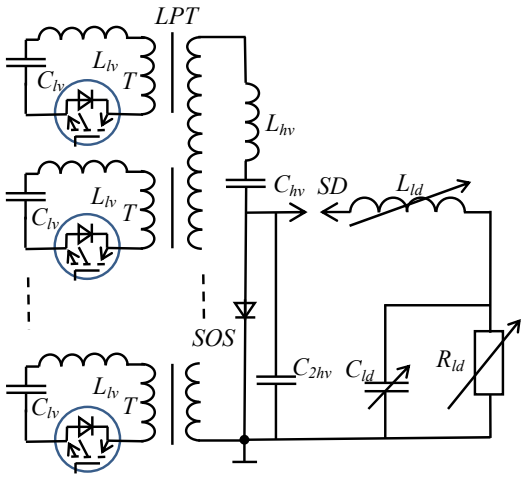

Fig. 1. Schematic circuit diagram of the generator with IGBT switches

Therefore, the duration of the transient response of the LPT is shorter than that of traditional PT. The transformation ratio of the step up transformer LPT is $k_t = n$, where n is the number of sections (or primary windings forming the total primary winding). In Fig. 2 $C_{lv\Sigma}=nC_{lv}$, $L_{lv\Sigma}=L_{lv}/n$, $L_{\mu\Sigma}= L_{\mu}/n$, L_{μ} – magnetization inductance of one section of LPT, T_Σ is a total IGBT switch consisting of n sectional IGBT switches T connected in parallel. Low values of L_s and L_{μ} lead to an increase of the current in the generator. This increases the switch requirements for the currents being passed. The modern IGBT module is capable of transmitting a current of 1200 A, can withstand a voltage of 3300 V and has an on-time of significantly less than 1 μs, and a shutdown time of approximately 1 μs (for example, IGBT module MIO 1200-33E10).

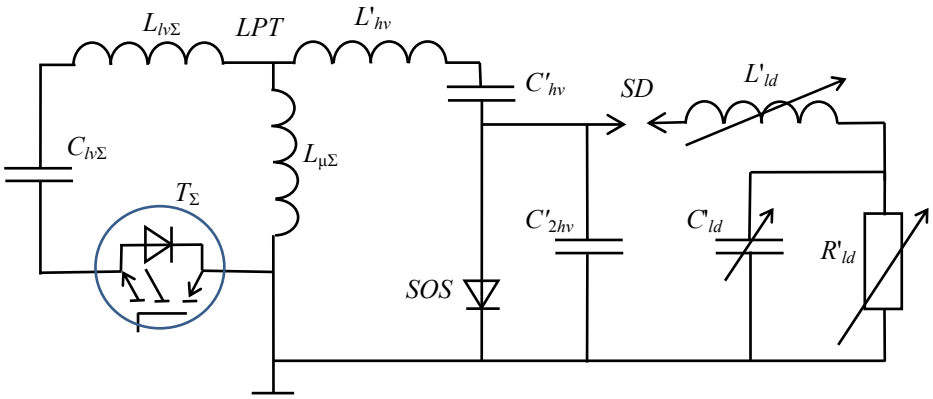

Fig. 2. Scheme of substitution for generator

Considering that the total primary winding consists of n constituent primary windings, each of which includes one MIO 1200-33E10 module with the corresponding driver as IGBT switch, at n = 25 the commutators of the total primary winding are able to pass the current I_{max} = 30 kA. And the calculated current I_{calc} in the discharge circuit through the total primary winding at R_{ld}=8 Ohm is approximately equal to $I_{calc}\approx U'_{hv}/R'_{ld}$. For U'_{hv}=300 V, $R'_{ld}=R_{ld}/n^2$=0.0128 Ohm, I_{calc}≈23.4 kA. $I_{max}>I_{calc}$ [8]. Hence, IGBT-switches can work together with SOS-switches in the discharge circuits of high-power high-voltage generators. Advantages of semiconductor switching systems with IGBT in high-power generators over of switching systems with spark gaps are a higher permissible repetition rate (up to hundreds of thousands of pulses per second), high stability of pulses on the load. In addition, such a switching system provides the ability to control the switching times of IGBT switches on and off and full synchronization of their operation in parallel operation. However, as a final high-voltage switch it is advisable to use a spark gap, since spark dischargers are the most high-speed high-voltage switches that allow obtaining the minimum (subnanosecond) durations of the high voltage pulse fronts on the load. The permissible frequency of following into a load of high-power high-voltage pulses with a nanosecond front is currently limited, probably, by spark gaps at a level of several thousand pulses per second by using forced cooling of their electrodes. The considered generators can find wide application in high-voltage electrotechnologies, including at disinfecting water treatment, water purification by means of electric discharges [9-11].

One of the most promising variants of the scheme of a high-power high-voltage generator operating on the R_{ld}-L_{ld}-C_{ld} load is shown in Fig. 2. After the SOS-diode is pumped back and the current is switched to the capacitance C'$_{2hv}$, this capacitance is charged during a time interval (half-cycle) $T/2\approx\pi[(L_{\mu\Sigma}+L'_{hv})\ C'_{2hv}]^{1/2}$, if $C'_{2hv}<<C'_{hv}$, the closing switch SD does not work, and $L_{\mu\Sigma}$ acts as an intermediate energy store. However, to switch the energy to the load R'_{ld}-L'_{ld}-C'_{ld}, the switch SD (spark discharger) should work, preferably closer to the end of the half-period $T/2$. Then C'_{2hv} with an energy close to the maximum is connected to the R'_{ld}-L'_{ld}-C'_{ld} load during the switching time. The shorter the switching time, the shorter the pulse front duration formed on the R'_{ld}-L'_{ld}-C'_{ld} load.

Such a scheme allows one to obtain nanosecond pulses with amplitude of hundreds of kilovolts and more on the load by using a linear pulse transformer as a step-up pulse transformer having one turn in the secondary winding and a high-speed spark gap as the closing switch SD. Such an arrester allows achieving switch times in units of nanoseconds or less.

Experimental results. Fig. 3 shows the oscillograms of the current and voltage pulses on the load R_{ld}-L_{ld}-C_{ld}. The load of the generator was a serial connection of a gas bubble in water with a discharge in it and a layer of water under the bubble, that is, the load was nonlinear. Therefore, in the diagram (Fig. 1, 2), the inductance, capacitance and active resistance of the load are shown by

variables (general case). The electrode system of the generator in which this nonlinear load was located was a «high-voltage metal rod – a low-voltage (grounded) metal ring under the rod». The oscillograms were obtained in an experimental setup using a simplified scheme in which there is no branch of C'_{hv}-*SOS*, and the capacitance C'_{2hv} is connected directly to the ends of the secondary winding of the *LPT* transformer. It follows from the oscillograms that the voltage and current curves are phase shifted relative to each other, the voltage amplitude on the load is approximately 23 kV and the current amplitude is about 15 A. The voltage and current pulse forms are aperiodic decaying with superimposed oscillations with a period of approximately 20 ns. The half-height duration for the voltage pulse was approximately 120 ns, and for the current pulse, about 60 ns. The duration of the pulse front, both voltage and current, over the levels 0.1-0.9 was approximately 10 ns. The repetition rate of pulses to the load ranged from 1200 to 5000 pulses per second. As a voltage sensor, a capacitive voltage divider was used, and a low-inductive current shunt was used as the current sensor. The recording device was a digital oscilloscope RIGOL DS1102E with a bandwidth of 100 MHz. Therefore, when recording pulses with characteristic times less than 10 ns, errors are possible.

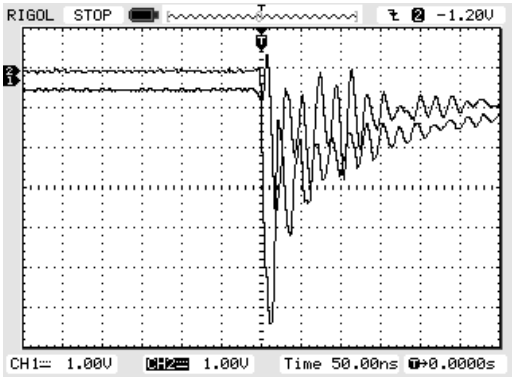

Fig. 3 Typical oscillograms of voltage pulse (1) and current pulse (2) on the load R_{ld}-L_{ld}-C_{ld}

The value of the division along the process axis for the voltage oscillogram (curve 1) is 7.65 kV/div, and for the current oscillogram (curve 2), 2.4 A/div.

Conclusions. A scheme of a high-voltage pulse generator based on a linear pulse transformer using IGBT-switches in its low-voltage circuits is proposed. In the high-voltage part of the generator it is proposed to use SOS-diodes as switches, and spark-gap dischargers as the final power switches. The advantages of the proposed scheme of a high-power generator with a R_{ld}-L_{ld}-C_{ld} load are shown: the possibility of obtaining high-voltage pulses with nanosecond and shorter fronts on the load at a repetition rate of up to several thousand pulses per second. These advantages are confirmed experimentally. A typical oscillogram of voltage and current pulses is shown on a nonlinear load in the form of a series connection of a gas bubble in water with a discharge in it and a layer of water under the bubble. The half-height duration for the voltage pulse was approximately 120 ns, and for the current pulse, about 60 ns. The duration of the pulse front, both voltage and current, over the levels 0.1-0.9 was approximately 10 ns.

The generators considered in this work can find wide application in high-voltage technologies, including decontaminating water treatment, water purification by electric discharges.

REFERENCES

1. Mesiats G.A. *Impul'snaia energetika i elektronika* [Pulsed power and electronics]. Moscow, Nauka Publ., 2004. 704 p. (Rus).

2. Muhammad H. Rashid. *Power electronics handbook: devices, circuits, and applications handbook*. Edited by Muhammad H. Rashid. 3rd ed. Butterworth-Heinemann is an imprint of Elsevier 30 Corporate Drive, Suite 400, Burlington, MA 01803, USA; Linacre House, Jordan Hill, Oxford OX2 8DP, UK, 2011. 1390 p.

3. Boyko N.I., Evdoshenko L.S., Zarochentsev A.I., Ivanov V.M., Konyaga S.F. The high-voltage complex with two high frequency generators that regulate modes of corona and barrier discharges when processing gaseous hydrocarbons. *Technical Electrodynamics*, 2012, no.2, pp. 105-106. (Rus)

4. Boyko N.I., Bortsov A.V., Evdoshenko L.S., Ivanov V.M. Generators of high-voltage pulses with a repetition rate of 50000 pulses per second. *Instruments and Experimental Techniques*, 2011, vol.54, no.4, pp. 533-541. **doi: 10.1134/s0020441211030225.**

5. Boyko N.I., Bortsov O.V., Evdoshenko L.S., Ivanov V.M., Ivankina A.I., Tur A.N. Pulsed corona discharge ionization with enlarged zone of ionization: physical fundamentals of obtaining and the perspective fields of application. *Electrical Engineering & Electromechanics*, 2004, no.3, pp. 98-104. (Rus). **doi: 10.20998/2074-272X.2004.3.20.**

6. Boyko N.I., Bortsov O.V., Evdoshenko L.S., Zarochentsev O.I., Ivanov V.M. Using pulsed corona discharge with enlarged zone of ionization for the conversion of toxic gaseous waste. *Electrical Engineering & Electromechanics*, 2007, no.4, pp. 64-65. (Rus). **doi: 10.20998/2074-272X.2007.4.16.**

7. Vasil'ev P.V., Lyubutin S.K., Pedos M.S., Ponomarev A.V., Rukin S.N., Sabitov A.K., Slovikovskii B.G., Timoshenkov S.P., Tsyranov S.N., Cholakh S.O. A SOS-Generator for technological applications. *Instruments and Experimental Techniques*, 2011, vol.54, no.1, pp. 54-60. **doi: 10.1134/s0020441211010118.**

8. Boyko N.I. Powerful high-voltage generators with the semiconductor switches. *Technical Electrodynamics*, 2014, no.5, pp. 92-94. (Rus).

9. Locke Bruce R. Environmental applications of electrical discharge plasma with liquid water – a mini review. *International Journal of Plasma Environmental Science & Technology*, 2012, vol.6, no.3, pp. 194-203.

10. Preis S., Panorel I.C., Kornev I., Hatakka H., Kallas J. Pulsed corona discharge: the role of ozone and hydroxyl radical in aqueous pollutants oxidation. *Water Science & Technology*, 2013, vol.68, no.7, p. 1536-1542. **doi: 10.2166/wst.2013.399.**

11. Vanraes P., Nikiforov A.Y., Leys C. Electrical discharge in water treatment technology for micropollutant decomposition. *Plasma science and technology – progress in physical states and chemical reactions*. 2016, Chapter 15, pp. 428-478. **doi: 10.5772/61830.**

Received 03.10.2017

N.I. Boyko, Doctor of Technical Science, Professor,
National Technical University «Kharkiv Polytechnic Institute»,
2, Kyrpychova Str., Kharkiv, 61002, Ukraine,
phone +380 57 7076245, e-mail: qnaboyg@gmail.com

How to cite this article:
Boyko N.I. Powerful generators of high-voltage pulses with nanosecond fronts. *Electrical engineering & electromechanics*, 2018, no.1, pp. 59-61. **doi: 10.20998/2074-272X.2018.1.09.**

UDC 621.315 **doi: 10.20998/2074-272X.2018.1.10**

Yu.N. Shumilov, V.G. Santotsky, E.D. Shumilova

ON THE NEED TO INCREASE THE RELIABILITY OF LINEAR INSULATORS FOR DISTRIBUTION NETWORKS 10-20 KV

Introduction. In Ukraine high voltage overhead distribution lines (OL) of class 6 and 10 kV are the most extended. Their total length exceeds 280,000 km. More than 95 % of the lines are made on line supports from reinforced concrete racks. On all poles of the overhead line, pin insulators are installed. According to the data of operation experience, up to 60-70 % of single-phase earth (SPE) faults due to «insulation» occurs on VL supports due to damage to line pin insulators, mainly during the thunderstorm period. Problem. Insufficient reliability of pin insulators leads to interruptions in power supply, accidents on the line, accidents in the area of reinforced concrete poles, where in the case of insulator damages, a long process of SPE occurs. Goal. The purpose of the work is to select the design and develop requirements for new linear insulators of 10-20 kV overhead lines that provide high resistance to lightning overvoltages with direct and inductive effects of lightning. Methodology. The research methodology consists in analyzing operational experience, calculating insulator parameters and laboratory tests. Results. Using statistical data on lightning parameters and data on mechanical loads on insulators, the main dimensions of line post insulators have been determined that will ensure their reliable operation under conditions of intense thunderstorm activity and extreme ice and wind loads. Conclusions. The main technical requirements for line post insulators for 10-20 kV distribution lines were formulated. On the 10 kV OL located in areas with increased thunderstorm activity it is recommended to use line post insulators instead of pin-type ones. On the OL-20 kV it is recommended to use only line post insulators. The use of high-lightning-resistant line post insulators on OL-10-20 kV will significantly increase the electrical safety and reliability of power supply to consumers. Increased by 2-3 times the cost of line post insulators in comparison with those used will be compensated for by the effects of reducing the number of collapsible supports, damage from under-supply of electricity, labor costs during transportation and restoration of destroyed supports, the moral side of reducing accidents in case of electric shock in the emergency zone. The insulators offered for OL-10-20 kV can be used for fixing both bare and protected wires. The exclusion from the design of the weakest elements – polyethylene caps and metal pins will increase the reliability of the power isolation unit. References 11, tables 2, figures 1.
Key words: **overhead power line, pin insulators, line post insulators, lightning over voltages, electrical breakdown, flashover of insulator, power supply interruptions, electrical safety, reliability.**

Статья посвящена выбору конструкций и разработке требований к новым линейным изоляторам для распределительных сетей 6-10-20 кВ, обеспечивающих высокую устойчивость воздушных сетей к грозовым перенапряжениям при прямых и индуцированных воздействиях молнии. Повышение грозостойкости изоляторов позволит сократить перерывы в электроснабжении потребителей и уменьшить электротравматизм персонала электрических сетей при восстановительных работах. Библ. 11, табл. 2, рис. 1.
Ключевые слова: **воздушная линия электропередачи, штыревые изоляторы, опорно-стержневые изоляторы, грозовые перенапряжения, электрический пробой, перекрытия изоляторов, перерывы электроснабжения, электробезопасность, надёжность.**

Introduction. In Ukraine, overhead transmission lines (OL) of voltage class 6 and 10 kV are the most extended. Their total length exceeds 280,000 km. More than 95 % of the OL is made on supports from reinforced concrete racks. On all supports of the OL, pin porcelain ШФ or glass ШС insulators are installed. Pin insulators comply with IEC recommendations and current Standards requirements, but are damaged during OL operation. According to [1] up to 60-70 % of single-phase earth faults (SPE) due to «insulation» occurs on OL supports due to damage of linear pin insulators, the remaining 30-40 % – due to the destruction of arresters, insulation damage on transformer substations, etc.

The overwhelming majority of 6, 10 kV electric networks are made on supports of reinforced concrete racks made of vibrating reinforced concrete, with fastening of wires with the help of pin porcelain or glass insulators. In these solutions, the inadequate resource and low reliability of OL-6-10 kV are implemented. In 35 % of cases, accidents occurred due to the destruction and electrical breakdown of the pin insulators in the power unit.

At a direct lightning strike into the wire (DLS), when the overvoltage wave steepness exceeds 1600 kV/μs, a capillary breakdown occurs in the insulator head [2, 3], and at induced overvoltages from nearby lightning strikes (IO), insulators overlaps take place[4]. In both cases, under certain conditions, a spark lightning strike can go into an arc, supported by the operating voltage. From the thermal action of the arc, the insulator head is usually broken/scattered. A single-phase short-circuit (SPSC) mode occurs [5, 6].

The SPSC mode on a OL-6-10 kV line can exist without switching off the OL line from 2 to 6 or more hours. At the same time, a capacitive current of 5-10 A flows through the reinforced concrete support, and caverns burn out in concrete, reinforcing steel begins to melt, the greatest destruction of concrete and reinforcement occurs at the site of penetration of the support in the ground. Destruction of concrete and reinforcement leads to an unexpected fall of supports, and because of the flow of capacitive current near the support, life-threatening touch voltages and step voltage appear when approaching the human to the support [7].

In the letters of the «State Mining and Industrial Supervision of Ukraine» No. 4824/0/41-8/6/13 and No. 2071/0/4.1-9.1/-6/14 the following is indicated: «*According to the analysis of occupational injuries in the energy sector in 2013, 171 people were injured, including*

20 – with a fatal outcome. The main types of events during which accidents with a fatal outcome were: electric shock and falling victim with altitude along with the support».

The SPSC mode also affects the isolation of other electrical equipment. This situation in the Ukrainian 6, 10 kV networks should be corrected.

The goal of the work is choice of design and development of requirements for new linear insulators of OL-10-20 kV providing high resistance to lightning overvoltages at direct and inductive effects of lightning.

Main research materials. In countries where the transition to reinforced concrete supports was accompanied by the use of support-rod insulators instead of pin insulators, such problems did not exist. In Russia and Belarus to improve the reliability of distribution networks 6, 10 kV in 2004-2009 they began to develop and install support-rod insulators (porcelain and polymer) for the replacement of the pin ones [8].

The cardinal solution of the problem of reducing the accident rate of OL-10-20 kV in Ukraine will be installation instead of pin insulators of support-rod insulators (porcelain and /or polymer). Their design is shown in Fig. 1. Taking into account ongoing developments of the application in Ukrainian distribution networks of 20 kV voltage, insulators with voltage of 20 kV are also included in the work program.

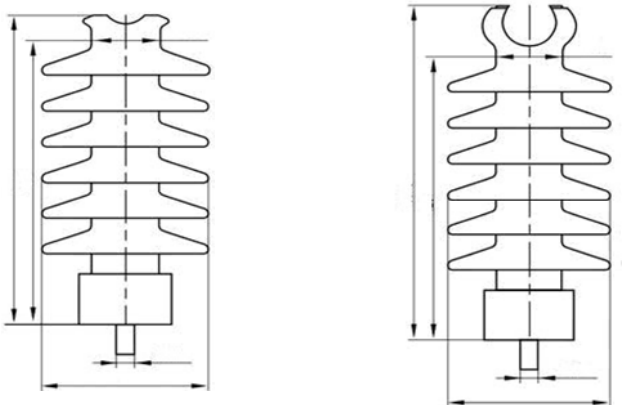

Fig. 1. Sketch of a support-rod insulator for OL 10-20 kV, options A and B

An even more effective solution would be the use of insulating traverses. The use of the traverses will greatly improve the impulse electrical strength, the moisture discharge voltage of the insulation and reduce the probability of lightning transfer to arc.

By improving these indicators, it is possible to reduce the specific number of switching off on the OL-6-10 kV by at least 7.6 times (Table 1).

For dead-end and non-ringed lines, the installation of support-rod insulators or traverses is practically the only cheapest way to solve the problem of unexpected power outage to consumers and reduce electro-injury and death of people. In Ukraine, support-rod insulators for OL-6-10 kV are not produced.

In this regard, the Research and Design Center for Development of the IPS of Ukraine, together with the PSC «Slavyansk High Voltage Insulators Works», at a meeting on September 25, 2017, considered the technical side of the development and production of reliable designs of support-rod insulators and traverses for OL-10 kV and OL-20 kV. The issue of the development of insulators and traverses in 2 versions – polymer and porcelain, suitable for use both on OL with insulated wires and on OL with protected wires was considered.

Table 1

Specific number of switching off of OL-6-10 kV, 1/100 km·100 thunderstorm hours in a non-forested zone (top estimation) [4]

Insulation	OL-6 kV		OL-10 kV	
	$N_{out..DLS}$	$N_{out.IO}$	$N_{out..DLS}$	$N_{out.IO}$
ШС-10А	13.0	11.0	17.3	21.1
ШС-10В	13.0	8.0	17.3	15.4
ШС-10Г	13.9	9.4	18.5	23.1
ШФ-10Г	12.2	8.8	16.2	19.7
ШФ-20В	11.4	3.7	15.2	8.4
ШК-10	11.8	8.8	15.7	18.6
ЛК 70/10	12.4	9.9	16.5	21.7
Insulating traverse ТИ	3.6	0.5	4.3	1.1
Note. DLS – direct lightning strike; IO – induced overvoltages.				

Particular attention was paid to the requirements for new insulators. Let us consider these issues.

Requirement for the normalized bending load. In the catalogs for pin insulators ШФ-10-20 kV and ШС-10-20 kV, the normalized mechanical force for bending F_{bend} = 12.5 kN is indicated. We explain the justification for the value of F_{bend} = 12.5 kN. This is important to understand when justifying the choice of F_{bend} for polymeric support-rod insulators.

The guaranteed fracture load in bending pins and hooks on all drafts does not exceed 3 kN and the crushing load on the support with three insulators – not more than 8 kN. Porcelain insulators with taking into account the possible heterogeneity of the raw material (clay, kaolin, sand), the conditions of firing, embrittlement and unpredictable aging were constructed with in advance inflated characteristics of strength to ensure the necessary (2-3 kN) bending strength during operation. In practice, a plastic cap applied between the pin and the porcelain insulator breaks at lower loads resulting from the bending pin: on the order of 1.5-2 kN load.

According to the conditions of the testing of pin porcelain insulators for mechanical loading, the insulator with a special high-strength rod (steel 40X, diameter at the base – 40 mm) is reinforced with a blind seal with cement-sand ligament. Only with a blind reinforcement with a special rod that does not bend under a load of 12.5 kN, tests can be carried out.

That is, in normal conditions, the «insulator – normal pin» assembly does not withstand more than 3 kN, so the use of insulators with a larger destructive load on the intermediate supports is economically inexpedient and can lead to the fall of the support itself, additional costs and time to rebuild the support. If the insulator breaks under load (for example, 4 kN) less than the strength of the support (8 kN), the power supply can be quickly restored by replacing the insulator. In this case, the wire

in most cases does not fall to the ground, as it remains to hang on the broken insulator, if, of course, the load impact is terminated (for example, the fall of the tree was the cause of the accident) [9].

In projects for reinforced concrete supports, maximum drafts are provided in the following values: 2; 4; 6; 8 kN. Does a polymer insulator need for a load of 12.5 kN? Such an insulator will be quite expensive. We suppose that for mass application it is advisable to develop two types of insulator: for loads of 4 kN and 8 kN. They will fully ensure the reliability with the operating mechanical loads.

Requirements for lightning resistance. To satisfy the requirements for high lightning resistance, two conditions must be fulfilled:

1. Do not allow through-breakdown of the dielectric at direct lightning strikes into the wire.
2. Do not block the insulators with induced overvoltages with following transition of a spark discharge into the arc one.

Satisfaction of these requirements will make it possible to exclude hazardous modes of SPE in the overhead lines due to low lightning resistance of insulators.

To avoid breakdown, it is necessary to increase the thickness of the dielectric in the insulating part (piece) of the insulator, and to avoid overlapping – to increase the discharge distance over the surface (the distance between the metal parts by air). In both cases, the goal is achieved by increasing the insulating height of the support-bar insulator h.

The discharge distance ℓ_d for support insulators is determined by the known expression [10]:

$$U_{\text{imp.+}} = 670 \cdot \ell_d, \quad (1)$$

where $U_{\text{imp.+}}$ is the impacting the insulator impulse voltage from induced waves at lightning discharge (amplitude value), kV_{max}; ℓ_d is the discharge distance, m.

The amplitude values of the impulse overvoltages $U_{\text{imp.+}}$ are of statistical nature. The experimental laws for the distribution of amplitudes of induced overvoltages in 6-10 kV networks were studied in [4]. In this work it is shown that at the level of probability $P(U_{\text{DLS}}) < 0.08 \div 0.05$ the amplitude values $U_{\text{imp.+}}$ are 200-300 kV_{max}.

Substituting these values in the formula (1), we find that ℓ_d can be taken in the range of 300-570 mm. Taking into account the sufficiently low probability of overlap at such discharge distances ℓ_d, as well as the coefficient of transition of the impulse overlap into the arc of 0.5-0.7 [4], the dangerous situation in the line caused by the appearance of the SPE AT induced overvoltages will be minimized.

For support-rod insulators of 6-20 kV, the ratio of ℓ_d is approximately 1.2; so at ℓ_d=300-570 mm thickness of the insulating piece along the axis of the insulator will be 250-475 mm. With such thicknesses, the internal breakdown of insulators is unlikely, that is, the first condition of lightning resistance is also satisfied.

On the basis of the above explanations, the basic requirements for support-rod insulators for 10-20 kV overhead lines presented in Table 2 were formulated.

Table 2

The main technical requirements for support-rod insulators for OL-10-20 kV

Indicator name	Porcelain insulators		Polymeric insulators	
	10 kV	20 kV	10 kV	20 kV
Mechanical force for bending F_{bend}, kN	8	8	4	4
Discharge distance ℓ_d, mm	400	450	400	450
Lightning impulse test voltage, kV_{max}	280	300	280	300
Length of leakage current path (not less than), mm	700	700	700	700
Probability of overlapping with induced overvoltages $P(U_{\text{IO}})$, not more than	0.08	0.075	0.05	0.075

Conclusions.

1. The main technical requirements for support-rod linear insulators for 10-20 kV OL are formulated.
2. On OL 10 kV located in areas with increased thunderstorm activity, it is recommended to use linear support-rod insulators instead of pin-type ones. On OL-20 kV it is recommended to use only support-rod insulators.
3. The use of support-rod insulators of high lighting resistance on OL-10-20 kV will significantly increase the electrical safety and reliability of power supply of consumers.
4. The cost of support-rod insulators increased by 2-3 times in comparison with those used will be compensated for by the effects of reducing the number of collapsible supports, damage from under-supply of electricity, labor costs during transportation and restoration of destroyed supports, the moral side of reducing accidents in case of damage by electric current in the emergency zone.
5. The insulators offered for OL-10-20 kV can be used for fixing both bare and protected wires.
6. Exclusion from the design of the weakest elements – caps and pins will increase the reliability of the power insulation unit.

REFERENCES

1. Santotskiy V.G. Some results of automatic detection of ground faults in 10 kV air grids. *Information collection of the UkrSilEnergoProject Institute «Distribution Grids»*, 2016, no.3-4, pp. 17-24. (Rus).

2. Ierusalimov M.Ye., Il'yenko O.S., Kozyura V.N., Sokolovskiy S.A. Investigation of impulse characteristics of pin insulators. *Technical electrodynamics*, 1983, no.5, pp. 3-9. (Rus).

3. Santotskiy V.G. On the residual electrical strength of 10 and 20 kV pin insulators, pierced by lightning impulses, and the duration of their stay in the 10 kV electric grid under operating voltage. *Abstracts of the workshop of the 4th Section of the Scientific Council on Theoretical and Electrophysical Problems of Increasing the Reliability and Durability of Isolating Networks with Isolated Neutral*. USSR, Tallin, 1981. 180 p. (Rus).

4. Malysheva Ye.P. *Povysheniye nadezhnosti raspredelitel'nykh setey ot 6 do 10 kV na osnove modelirovaniya i usileniya grozoupornosti. Diss. cand. techn. nauk* [Increase of reliability of distribution networks from 6 to 10 kV on the

basis of modeling and strengthening of lightning resistance. Cand. tech. sci. diss.]. Novosibirsk, 2006. (Rus).
5. Arays R.Zh., Stelmanis I.O. *Ekspluatatsiya elektricheskih setey sel'skoy mestnosti*. [Operation of rural electric grids]. Moscow, Energiya Publ., 1977. 280 p. (Rus).
6. Fedoseyenko R.Ya., Melnikov A.Ya. *Ekspluatatsionnaya nadezhnost elektrosetey selskokhozyaystvennogo naznacheniya*. [Operational reliability of agricultural grids]. Moscow, Energiya Publ., 1997. 320 p. (Rus).
7. Sherstobitov R.M., Yundin M.A. Influence of single-phase earth faults in the 10 kV overhead line on reliability of power supply to consumers. *Safety & Reliability of Power Industry*, 2010, no.10, pp. 63-66. (Rus).
8. *The nomenclature of high-voltage polymer insulators. The main linear pin polymer insulators for VLEP 20 kV*. Catalog of ZAO «Rebar-insulator plant». Lytkarino, 2013. (Rus).
9. *Supporting linear rod polymeric insulators*. Available at: https://elektro-montagnik.ru/lectures/part2/file/OLK.pdf (accessed 02 May 2013). (Rus).
10. Sinyavskiy V.N. *Raschet i konstruirovaniye elektrokeramicheskikh izolyatorov*. [Calculation and construction of electroceramic insulators]. Moscow, Energiya Publ., 1977. 192 p. (Rus).
11. Sangkasaad S. Research and experience with new insulator technologies in Thailand. *Proceeding of 2001 World insulator congress: applying new technologies for better reliability and lower costs*. Shanghai, 2001, pp. 154-167.

Received 10.11.2017

Yu.N. Shumilov[1], *Doctor of Technical Science, Professor,*
V.G. Santotsky[2],
E.D. Shumilova[3], *Candidate of Technical Science, Associate Professor,*
[1] PSC «Slavyansk High Voltage Insulators Works»,
79, Kramatorskaya Str., Slavyansk, Donetsk Reg., 84105, Ukraine,
phone +380 95 1813515,
e-mail: sumilovurij2@gmail.com
[2] Research & Design Center for development of the IPS of Ukraine,
11/8, Dorohozhytska Str., Kyiv, 04112, Ukraine,
phone +380 95 2757375,
e-mail: npcr-kanc@ua.energy
[3] Donbass State Pedagogical University,
19, G. Batyuka Str., Slavyansk, Donetsk Reg., 84116, Ukraine,
e-mail: shumilov3@ukr.net

How to cite this article:
Shumilov Yu.N., Santotsky V.G., Shumilova E.D. On the need to increase the reliability of linear insulators for distribution networks 10-20 kV. *Electrical engineering & electromechanics*, 2018, no.1, pp. 62-65. **doi: 10.20998/2074-272X.2018.1.10.**

UDC 621.316.9 **doi: 10.20998/2074-272X.2018.1.11**

D.G. Koliushko, S.S. Rudenko

EXPERIMENTAL SUBSTANTIATION OF THE CALCULATION PROCEDURE OF NORMALIZED PARAMETERS OF GROUNDING DEVICE BASED ON THE THREE-LAYER SOIL MODEL

Purpose. Experimental substantiation of the possibility of using the calculation procedure of normalized parameters grounding devices on the basis of a three-layer model soil. Methodology. The research was based on comparison of the results of experimental measurements for the existing high voltage energy facilities of Ukraine with the results of the calculation. Results. Comparison showed that the average error decreased from 18 % for the two-layer model to 10 % for the three-layer model. The analysis of the calculated and experimentally determined values of the touch voltage showed a high degree of coincidence. Originality. The adequacy of the calculation procedure of the normalized parameters of the grounding device for model with three-layer soil is substantiated by the results of experimental research on the existing energy objects. Practical value. The obtained results allow us to use calculation procedure to create software to determine with increased accuracy the normalized parameters of grounding device located in three-layer soils. References 10, tables 4, figures 3.
Key words: **grounding device, resistance, touch voltage, three-layer soil model.**

Выполнен анализ возможности применения разработанной методики определения нормируемых параметров заземляющего устройства, расположенного в трехслойном грунте, путем сравнения результатов экспериментальных измерений с расчетными значениями для действующих высоковольтных подстанций Украины. Показано, что средняя погрешность определения значения сопротивления заземляющего устройства снизилась с 18 % для двухслойной модели до менее 10 % для трехслойной модели. Сравнение расчетных и экспериментально определенных значений напряжения прикосновения показало высокую степень их совпадения. Библ. 10, табл. 4, рис. 3.
Ключевые слова: **заземляющее устройство, сопротивление, напряжение прикосновения, трехслойная модель грунта**.

Problem definition. Determination of the values of the normalized parameters (NPs) of the grounding devices (GD) of the operating electric power stations and substations, namely the voltage of the contact, the voltage on the GD and the resistance of the GD [1, 2] experimentally leads, as a rule, to significant difficulties (absence of a free space for removal measuring electrodes at a sufficient distance, communications that go beyond the electrical installation, the impossibility of measuring at a real current of ground fault). Therefore, normative documents [2] provide for the possibility of using experimental and calculation methods [3-7]. The main method of monitoring the state of GD is currently electromagnetic diagnostics (EMD), which includes the experimental and calculation stages, as well as the stage of development of recommendations for bringing the GD in line with the requirements of regulatory documents. In the first stage, the actual layout of the GD, the corrosion state and the section of horizontal groundings (HG) are determined, the vertical electrical sensing (VES) is carried out and the electrical parameters of the GD are measured for further calculation. At the second stage, an interpretation of the results of the VES is carried out to determine the structure and specific electrical resistance (SER) and the thickness of the soil layers, and the calculation of the NP of the GD in the mode of single-phase ground fault is conducted. Currently, the most commonly used to calculate NPs are software that is based on a mathematical model of GD located in a two-layered soil [6].

In [8], based on a statistical database of more than 600 energy objects in Ukraine, it has been shown that in most cases the soil has a three-layer structure (72.7 %), sometimes two-layer (about 8.7 %), or it has more than three layers (about 19 %). Proceeding from this, in order to increase the accuracy of the calculation, the authors proposed a mathematical model of non-potential GDlocated in a three-layered soil [9] and a new calculation method is developed on its basis.

However, the developed method for calculating the NP of the GD on the basis of a three-layer soil model has no experimental substantiation which limits its practical application.

The goal of the work is experimental substantiation of the method of calculation of normalized parameters of grounding devices on the basis of a three-layer soil model.

Materials of research. The verification of the calculation methodology was carried out by comparing the results of experimental studies for existing high voltage power units of Ukraine with the calculated values.

For the implementation of the calculation methodology, a test version of the software package «LiGro» was developed for the determination of the NP of the GD of the existing power stations and substations under the three-layered structure of the soil. From the existing software [3-7] the specified software package is distinguished by:

- taking into account the three-layered structure of the soil with the stored calculation duration at the level of two-layered models;
- the calculation of the electric field occurs on the basis of solving the problem of the potential of the field of a point source of current in a three-layered half-space;
- taking into account non-potential groundings;
- the possibility of arbitrary orientation of the grounding.

The verification of conformity of the calculation method with the experimental data is performed according to the following criteria:

- comparison of the experimentally determined and calculated resistance value of the GD (R_G);

• comparison of the experimentally determined and calculated touch voltage value on several selected substation equipment units (U_t).

Analysis of the results of determination of the resistance of the GD. For the analysis the database on the results of the EMD of the state of the GD of 70 electric substations (SS) of the 35 kV voltage class located in the north of Ukraine was used. The choice of this group of power objects is explained as follows:

• measurements were made in the same weather conditions;

• substations are located in the open area and do not have a galvanic connection with industrial objects (which ensures accuracy of measurements), except for SS No. 12 (see Table 1);

Table 1

Results of experimental and calculation determination of R_G

SS Number	R_{Ge}, Ω	R_{G2}, Ω	R_{G3}, Ω	SS Number	R_{Ge}, Ω	R_{G2}, Ω	R_{G3}, Ω
1	0.620	0.5953	0.644	36	5.600	6.133	5.527
2	0.700	0.749	0.7349	37	1.170	1.236	1.346
3	1.270	2.084	1.530	38	1.000	0.7291	0.7756
4	0.750	0.7149	0.684	39	0.560	0.5375	0.5917
5	1.160	1.304	1.218	40	1.000	0.8848	0.9036
6	0.990	0.9278	0.9138	41	1.150	1.250	1.227
7	0.955	1.152	1.252	42	9.700	9.000	8.372
8	0.600	0.5419	0.6788	43	1.330	2.428	1.467
9	0.814	0.9386	0.9175	44	2.600	2.918	2.662
10	1.060	1.607	1.396	45	0.760	0.8873	0.898
11	1.120	1.244	1.206	46	0.898	1.29	0.9515
12	0.394	0.6461	0.6448	47	1.790	1.862	1.792
13	2.370	2.318	2.465	48	1.250	1.796	1.491
14	0.960	0.5622	0.764	49	0.500	0.523	0.5225
15	0.710	0.6598	0.5931	50	2.000	2.526	2.524
16	0.870	0.4934	0.7422	51	0.530	0.7412	0.8197
17	0.697	0.6848	0.7046	52	0.622	0.541	0.6842
18	0.873	0.7781	0.828	53	0.990	0.8837	0.8393
19	0.775	0.882	0.849	54	0.670	0.8287	0.9077
20	0.600	0.6185	0.6017	55	1.100	0.8556	0.9265
21	7.200	8.216	7.543	56	0.950	1.575	1.032
22	1.200	1.459	1.316	57	0.630	0.6615	0.63
23	0.840	1.579	0.961	58	0.441	0.5143	0.4982
24	1.088	1.398	1.233	59	3.810	3.969	3.802
25	0.790	0.7408	0.7919	60	2.800	2.840	2.833
26	0.875	1.024	1.111	61	1.740	1.932	1.731
27	0.605	0.5522	0.560	62	10.10	9.591	10.1
28	1.370	1.661	1.372	63	0.680	0.7406	0.694
29	0.900	0.9658	0.9637	64	0.870	0.9517	1.006
30	2.600	2.25	2.746	65	1.060	1.453	1.136
31	0.300	0.3829	0.327	66	2.236	2.171	2.173
32	0.500	0.517	0.4815	59	0.530	0.5849	0.64
33	21.10	17.66	23.66	68	0.986	1.28	1.182
34	0.610	0.6879	0.6903	69	0.610	0.7621	0.7084
35	1.290	1.073	1.220	70	0.560	0.5695	0.5713

• the presence of an area free of underground communications around the objects, which allowed to obtain the curves of the VES with sufficient accuracy of interpretation (the deviation of the estimated curves of the VES from the experimental values did not exceed 10 %);

• ground soils where the objects are located have a wide range of SER values and allow to evaluate all types of soils (for example, the minimum and maximum values of the SER of the first layer lies in the range from 17 Ω·m to 5690 Ω·m).

In the course of the research, it was compared experimentally measured resistance values of the GD R_{Ge} with the values R_{G2} and R_{G3} calculated by means of the method of determining the NP of the GD located in a two-layered soil (the software complex «Grounding 1.0») [6], and developed by the authors in [9] for the GD located in a three layer soil (software complex «LiGro»). In Table 1, the results of measurements of R_{Ge}, the calculation by using two-layer R_{G2} and three-layer model R_{G3} values, respectively, are presented.

It should be noted that for a fairly significant number of substations (28.5 %) a four-layered soil was characteristic and for calculations the equivalence technique had to be applied with bringing the existing structure of soil to the calculated two- and three-layer models. In particular, this is true for substations No. 7-10, 24-28, 37, 52-61 (see Table 1). The GD of the substation No. 50 is located in five-layer soil. For all other energy objects, a three-layered soil structure is characteristic, so when calculating with the help of «LiGro» the initial soil structure was used, and in the case of «Grounding 1.0» simulation, in all cases an equivalence technique was used.

As can be seen from the results presented in Table 1, for most cases (71 %), the calculation error using a three-layered structure of the soil by the software complex «LiGro» δ_3 is less than the error δ_2 (calculation using the two-layer model «Grounding 1.0»). In addition, it should be noted that for a three-layer model (about 74 %), the error is a positive value. This is due to the fact that the simulation did not take into account the presence of natural groundings (the foundations of equipment and cable lightning rods, the connection of the GD to the outer metal fence, etc.).

However, for three substations, a significant error ($\delta_3 > 35$ %) is recorded in the calculation of the resistance of the GD. Therefore, in order to check the results of the determination of the resistance of the GD (namely, the error value module δ_3) for the presence of random differences in the sample, the Grubbs criterion [10] was used. At the same time, the level of statistical significance for determining the table value of the criterion was 0.05.

As a result of the analysis, the results of determination of the resistance of the GD for substations No. 12, 51, 54 were excluded in stages from the sample volume.

From a physical point of view, a significant deviation of the calculated and experimental data for substation No. 54 is due to the influence of the methodological error that arose when using the equivalence technique to bring the four-layer soil structure to the calculated three-layer. And in two other cases due to the removal of potential outside the power plant: for the substation No. 12 by cables, and for the substation No. 51 by two cable lightning rods which in turn are connected to the metal supports of overhead lines with a voltage class of 35 kV and are natural additional groundings.

The analysis results for a sample of 67 objects (excluding switched off substations) are presented in Table 2.

As can be seen from Table 2, the technique of calculating a non-potential GD located in a three layer soil realized in the form of the software complex "LiGro" has a significantly lower average error (1.8 times) for the determining resistance of the GD in comparison with the two-layer model [6].

Table 2

Comparison of the accuracy of determining the resistance of the GD for 67 substations

Model type	Average error δ, %	Number of substations that fall into the range of error			
		± 5 %	± 10 %	± 15 %	± 20 %
Two-layer "Grounding 1.0"	18.22	14	28	41	47
Three-layer "LiGro"	9.91	22	40	50	59

Also, for the developed method of calculating the NP of the GD located in the three-layer soil, a greater number of falls of the experimentally determined values in the permissible error ranges (by an average of 31 %) is recorded. This is especially true for ranges of ± 5 % and ± 10 % where the number of such falls increased by 57 % and 42 % respectively.

Analysis of the results of determining the touch voltage. The test was based on a comparison of the touch voltage on several selected substation equipment units when simulating a single-phase ground fault. The analysis was carried out on three substations with voltage class 110 (150) kV. In this case, the traditional method of the set of experimental data was used to assess the adequacy of the mathematical models of the GD which is presented in [6]. The substations were selected in such a way that each of them had one of the most common types of soil: Q, H and K which make up more than 99 % of all three-layered soils of Ukraine in the locations of power facilities. Type A soil was not considered, since it occurs in less than 1 % of cases [8].

Fig. 1-3 show the layouts of the GD locations for the specified substations. The horizontal groundings are marked with a thick black line, the grounding conductors connecting the equipment with grounding are marked by points, and the name of the equipment QS-1–QS-6 on which the measurements have been carried out as well as the power transformers 1T and 2T are shown.

The result of the calculation is the maximum and minimum value of the touch voltage within a radius of 0.8 m around the point of study.

The evaluation of the results of the calculation was as follows: the experimentally measured value of the touch voltage U_t should be in the interval between the minimum and maximum calculated values for the corresponding point. Table 3 shows the results of comparison of U_t for disconnectors of substations SS No. 1, 2, 3. Resistance of the base (plate) R_o is the experimentally determined value according to [6] which is necessary for calculation and is an own characteristic for each point:

$$U_t = \left|\varphi_{k0} - \varphi_{0.8}\right| \frac{R_{body}}{R_{body} + R_o}, \qquad (1)$$

where φ_{k0} is the potential on the k-th equipment unit, $\varphi_{0.8}$ is the potential on the soil surface determined by the results of calculations, within a radius of 0.8 m around the k-th equipment unit; R_{body} is the resistance of the human body of 1 kΩ [6].

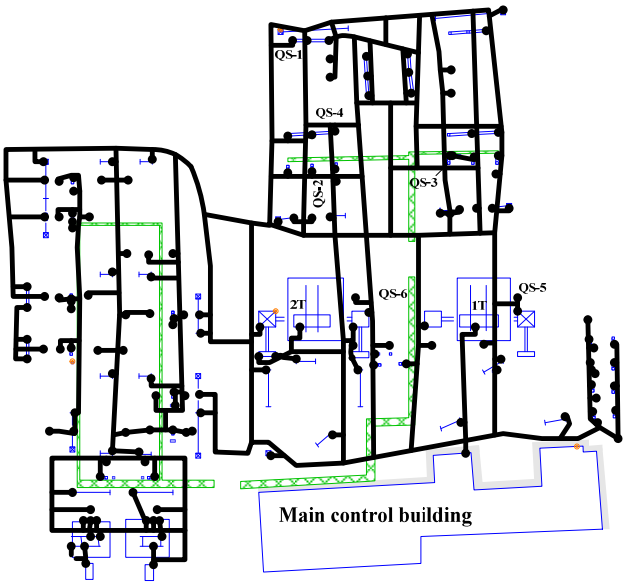

Fig. 1. Schematic diagram of the operating substation SS No. 1 of the voltage class 150 kV in the central part of Ukraine

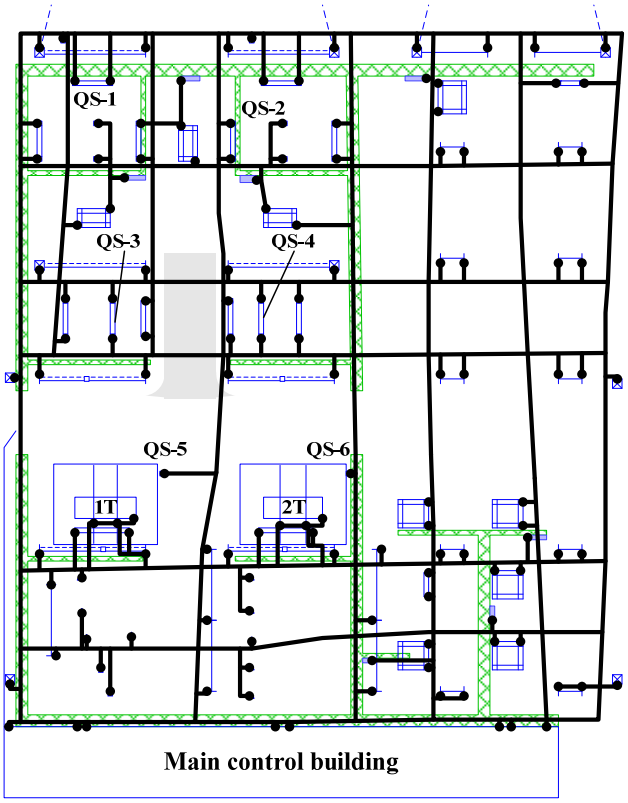

Fig. 2. Schematic diagram of the operating substation SS No. 2 of the voltage class 110 kV in the central part of Ukraine

Input data for the calculation (grounding parameters, specific electrical resistance of soil layers ρ and their thicknesses h, and the value of the measuring current) are given in Table 4.

For SS No. 1 and SS No. 3, the experimentally determined value of the touch voltage for all points (that is, in 100 % of cases) lies in the calculated range.

For SS No. 2, the experimentally determined value of the touch voltage for 5 points of 6 (i.e. 83.3 % of cases) lies in the calculated range, and for the QS-4 equipment, the deviation of the nearest calculated value from U_t is 20.8 %. For specified point such a deviation can be explained by the difference in the cross section of the local grounding, its corrosion wear, or the difficult path of the grounding trail (the depth of bedding is variable, and the grounding itself has not a straight line, but an arbitrary shape at a distance of less than 0.2 m which can not be determined).

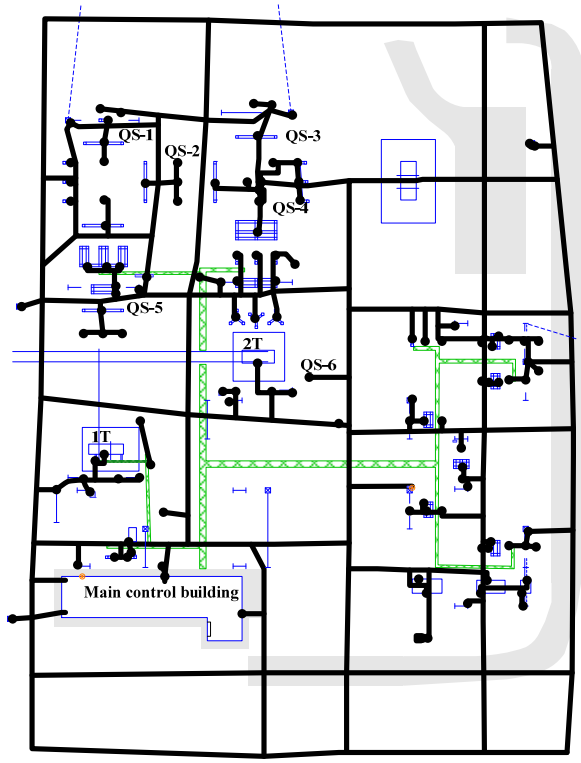

Fig. 3. Schematic diagram of the operating substation SS No. 3 of the voltage class 150 kV in the south of Ukraine

Table 3

Comparison of experimental and calculated value of the touch voltage

Object name	Conditional name of the equipment	Experimental results		Calculated results		Fall into the definition range U_t
		U_t, mV	R_o, Ω	$U_{t\,max}$, mV	$U_{t\,min}$, mV	
SS No. 1	QS-1	20	273	21.40	16.10	+
	QS-2	19	92	21.40	18.40	+
	QS-3	30	130	30.50	25.40	+
	QS-4	18	213	19.90	14.00	+
	QS-5	35	162	51.35	32.50	+
	QS-6	42	114	58.00	41.90	+
SS No. 2	QS-1	33	38	34.6	19.5	+
	QS-2	17	42	24.0	16.2	+
	QS-3	16	61	20.3	15.2	+
	QS-4	13	87	21.5	15.7	–
	QS-5	24	123	31.1	23.1	+
	QS-6	38	116	61.4	36.5	+
SS No. 3	QS-1	95	266	97.5	78.13	+
	QS-2	117	239	120.1	85.20	+
	QS-3	99	315	99.3	65.60	+
	QS-4	190	252	238.4	129.70	+
	QS-5	60	298	70.8	56.60	+
	QS-6	107	1169	259.0	106.80	+

Table 4

Input data to calculate the touch voltage

Parameter:	SS No. 1	SS No. 2	SS No. 3
HG cross section, mm	band 20×6	band 40×4	bar Ø16
ρ_1, Ω·m	92.5	42	150
ρ_2, Ω·m	61	3,3	43
ρ_3, Ω·m	13	22	12
h_1, m	0.9	0.3	0.3
h_2, m	3.2	5.3	9.8
Measuring current I_i, A	4.76	4.76	4.76

In order to take into account this, it is necessary to carry out additional research with the introduction of the corresponding results into the calculation model. However, the proximity of the experimental value to the calculated one for this point and the fall into the calculated range for other points makes it possible to conclude that the model for the GD of this substation is adequate.

Thus, the total fall in the calculated range is observed in 17 points of 18, which is 94.4 %.

The results of the performed research confirm the adequacy of the developed method of calculating the GD based on the three-layer soil model, the experimental value of the touch voltage obtained at simulating a single-phase ground fault on the real GDs that are in service.

Conclusions.

1. The adequacy of the method of calculation of the normalized parameters of the grounding device based on the three-layer soil model is substantiated by comparing the results of experimental research for the operating high-voltage power facilities of Ukraine with the calculation results.

2. It is shown that the developed method of calculation allows to improve the accuracy of the determination of normalized parameters of grounding devices. In this case, the average error of determining the resistance of grounding devices does not exceed 10 %, and when determining the touch voltage, the fall in the calculated range is recorded for 94 % of the experimental points.

3. The obtained results allow to use the developed method of calculation for the creation of software tools for determining the normalized parameters of grounding devices of arbitrary configuration located in a three layer soil.

REFERENCES

1. IEEE Standard 81-2012. IEEE Guide for measuring Earth resistivity, ground impedance, and Earth surface potentials of a grounding system. [Amended by 2012-12-28]. New York: IEEE, 2012. 86 p. **doi: 10.1109/ieeestd.2012.6392181**.

2. *Natsional'nyy standart Ukrayiny. SOU 31.2-21677681-19:2009. Viprobuvannya ta kontrol' prystroyiv zazemlennya elektroustanovok. Tipova instruktsiya.* [National Standard of Ukraine SOU 31.2-21677681-19:2009. Test and control devices, electrical grounding. Standard instruction]. Kyiv, Minenergovugillya Ukrayiny Publ., 2010. 54 p. (Ukr).

3. Tabatabaei N.M., Mortezaeei S.R. Design of grounding systems in substations by ETAP intelligent software. *International Journal on «Technical and Physical Problems of Engineering» (IJTPE)*, 2010, iss.2, vol.2, no.1, pp. 45-49.

4. Turri R., Andolfato R., Cuccarollo D. A numerical simulation tool for cathodic protection and electromagnetic

interference analysis. *NACE Milano Italia Section – Conference & Expo 2016 «A European event for the Corrosion Prevention of Oil&Gas industry»*. 17 p. Available at: https://www.researchgate.net/publication/303685228_A_NUMERICAL_SIMULATION_TOOL_FOR_CATHODIC_PROTECTION_AND_ELECTROMAGNETIC_INTERFERENCE_ANALYSIS (accessed 22 September 2016).

5. Zubov K.N. *Sovershenstvovanie raschetnykh metodov molniezashchity i zazemliaiushchikh ustroistv v neodnorodnykh gruntakh. Diss. cand. techn. nauk* [Improved computational methods for lightning protection and grounding devices in heterogeneous soil. Cand. tech. sci. diss.]. Vologda, 2011. 158 p. (Rus).

6. Koliushko D.G. *Sovershenstvovanie diagnostiki zazemliaiushchikh ustroistv elektroenergoob»ektov. Diss. cand. techn. nauk* [Improving the diagnosis of grounding devices for electric power objects. Cand. tech. sci. diss.]. Kharkov, 2003. 172 p. (Rus).

7. Unde M.G., Kushare B.E. Grounding grid performance of substation in two layer soil – a parametric analysis. *International Journal of Engineering Sciences & Emerging Technologies*, 2012, vol.1, no.2, pp. 69-76. **doi: 10.7323/ijeset/v1_i2_8.**

8. Koliushko D.G., Rudenko S.S., Koliushko G.M. Analysis of electrophysical characteristics of grounds in the vicinity electrical substation of Ukraine. *Electrical engineering & electromechanics*, 2015, no.3, pp. 67-72. (Rus). **doi: 10.20998/2074-272X.2015.3.10.**

9. Koliushko D.G., Rudenko S.S. Mathematical model of grounding connection of a power plant with under layer. *Electronic modeling*, 2014, vol.36, no.2, pp. 89-97. (Rus).

10. International Organization for Standardization. ISO 5725-2: 1994: Accuracy (Trueness and Precision) of Measurement Methods and Results-Part 2: Methods for the Determination of Repeatability and Reproductibility. International Organization for Standardization, 1994.

Received 10.12.2017

D.G. Koliushko[1], *Candidate of Technical Science, Senior Research Associate,*
S.S. Rudenko[1], *Research Associate,*
[1] National Technical University «Kharkiv Polytechnic Institute», 2, Kyrpychova Str., Kharkiv, 61002, Ukraine,
e-mail: nio5_molniya@ukr.net

How to cite this article:
Koliushko D.G., Rudenko S.S. Experimental substantiation of the calculation procedure of normalized parameters of grounding device based on the three-layer soil model. *Electrical engineering & electromechanics*, 2018, no.1, pp. 66-70. **doi: 10.20998/2074-272X.2018.1.11.**

Матеріали приймаються за адресою:
Кафедра "Електричні апарати", НТУ "ХПИ", вул. Кирпичова, 21, м. Харків, 61002, Україна
Електронні варіанти матеріалів по e-mail: a.m.grechko@gmail.com

Довідки за телефонами: +38 050 653 49 82 Клименко Борис Володимирович
+38 067 359 46 96 Гречко Олександр Михайлович